

Theory and Modelling of Single-Electronic Systems

Sharief Fadul Babikir

October 1993

A Thesis presented to the University of Glasgow
Department of Electronics and Electrical Engineering
for the degree of Doctor of Philosophy

© Sharief Fadul Babikir, 1993

ProQuest Number: 13833803

All rights reserved

INFORMATION TO ALL USERS

The quality of this reproduction is dependent upon the quality of the copy submitted.

In the unlikely event that the author did not send a complete manuscript and there are missing pages, these will be noted. Also, if material had to be removed, a note will indicate the deletion.



ProQuest 13833803

Published by ProQuest LLC (2019). Copyright of the Dissertation is held by the Author.

All rights reserved.

This work is protected against unauthorized copying under Title 17, United States Code
Microform Edition © ProQuest LLC.

ProQuest LLC.
789 East Eisenhower Parkway
P.O. Box 1346
Ann Arbor, MI 48106 – 1346



Theis

9913

Copy 1

Abstract

In this thesis a theoretical study is made of the behaviour of single-electronic devices and systems. It is argued that the properties of single-electronic systems can be determined if the densities of the legal soliton states are known. The dynamics of the tunnelling electrons in such systems are modelled as a traffic process. An exact analytical technique based on the conventional Traffic Theory is formulated in the thesis. This new technique is compared with the traditional Monte-Carlo method and is shown to be superior, both in accuracy and speed. An algorithm that correctly and efficiently determines the set of active soliton states and the relationship between the states is also described.

Tunnelling dynamics in a double-junction system are modelled as a Birth-Death process and an exact analytical solution is obtained. The model is then used to study the effects of discrete energy spectrum at the central dot of a double-junction system.

A numerical solution for the Fokker-Planck like equation of the charge density function in a single tunnel junction circuit is implemented and used to study the coherence of the single-electron tunnelling (SET) oscillations. To avoid the heavy computations involved in the numerical solution a simple technique based on the distribution of the time between successive tunnel events is presented. It is shown that the SET oscillations do exist but the predicted ensemble average oscillations damp out exponentially with time.

The regimes of operation of the double-junction system, the turnstile, are investigated. It is argued that the addition of resistive components to the circuit will enhance the reliability of the device and dramatically reduce the probability of unwanted events at the cost of reduced clocking rate. The Master-Equation formalism is extended to the double-junction system. The charge fluctuations are shown to be less than the fluctuations in a single-junction case.

The processes degrading the reliability of single-electronic systems are studied. These include thermal and quantum fluctuations, the charge macroscopic quantum tunnelling and single charges that are being momentarily or permanently trapped in the vicinity of the system's electrodes. The Traffic model is extended to include these processes

Acknowledgements

I would like to thank Professor John Barker for the assistance and encouragement he provided throughout the period of study and for many fruitful and stimulating discussions.

I am deeply grateful to all Members of Staff at the Electronics and Electrical Engineering Department. Many thanks are due to the members of the Modelling Group and the Single-Electronics Group for their full collaboration and assistance throughout my stay at Glasgow University. I would like to thank in particular Dr. Asen Asenov for helping in many aspects of this work, Dr. John Davies for the excellent series of lectures he delivered, Dr. John Williamson and Dr. John Weaver for many useful discussions. Particular thanks are due to Scott Roy and Don Reid for the assistance and encouragement. Thanks are due to Mr. Ibrahim O'Keir of Strathclyde University for providing many (Mathematics) references.

I would like to thank the staff at the Registry Office and staff of the International Programme Office ,in particular Avril McGregor, for the understanding, appreciation and help during periods of difficulties.

My *special* thanks must be to my wife, *Maha*, for her patience and encouragement throughout the period of study and for the elegant typing of the thesis.

It is a pleasure to acknowledge the continual encouragement of *our* parents in the Sudan and their endless concern about *us*.

Thanks are due to the Sudanese Government for giving me the opportunity to study at Glasgow and I am grateful to the Cultural Attaché at the Sudanese Embassy (London). I finally acknowledge the unlimited moral support we received from the small Sudanese Community at Glasgow; I mention in particular Dr. Hasan and his family, A/Wahab, Zakariea and Elkhatim.

TO MY MOTHER

with love, gratitude and respect.

Table of Contents

Abstract	I
Acknowledgements	II
Dedication	III
Publications	VI
List of Illustrations	VII
1- Chapter (1): Introduction	1
1.1 Outlines of the Thesis	1
1.2 Historical Background	3
1.3 Semiclassical Model	9
2- Chapter (2): Models of the Single Junction	15
2.1 Introduction	15
2.2 Tunnelling Rate	15
2.3 Master-Equation Formalism	19
2.4 Solution of the Master Equation	21
2.4.1 Coulomb-Blockade Regime	22
2.4.2 Single-Electron Tunnelling	24
2.4.3 Numerical Solution	26
2.4.4 Results of Numerical Simulations	29
2.5 Time between Tunnel Events	30
2.5.1 I-V Characteristics	34
2.5.2 Voltage-Biased Junction	34
2.5.3 Current-Biased Junction	35
2.5.5 Q-Factor of SET Oscillations	38
Summary	39
3- Chapter (3): The Double-Junction System	46
3.1 Introduction	46
3.2 Experimental Structures	46
3.3 Semiclassical Model	49
3.4 Finite-State Machine Model	53
3.5 Static Monte-Carlo Simulation	57
3.6 Dynamic Monte-Carlo Simulation	60
3.7 Master-Equation Formalism	64
3.7.1 Charge Fluctuations	66
Summary	67

4- Chapter (4): Single-Electronic Systems	72
4.1 Introduction	72
4.2 The Single-Electron Pump	72
4.3 Arrays of Tunnel Junctions	73
4.4 Modelling the Multi-Junction Systems	75
4.5 Single-Electron Solitons	75
4.6 Monte-Carlo Modelling	78
Summary	80
 5- Chapter (5): Traffic Theory	 83
5.1 Introduction	83
5.2 Traffic Model for Tunnelling Dynamics	83
5.3 Density of Soliton States	91
5.4 Birth-Death Model	97
5.5 The Quantum Dot	103
5.6 Multi-Junction Arrays	110
5.7 Evolution of Soliton States	111
5.8 Algorithm to discover the Active States	113
Summary	115
 6- Chapter (6): Killer Processes	 121
6.1 Introduction	121
6.2 General 1 Model	121
6.3 Thermal and Quantum Fluctuations	124
6.4 Charge-Macroscopic Quantum Tunnelling	130
6.5 Effect of External Resistance	133
6.6 MQT in Multi-Junction Arrays	135
6.7 Trapped Charges Effects	137
6.8 Killer Processes and the Traffic Model	143
Summary	144
 Conclusion	 149
 References	 151
 Appendices	 159

Publications

During the course of this research, some aspects of the work have been published:

Theory, modelling and construction of single-electronic systems, Barker J, Weaver J, Babikir S and Roy S, Proceedings of Second International Symposium on New Phenomena in Mesoscopic Structures, Hawaii (1992)

Trajectory representations, fluctuations and stability of single-electronic systems, Barker J, Roy S and Babikir S, Chapter (22) in 'Science and Technology of Mesoscopic Structures', edited by Namba S., Hamaguchi C. and Ando T., Springer-Verlag: London, Tokyo and New York (1992)

Queuing-theoretic simulation of single-electronic metal-semiconductor devices and systems, Babikir S, Barker J and Asenov A, Proceedings of the International Workshop on Computational Electronics, Leeds (1993).

List of Illustrations

Figure Page

1.1	6	Zeller and Giaever's structure.
1.2	6	Lambe and Jacklevic's structure.
1.3	10	Potential profile of a single tunnel junction.
1.4	11	Electric forces acting on a tunnelling electron.
2.1	19	Current-biased tunnel junction.
2.2	31	Evolution of charge on a single junction with time.
2.3	35	Relationship between current and voltage sources.
2.4	40	Average charge on the junction in the full Coulomb-blockade regime calculated using both analytical numerical solutions.
2.5	40	Standard deviation of the charge, analytical vs. numerical.
2.6	41	Evolution of charge with time, the SET oscillations. Calculated from the numerical solution.
2.7	42	Frequency spectrum of SET oscillations.
2.8	43	Distribution of the time spent above the Coulomb barrier before the tunnel event.
2.9	43	Distribution of the time between successive tunnel events.
2.10	44	I-V ch/cs of a single tunnel junction.
2.11	45	Quality factor of SET oscillations.
3.1	46	The double-junction system (The turnstile).
3.2	47	Fulton's structure.
3.3	48	Scott-Thomas's structure.
3.4	49	Meirav's structure.
3.5	49	Pasqueir's structure.
3.6	51	Potential profile for the double-junction system.
3.7	56	Finite-State Machine model for the turnstile.

3.8	56	Operational areas obtained from the Linear Programming method.
3.9	61	Damped double-junction circuit.
3.10	62	operational areas for the damped double-junction circuit.
3.11	68	I-V ch/cs of a double junction system (Static MC method).
3.12	69	Transfer ch/cs of the double-junction circuit.
3.13	69	Average number of excess electrons at the central electrode as a function of the gate voltage.
3.14	70	Evolution of the charge on the junction of a damped double-junction system with time.
3.15	70	Distribution of the time that elapses before the event $T(M,R,1)$ occurring in (3.14)
3.16	71	Similar to (3.14) with different initial bias conditions.
3.17	71	Distribution of the time that elapse before the event $T(L,M,0)$.
4.1	72	The single-electron pump.
4.2	72	Schottky-dot structure (Glasgow).
4.3	77	Equivalent circuit for the multi-junction array.
4.4	81	I-V ch/cs of an 8-junction array.
4.5	82	Transfer ch/cs of a 3-junction system. Shown also the dependence of the excess charges at the inner electrodes on the gate voltage.
5.1	84	Single-electronic systems, tunnel and non-tunnel nodes.
5.2	84	Traffic Model for tunnelling dynamics.
5.3	92	Relationship between the soliton states of a single-electronic system.
5.4	92	Soliton states of a double-junction system. Birth-Death relationship.
5.5	105	Single-quantum dot structure. Discrete energy levels.
5.6.A	116	I-V ch/cs of a symmetric double-junction structure.

- 5.6.B 117 I-V ch/cs of an asymmetric double-junction system.
- 5.7 118 Transfer ch/cs of a double-junction system. Comparison between the results of the Traffic and MC methods.
- 5.8 119 I-V ch/cs and number of soliton states contributing to the conduction process in a quantum-dot structure with discrete energy levels at the central dot.
- 5.9 119 Effect of discrete energy levels on the transfer ch/cs of a double-junction system.
- 5.10 120 Differential conductance of a 3-junction system. Shown also the number of active soliton states.
- 5.11 120 I-V ch/cs of an asymmetric 3-junction system.
- 6.1 123 Potential profile in a single-junction system. This is the relevant profile when studying the thermally activated events.
- 6.2 123 Potential profile used to investigate the q-MQT events.
- 6.3 138 Distribution of induced charges at the three segments of the 1-DEG of the Meirav's structure due to a single trapped charge.
- 6.4 140 Electric field strength due to a uniformly distributed (line) charge.
- 6.5 143 Model used to estimate the effects of surface charges on the metallic quantum structures.
- 6.6 145 Conductance of the single junction vs. temperature.
- 6.6.A 146 Conductance of the single junction due to the MQT of the charge.
- 6.7 147 Effects of the environmental impedance on the zero-bias resistance of the single junction.
- 6.8 147 Zero-bias resistance of the single junction vs. temperature.
- 6.9 148 Induced potential difference across the tunnel junctions of Meirav's double-junction structure due to single trapped charges.

Chapter (1)

Introduction

Recent advances in fabrication technology have made it possible to fabricate ultra-small normal (non-superconducting) tunnel junctions in which the flow of the electric charge in the form of discrete single electrons can be observed and controlled. The new devices exhibit two distinct modes of operation; viz. (a) the Coulomb-blockade regime where the flow of electrons is completely suppressed by the Coulomb gap and (b) the correlated flow of single electrons where a single tunnel event will block other events until some certain charge is fed to the junction from the external source. These exciting properties suggest that these devices may be used in a wide range of applications including the single-electron logic circuits and current standards.

This has motivated the investigation into the single junction as a basic element of the new class of single-electronic devices and into multi-junction systems which are expected to provide higher reliability and versatility.

The objective of this thesis is to study the properties of some devices that are expected to form the backbone of the wider range of the single-electronic systems and to develop some simulation tools to facilitate the studies.

The behaviour of single-electronic devices is affected by thermal and quantum fluctuations induced by the environment. Trapped charges in the bulk insulating medium or at the surface modulate the potential at the different nodes of the system. It is therefore an important issue to investigate these factors and look at ways of eliminating or reducing their detrimental effects.

1.1 Outlines of the Thesis:

Chapter (1): is an introductory chapter, a historical background of the field of Single-Electronics is presented, and the physics behind the Coulomb-blockade phenomenon is outlined.

Chapter (2): the single junction is studied, two models are used to analyse the device; these are: (a) the solution of the Master Equation relating the charge distribution function to the parameters of the single-junction circuit and (b) a simpler technique based on the investigation of the distribution of the time between successive tunnel events.

Chapter (3): the double-junction structure has received a lot of attention in the last few years and several experiments have been performed on different double-junction structures. The device is described in this chapter with reference to several experimental structures. Modelling techniques used in this chapter include: (a) a semiclassical model describing the origin of Coulomb blockade in such circuits, (b) Finite-State-Machine model describing the State-Input-Transition relationship in single-electronic systems, (c) static and dynamic Monte-Carlo methods and (d) Master-Equation model. Emphasis is placed on the double-junction as a memory element in logic circuits (the turnstile).

Chapter (4): is intended to be an extended introduction to chapter (5). The long array of tunnel junctions is studied and is shown to sustain soliton modes. The conventional Monte-Carlo techniques, as applied to modelling single-electronic devices and circuits, are briefly outlined.

Chapter (5): an exact analytic technique based on the conventional Traffic Theory is presented as a solution of the model of multi-junction systems. This technique is shown to be much faster than the standard Monte-Carlo method. An algorithm which systematically and efficiently determines the set of active states is described and implemented. A version of this technique (the Birth-Death Model) is applied to the double-junction system.

Chapter (6): the flow of single electrons in single-electronic systems is affected by thermal and quantum fluctuations; unwanted tunnel events will degrade the reliability of these devices. Fluctuations of the potential due to single charges being trapped/detrapped in the vicinity of the junctions may also cause such events. These killer processes are investigated in this chapter.

The following sections give a review of the field of single-electronics. The first structures in which the Coulomb-blockade phenomenon was observed are briefly described. In this chapter, the semiclassical model of tunnelling in a metallic tunnel junction is presented.

1.2 Historical Background:

The electrical conduction mechanism through small metal particles has been a subject of interest since the early fifties. The first studies were conducted on thin metal films a few tens of angstroms thick prepared by evaporation onto a substrate. These films consist of an array of small individual metallic islands separated by distances of the order of a few angstroms. The size of the islands and the separation between the granules determine the electrical properties of the film. The behaviour was found to be dominated by the bulk metal properties if the film contains large metal granules with small inter-grain separation. Due to strong scattering from the dielectric inclusions and grain boundaries, the electrical conductivity will be less than the crystalline value, see Abeles (1976) for a review.

In the metallic region, the resistivity is relatively low and the temperature coefficient of resistivity is positive. A film of small metallic particles imbedded in a continuum of a dielectric medium (the dielectric region) behave in a different way and its electrical properties are greatly affected by the isolated metal particles and the insulating medium as well. In the dielectric region, the resistivity decreases with temperature; and the resistivity is strongly field dependent at high electric fields and low temperatures. In the transitional region, between metallic and dielectric regions, the resistivity rises sharply because of the breaking up of the metal continuum and the subsequent formation of a series of isolated metal granules, see e.g. Abeles (1976).

For electrical conduction to occur in thin film structures, electrons must be transferred from one particle to the other across the gaps, and it is this mechanism of transfer that determines the electrical properties of the film. Such films were

extensively studied, both in the normal state (e.g. by Neugebauer and Webb (1962)) and in the superconducting state (e.g. Giaever and Zeller (1968)). A recent study was conducted by Cohn et al (1990) on oxidised films of bismuth. A negative temperature coefficient of the resistance of such films was observed. This indicates that the conduction mechanism in these structures is an activated process; i.e. the addition of thermal energy to the system tends to enhance the conduction process.

As early as 1951, Gorter has pointed out the importance of the energy required to transfer an electronic charge from an initially neutral island to another. This energy is estimated to be of the order of $e^2/4\pi er$ where r is the radius of the granule. Neugebauer and Webb (1962) argued that only electrons or holes excited to states of at least this energy above the Fermi level will be able to tunnel from one neutral island to the other and referred to this energy as the 'activation energy', which is the energy required to charge a sphere of radius r by a single electronic charge.

The transfer of charge from an initially charged island to a neutral grain was assumed to be an inactivated process because it does not lead to a net increase in the energy of the system, in contrast to the case of two neutral islands. It will be shown that the transfer of electrons between the granules of such structures may be treated within a unified theory where no distinction between initially charged and initially neutral islands is needed. The activation-energy model used by Neugebauer and Webb predicted a (negative) exponential dependence of the (low temperature) low-bias conductance of the film on the reciprocal of temperature. Although this model neglected the interaction between the charged particles, the authors had pointed out the importance of the interaction energy when it becomes of the order of the thermal energy, $k_B T$, or when the size of the islands and distance between the particles are made extremely small. This model also neglected the potential differences between neighbouring islands due to the existence of an excess electron at another grain.

Hill (1969) suggested a model that accounts for the interaction energy between the grains. Hill assumed that the metallic granules are identical and all of spherical shape with equal distances apart. The interaction energy is then calculated from the knowledge of the capacitive coupling between the neighbouring grains. The interaction energy between the spheres was calculated as an approximate function of the geometry of the structure.

Full electrostatic considerations of the two-sphere model (Hill's model) were taken into account by Abeles et al (1975) who obtained an exact expression for the capacitance between two neighbouring spheres. Roy (1993), in modelling single-electronic devices, has obtained similar expressions for the capacitance between two identical spheres. The structures studied by Roy consist of metallic dots (40nm diameter and 12nm apart) deposited on p-silicon substrate, Barker (1993).

All previous models neglected the solitary nature of the excess charges located at other grains. Electrons situated at any point in the coupled structure will polarise the whole structure, and the dynamics of charge transfer between two neighbouring grains will be affected by the distribution of charges on the whole array. Furthermore, the event- when accomplished- will induce potentials along the structure and will subsequently affect other events (what is normally called 'space correlation').

In 1968, Zeller and Giaever experimentally studied the transport properties of an Al-Al₂O₃-Al structure containing Sn particles in the oxide layer, figure (1.1). They observed that the structure exhibits a small conductance at low voltages while the conductance saturates to a constant value at voltages greater than some threshold voltage level. This threshold voltage was found to strongly depend on the size of the Sn inclusions. Together with these very important observations, Zeller and Giaever explained the zero-bias anomalies in terms of the Coulomb interaction and derived the correct condition for the onset of conduction through

these structures in the absence of thermal fluctuations (conditions will be discussed in the thesis).

Zeller and Giaever (1968) stated that the condition, at low temperatures, for the flow of current through the single tunnel junction is simply : $|V| > e/2C$. The voltage gap appearing in the I-V characteristics of the single junction has since been known as the Coulomb gap. Another important feature of Zeller and Giaever's observations is the clear negative temperature coefficient of differential resistance ($R(V=0) \propto 1/T$).

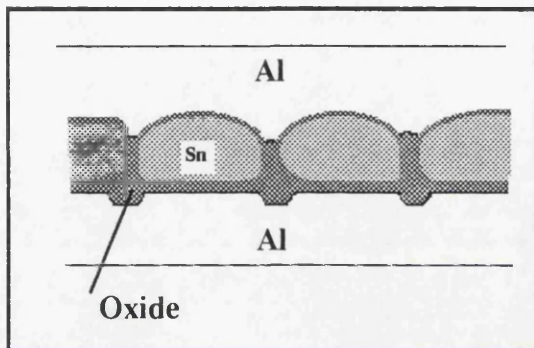


Figure (1.1): Structure studied by Zeller and Giaever.

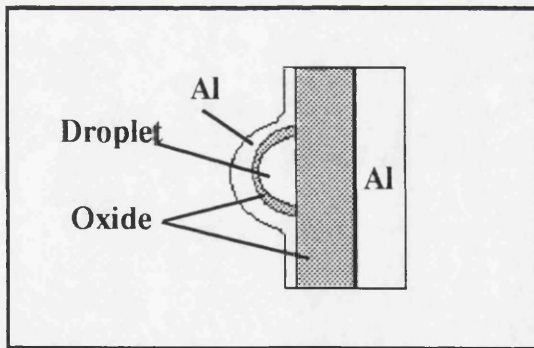


Figure (1.2): Lambe and Jaklevic's Structure.

Lambe and Jaklevic (1969) studied a structure of a metal electrode and a metallic droplet, figure (1.2). This structure has an equivalent circuit of a tunnel junction connected in series with a non-tunnel junction. They showed that the average number of electrons present on the droplet increases with the applied

voltage. A model of a variable capacitor was introduced to account for the behaviour.

The structures of metallic grains imbedded in the oxide layer were later theoretically studied by Shekhter (1973) who showed that $R(V=0) \propto 1/T$ in agreement with Zeller and Giaever's observations. Shekhter also predicted oscillations in the I-V characteristics of structures having a single grain in the oxide layer (a double-barrier system) due to single electrons being permanently trapped in the central island. It was later shown that the line current does increase with the terminal voltage but there are oscillations in the differential conductance of the double-barrier system that are attributed to more and more electrons contributing to the conduction process.

Kulik and Shekhter (1975) used the Gibbs distribution function to determine the occupation numbers of the central island in a double-barrier structure and then to calculate the I-V curves of the structure. They also used the concept of a varying capacitance to account for the non-linear relationship between the voltage and the average charge monitored at the central island. It was shown that the conductance of the double-junction structure oscillates in a uniform manner with the excess charge at the central electrode. The period of oscillations corresponds to the addition of an exact single electronic charge to the central electrode. The conclusions regarding the periodic increase of the average charge at the central island had later inspired many to think of a single-electron transistor in which the line current may be controlled by some 'gate' voltage that modifies the potential of the central grain. The single-electron transistor is also suggested to function as a memory element in the new class of single-electronic systems. Conditions of operation and problems associated with the this device will be discussed in chapter (3).

The Coulomb-blockade and single-electron tunnelling phenomena have attracted a lot of attention, both theoretically and experimentally, in the last few years as it became possible to fabricate junctions with capacitance of the order of,

or less than, 10^{-15}F (critical temperatures greater than $\sim 1\text{K}$). Very few experimental data have appeared for single tunnel junction circuits. The difficulties with such circuits arise from the detrimental effects introduced by the stray capacitance of the connecting leads. The stray capacitance, C_s , is usually comparable in value to the junction capacitance itself, and the charging energy, $e^2/2(C+C_s)$ is therefore drastically reduced. The large stray capacitance will present an impedance of the order of $10^2\text{-}10^3 \Omega$ at high frequencies. This high capacitance together with a low series external resistance tend to smear out the Coulomb gap. The equivalent line impedance, Z , allows the junction to discharge its energy in a finite time $\approx CZ(\omega)$. If the energy uncertainty associated with this time is comparable to the charging energy, $e^2/2C$, the blockade will be weakened, Girvin et al (1990). This implies that the condition to observe the Coulomb gap is: $Z(\omega) \gg R_Q$, where R_Q is the universal quantum resistance. Under this condition, the time between successive tunnel events is long and coherence effects are neglected. The charge will be a well-defined variable.

Experiments on single Al junctions of area $0.01(\mu\text{m})^2$ and capacitance of few fF's were conducted by Geerligs et al (1989). The Coulomb gap was observed with junctions having high tunnel resistance. Cleland et al (1990) fabricated single junctions with metallic electrodes having area of the order of $0.02\text{-}0.04(\mu\text{m})^2$ and capacitance $1\text{-}10\text{fF}$. These structures have revealed a Coulomb gap at $T=20\text{mK}$. The thermal and quantum fluctuations do wash out the Coulomb gap; but the existence of a voltage offset in the I-V curves at higher voltages is a clear indication of the Coulomb-blockade effects $\{I \propto (V - e/2C), V \gg e/2C\}$.

Concrete confirmation of the theory of Coulomb blockade and single-electron tunnelling has been reported on double-junction structures, e.g. Fulton and Dolan (1987), Kuzmin and Likharev (1987), Thomas et al (1989), Meirav et al (1990), etc., {some of these structures will be discussed in chapter (3)}. The Coulomb staircase has been observed using the Scanning Tunnelling Microscope,

e.g. van Bentum et al (1988) and Wilkins et al (1989). Experiments on one-dimensional arrays of tunnel junctions have also confirmed the oscillatory nature of the line conductance with gate voltage, see Kuzmin et al (1989) and Geerligs et al (1989).

1.3 The Semiclassical Model:

In the following part of the introduction, the single normal tunnel junction will be described. The understanding of the physics underlying the operation of the single junction is crucial to all parts of the thesis. Consider a tunnel junction with normal metallic electrodes. The properties of the junction can be investigated by examining the factors affecting the tunnelling process.

In the absence of an applied bias voltage, the potential energy diagram corresponding to the metal-insulator-metal (MIM) junction is shown in figure (1.3). The shaded areas represent the eigenstates that are fully occupied at zero temperature. During the tunnelling process the electron will be found in the area between the plates; it will polarise the two electrodes and produce two image charges on them. These image charges will in turn polarise the facing electrodes and, consequently, an infinite number of image charges is formed. Each image charge contributes to the total potential sensed by the tunnelling electron. The total image potential, $U(x)$, is a function of position and is given by:

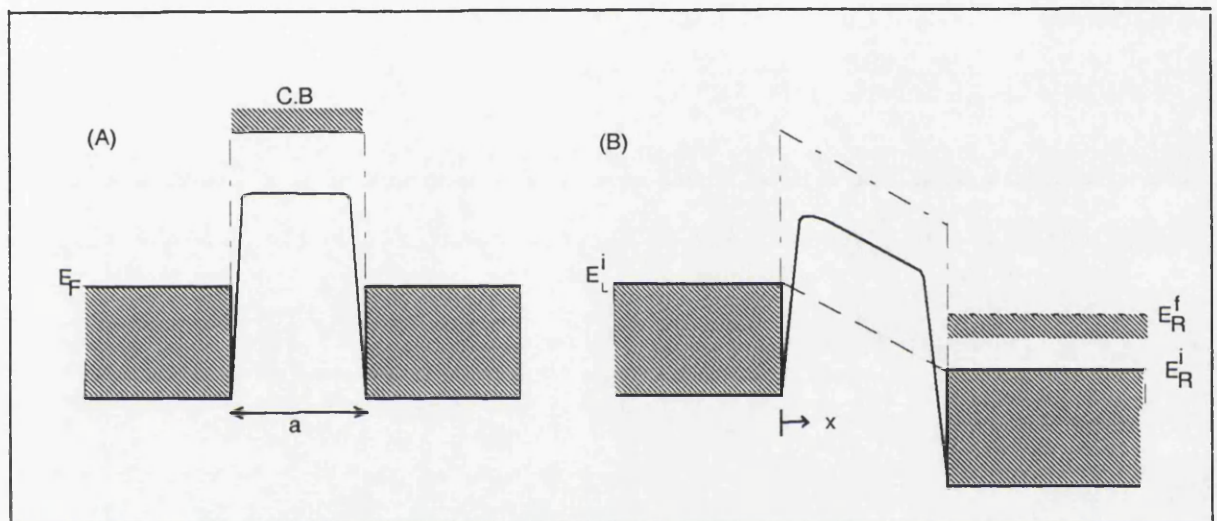
$$U_i(x) = -\frac{e^2}{8\pi\varepsilon} \left[\frac{1}{2x} + \sum_{n=1}^{\infty} \left(\frac{na}{(nx)^2 - x^2} - \frac{1}{na} \right) \right] \quad (1.1)$$

In the absence of any image forces, the potential profile in the region between the plates is determined by the band structure of the insulating material and the applied voltage. The additional potential due to the image forces reduces the barrier between the electrodes, rounds off the sharp edges at the interfaces and reduces the width of the barrier. Equation (1.1) implies that the potential energy of the electron at the MI interfaces is $=-\infty$. This can be circumvented by assuming that the image potential expressed by equation (1.1) holds only in the range

$x_0 \leq x \leq a - x_0$ where x_0 is some critical value, Simmons (1964). The barrier potential shown in figure (1.3.A) can be expressed by:

$$U_0(x) = E_F + \phi + U_i(x) \quad (1.2)$$

where E_F is the Fermi energy of the electrodes and ϕ is the work function. The diagram of figure (1.3) represents a symmetrical MIM junction where the metallic electrodes have the same Fermi energy and hence the bottoms of the conduction bands lie at the same level. Asymmetrical junction, with electrodes made from different metals, can be described in a similar way taking the different Fermi energies into account, Duke (1969).



Figure(1.3): Potential Profile

If a voltage is applied across the symmetrical MIM junction, the Fermi levels of the two electrodes will be separated by a value eV, figure (1.3.B). The Fermi levels in the bulk metals of each electrode remain flat as the voltage drop across the metallic electrode is assumed negligibly small. In the case of a large capacitance junction with a charge on the electrodes just before the tunnelling event that is much larger than the electronic charge, $|q| \gg e$, the charges on the electrodes before, during and after the tunnel event can be assumed constant. The

electric field strength due to the charges on the electrodes will not be affected by the changes of $\pm e$; thus the barrier potential may be expressed as:

$$U'(x) = E_F + \phi + U_i(x) - eV \frac{x}{a} \quad (1.3)$$

where a is the distance between the electrodes.

Now, consider the case of small tunnel junctions in which the initial charge on the electrodes is of the same order as the electronic charge. The changes of $\pm e$ can no longer be ignored in this case. Let the charges on the electrodes before the tunnelling event be $+q$ and $-q$. During the tunnelling event the charge on the initially negatively charged electrode will be $-(q-e)$ while the charge on the other electrode is maintained at $+q$, see figure (1.4). If the plates are considered to have large surface areas (A), then the electric field acting on the electron during the course of the tunnelling event is:

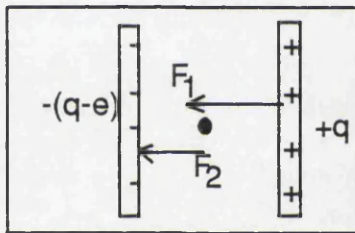


Figure (1.4)

$$F = \frac{1}{2\varepsilon A} (q - e) + \frac{1}{2\varepsilon A} q = \frac{1}{\varepsilon A} \left(q - \frac{e}{2} \right) = \frac{1}{a} \left(V - \frac{e}{2C} \right) \quad (1.4)$$

Investigating this electric field strength, one will realise the importance of this force. The term tells the fact that when the initial charge on the junction is less than $e/2$ the force acting on the electron during the course of the tunnelling event will be in a direction opposite to the direction of motion of the tunnelling electron. In other words, when $q < e/2$ the Coulomb force will suppress any electron trying to tunnel through the barrier and this is the origin of the so called 'Coulomb blockade of tunnelling'. On the other hand, the Coulomb force will act on the electron in the same direction of motion when the initial charge is greater than $e/2$.

Knowing the electric field strength and the image force potential, the full barrier potential profile can be expressed as:

$$U(x) = E_F + \phi + U_i(x) - e(V - \frac{e}{2C})\frac{x}{a} \quad (1.5)$$

The classical picture of the image potential described above was used in modelling transport in thin metallic films, e.g. Simmons (1964), Simmons et al (1964), Williams et al (1972) and Uozomi et al (1977). Photon-assisted tunnelling measurements have shown that the classical image force theory is not adequate in describing the interaction between the tunnelling electrons and the metals from which they emerge, e.g. Weinberg and Hartstein (1976), Hartstein et al (1977 & 1982) and Dietz (1980). Weinberg and Hartstein suggested a quantum mechanical model to calculate the transmission probability through the metal-insulator interface. This model assumes that the wave-function of the plasma in the metal is the image of the part of the wave-function of the incident electron that lies in the insulator region.

The barrier potential described above ignores the penetration of the electric field into the metal electrodes and assumes that the whole voltage drop is maintained in the insulator region. The charge on the electrodes is then a surface charge accumulated on the metal-insulator interface. However, even in the presence of a surface charge, the field does not vanish abruptly at the M-I interface but drops rapidly to zero in the metal, Duke (1969).

The description of the Coulomb blockade phenomenon given so far is pivoted on the classical picture of the electric field during the course of the tunnel event. Simple considerations of the state of the junction prior to and after the event would lead to the same conclusions. Let the initial charge on the junction be equal to q . The electrostatic energy stored in the junction is then given as $E_i = q^2/2C$. If it is assumed that the tunnel event can occur only in the forward direction, i.e. an electron may tunnel from the electrode with the negative charge to the other, the charge on the junction after the event will drop to the value $(q-e)$

and the electrostatic energy becomes $E_f = (q-e)^2/2C$. The change in the energy is then:

$$\Delta = E_i - E_f = \frac{e}{C} (q - \frac{e}{2}) \quad (1.6)$$

The event will be allowed if the final energy is less than the initial energy, i.e. $q > e/2$. This argument is valid provided that the thermal and quantum fluctuations are negligibly small. At finite temperatures the thermal and/or quantum fluctuations may provide the energy required to make a tunnel event possible even if $q < e/2$. Thermal effects can be dramatically reduced by carefully choosing the operating temperature; and the condition:

$$k_B T \ll E_c = \frac{e^2}{2C}$$

will reduce the possibility of occurrence of any thermally activated events. The thermal and quantum fluctuations and their effects on the performance of the single junction will be discussed in chapter (6).

It should be mentioned that the charge redistribution time is assumed to be negligibly small. Once the electron lands on the other electrode, the charge on the junction can be represented by $q-e$. The tunnelling process across the single junction in this case is not affected by the external circuit and the junction is assumed to be completely isolated from the environment. The external circuit will be sensed during the subsequent recharging process, that follows the tunnel event.

Finally, let the leads connecting the junction to the source have zero impedance, $Z=0$. Let the initial charge on the junction be equal to q where q is essentially the steady state charge delivered to the junction from the voltage source. Let a tunnel event occur at some time from an electrode to the other. The charge on the junction following the event will instantaneously relax to its previous value, i.e. it takes the system zero time to recharge the junction from the level $q-e$ to the level q . Thus, the change in the energy is simply:

$$\Delta=0, \forall q$$

and it is concluded that: if the single junction is voltage-biased ($Z=0$), the tunnelling process may take place at any bias level and it is no longer possible to observe the Coulomb gap.

The former case, $Z=\infty$, corresponds to the current-biased junction where the Coulomb gap will be observed. Effects of finite external impedance will be addressed in chapter (6).

Chapter (2)

Models of the Single Junction

2.1 Introduction:

The potential profile in a single-junction circuit was discussed in the previous chapter. In this chapter the tunnelling rate across the junction will be studied using the quantum golden rule. A numerical solution is implemented for the Master Equation that governs the evolution of the charge with time. It includes the fluctuations introduced by the thermal noise and by the stochastic nature of tunnelling. Another approach suggested to study the coherence of single-electron tunnelling events uses the distribution function of the time between successive tunnel events.

2.2 Tunnelling Rate:

Tunnelling through the barrier is a pure quantum mechanical process. If an electron with energy $E < V_{\max}$ falls on the barrier from either side then there is a finite non-zero probability that this electron will penetrate the barrier and eventually be found at the other side of the barrier. The particle will spend some time beneath the barrier, a time that is referred to as the 'traversal time for tunnelling'. The traversal time for tunnelling is normally much smaller than other characteristic times in the systems under study, e.g. the time between tunnel events, and can be ignored. The transmission probability may be determined from the solution of the one dimensional Schrödinger equation in the regions to the left, right and under the barrier. Clearly, the transmission factor is a function of the form of the potential profile and the energy of the incident electron and can be written as $D(E, V)$. An approximate expression for $D(E, V)$ can be evaluated using the WKB approximation method. No expression for the transmission factor will be pursued in the thesis and a constant value, independent of the energy, will be used and then absorbed into a phenomenological parameter (the tunnel resistance) which can be determined from experiments.

For the MIM junction, with the potential profile shown in figure (1.3), the total transmission probability can be obtained by adding the contributions of all conduction electrons in the metals, taking into account the occupancies of the energy levels involved.

Let E_L^i and E_R^i be the Fermi energy levels of the left and right electrodes just before the tunnel event. The levels are separated by an amount eV, (see figure (1.3))

$$E_R^i = E_L^i - eV \quad (2.2.1)$$

If a tunnel event takes place from the left to the right electrode, the Fermi levels then modify to E_L^f and E_R^f . The additional electron on the right electrode will shift -up- all the electronic energy levels there by an amount equal to the electron charging energy, $E_C = e^2/2C$. Thus,

$$E_R^f = E_R^i + e^2/2C = E_L^i - eV + e^2/2C = E_L^i - \Delta \quad (2.2.2)$$

where Δ is the change in the free energy, $\Delta = eV - e^2/2C$, defined in equation (1.6).

The levels of the left electrode are reduced by the same amount, $e^2/2C$, i.e.

$$E_L^f = E_L^i - e^2/2C \quad (2.2.3)$$

It is to be noticed that if the initial potential difference between the electrodes is less than the threshold value, $V < e/2C$, and an electron with energy $E < E_L^i$ at $T=0$ K is to tunnel to the right electrode, it will arrive at a level below the Fermi level, E_R^f . This implies that the tunnelling process is suppressed at low temperatures if the voltage is less than the threshold value, $e/2C$.

The wave-vectors of the electrons incident on the barrier from the left can be decomposed into transverse and longitudinal components. The total transition probability is calculated by adding the contributions of all possible vectors, taking into account their distribution, and can be written as:

$$\Gamma = \int dE_x \int dE_\perp f_L(E) (1 - f_R^f(E)) D(E, V) \rho_L(E) \rho_R(E) v_L v_R \quad (2.2.4)$$

where:

E_x = the longitudinal component of the energy of the incident electron,

E_\perp = the transverse component of the energy, and the total energy is therefore $E=E_x+E_\perp$.

f_L = Fermi distribution function at the left electrode before the tunnel event. This function is characterised by the Fermi level E_L^i ,

f_R^f = Fermi function characterised by E_R^f ,

ρ_L , ρ_R are the densities of energy states on the left end right electrodes respectively,

v_L , v_R are the volumes of the left and right metallic electrodes and $D(E,V)$ is the elastic transmission probability.

Equation (2.2.4) ensures the conservation of momentum and energy of the tunnelling electron. In general, the elastic transmission probability depends only on the longitudinal component of the wave-vector of the incident electron, thus the tunnel rate can be written as:

$$\Gamma = \int dE_x D(E_x, V) N(E_x) \quad (2.2.5)$$

where the function $N(E_x)$ is termed the supply function and is given by:

$$N(E_x) = v_L v_R \int dE_\perp f_L(E) \{1 - f_R^f(E)\} \rho_L(E) \rho_R(E) \quad (2.2.6)$$

The supply function can be simplified if it is assumed that the transverse component of the energy is much smaller than the longitudinal part, $E_\perp \ll E_x$, Duke (1977), Mullen et al (1988) and Ueda (1990). Thus:

$$N(E_x) = v_L v_R \rho_{Lx}(E_x) \rho_{Rx}(E_x) f_L(E_x) \{1 - f_R^f(E_x)\} \quad (2.2.7)$$

This assumes that the density of states on the electrodes is:

$$\rho(E) = \rho_x(E_x) \delta(E_\perp) \quad (2.2.8)$$

The total tunnel rate can now be evaluated if the transmission factor $D(E_x, V)$ is known. To simplify the analysis further, this factor may be considered as a constant that is equal to the value of the transmission factor at the Fermi

surface. This assumption is valid if the change in the free energy of the tunnelling electron, Δ , is much smaller than the Fermi energy. At low temperatures, all levels below the Fermi energy will be full, while those above will be empty. Therefore, for an electron to have a chance to tunnel through the barrier, it must have an energy E such that $E_L^f \leq E \leq E_R^i$. Thus, the density of states in the integral can be approximated by a constant value corresponding to that at the Fermi level.

Substituting equation (2.2.7) in (2.2.5), the tunnel rate is found to be:

$$\Gamma_x = \frac{1}{e^2 R_{tx}} \frac{\Delta}{1 - e^{-\beta\Delta}} \quad (2.2.9)$$

where $\beta = (k_B T)^{-1}$ and R_{tx} is the tunnel resistance given by:

$$R_{tx} = \left\{ e^2 \nu_L \nu_R \rho_{Lx}(E_F) \rho_{Rx}(E_F) D(E_F, V) \right\}^{-1} \quad (2.2.10)$$

Let the incident electron have a transverse component together with the longitudinal component. Again, the condition $\Delta \ll E_F$ is imposed to allow the densities of states and the transmission constant to be approximated by their values at the Fermi surface. The supply function turns out to be:

$$N(E_x, V) = \frac{\rho_L \rho_R \nu_L \nu_R}{\beta} \frac{1}{1 - e^{-\Delta\beta}} \left\{ \Delta\beta - \ln \left[\frac{1 + e^{\beta(E_x - E_F + \Delta)}}{1 + e^{\beta(E_x - E_F)}} \right] \right\} \quad (2.2.11)$$

The tunnel rate, at low temperatures, can be evaluated using equation (2.2.5) and is found to have the following form:

$$\Gamma = \rho_L \rho_R \nu_L \nu_R D(E_F, V) E_F \frac{\Delta(1 - \Delta/2E_F)}{1 - e^{-\Delta\beta}} \quad (2.2.12)$$

The dependence on the change of the free energy of the first term of this equation is similar to relation (2.2.9). The second term is a small negative correction term due to the distribution of the total energy of the incident electrons in the transverse as well as longitudinal directions. For a metallic tunnel junction, the Fermi energy is of the order of few electron volts. If the capacitance of the junction is as small as $10^{-18} F$, the charging energy will be of the order of 80 meV.

Therefore, for a practical metallic tunnel junction the tunnel rate can be approximated by

$$\Gamma \approx \rho_L \rho_R v_L v_R D(E_F, V) E_F \frac{\Delta}{1 - e^{-\Delta \beta}} \quad (2.2.13)$$

and the tunnel resistance will then be given as

$$R_t = (e^2 \rho_L \rho_R v_L v_R D(E_F, V) E_F)^{-1} \quad (2.2.14)$$

Equation (2.2.14) agrees qualitatively with the results obtained by Fulton and Dolan (1987). Their data indicates that the tunnel resistance is lower for junctions with higher electrode area.(volume).

2.3 Master-Equation Formalism:

The Hamiltonian of a current-biased tunnel junction, figure (2.1), is:

$$H = Q^2 / 2C + H_1 + H_2 + H_T + H_s \quad (2.3.1)$$

where

$Q^2/2C$ is the junction charging energy,

H_1, H_2 and H_s describe the internal degrees of freedom of the junction electrodes and the shunt path respectively and

H_T represents the single-electron tunnelling.

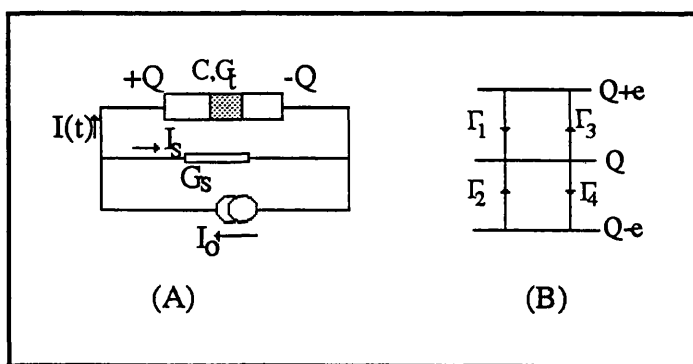


**Figure (2.1): A: Current-biased Tunnel Junction.
B: Possible tunnel events and their rates.**

If the tunnel and external shunt conductances are much smaller than the universal quantum conductance,

$$G_t, G_s \ll 1/R_Q , \quad (R_Q \approx 6.5 \text{k}\Omega) \quad (2.3.2)$$

the charge on the junction can be considered as a well-defined classical variable; and in this case, the flow of current from the source into the junction is a continuous process, Averin and Likharev (1986 & 1990). The Hamiltonian,

$$H_o = Q^2/2C + H_1 + H_2 + H_s \quad (2.3.3)$$

can be considered as a basic Hamiltonian and the remaining term can be treated as a weak perturbation. Averin and Likharev (1986) have shown that the equation of motion of the density matrix of the system in Q-space reduces to the following simple Master Equation:

$$\frac{\partial s}{\partial t} = -I_o(t) \frac{\partial s}{\partial Q} + F_T + F_s \quad (2.3.4)$$

where $s(Q,t)$ is the classical charge density function, F_s is a contribution from the shunt path and is given by the following expression:

$$F_s = \frac{G_s}{C} \frac{\partial}{\partial Q} \left(Ck_B T \frac{\partial s}{\partial Q} + Qs \right) \quad (2.3.5)$$

The tunnelling term, F_T , in equation (2.3.4) depends on the distribution function as well as the tunnelling rates and is expressed as:

$$F_T = \Gamma_1 s(Q+e) + \Gamma_2 s(Q-e) - (\Gamma_3 + \Gamma_4) s(Q) \quad (2.3.6)$$

where $\Gamma_1, \dots, \Gamma_4$ are the tunnel rates defined according to figure (2.1.B). The first two terms of F_T give the rate of increase of the density function due to the possible tunnel events from $Q+e$ and $Q-e$ levels to the Q level, at rates given by Γ_1 and Γ_2 respectively, giving rise to a change of $\pm e$ in the initial charge on the junction. The last term is the decay rate of $s(Q,t)$ due to tunnel events at charge Q into the levels $Q \pm e$, at a total rate of $\Gamma_3 + \Gamma_4$. The tunnelling rates are evaluated according to equation (2.2.9) or (2.2.12).

Equation (2.3.4), with the tunnelling term set equal to zero, is similar to the Fokker-Planck equation which was first used to represent the Brownian motion of small particles. It is also used to study the noise in lasers.

Equation (2.3.4) is an important and interesting relation as it incorporates the charge fluctuations and the variation of these fluctuations with time. It also includes the effect of the tunnelling events on the fluctuations. It serves as a basis for determining the ensemble time-average behaviour of the junction and the steady-state I-V characteristics. Both the Coulomb blockade of tunnelling and single-electron tunnelling oscillations are described by this Master Equation.

Ben-Jacob et al (1988), Geigenmuller and Schön (1988), and Muller et al (1988) investigated the fluctuation of the charge on the junction by looking at the possible events that can modify the state of the junction, viz. the charge delivered to the junction from the source and the tunnel events. It was shown that the charge distribution function satisfies the relation:

$$\frac{\partial s}{\partial t} = -I_o \frac{\partial s}{\partial Q} + F_T \quad (2.3.7)$$

where F_T is identical to the tunnelling term defined before. Clearly, the two expressions (2.3.4) and (2.3.7) will be equivalent if F_s is negligibly small, i.e. if R_s is sufficiently large. Equation (2.3.7) contains no diffusion term and tells nothing about the thermal and quantum fluctuations of the charge; the only fluctuations involved in (2.3.7) are those introduced by the tunnelling process.

2.4 Solution of the Master Equation:

In this section the Master Equation is solved both in the Coulomb-blockade and in the single-electron tunnelling regimes. The charge fluctuations and the dependence on time are also investigated. It is important to note that the equation at hand does not include the fluctuations introduced by the charge-macroscopic quantum tunnelling process, which will be addressed in chapter (6).

2.4.1 Coulomb-Blockade Regime:

The Fokker-Planck like Master Equation described above is a key relation in describing the behaviour of the single junction. It is possible to derive exact expressions for the total averaged charge and the charge fluctuations as a function of time if the junction is operated in the Coulomb-blockade region, i.e. if $I_o < e/2\tau_s$, where $\tau_s = R_s C$. Let the charge on the junction be gaussian distributed with mean \bar{Q}_o and variance σ_o^2 . It is assumed that as the charge is delivered to the junction, the charge distribution will stay gaussian but the mean value and the fluctuations of the charge will evolve with time and are denoted by $\bar{Q}(t)$ and $\sigma^2(t)$. The charge distribution function at any time may be written as:

$$s(Q, t) = \frac{1}{\sqrt{2\pi\sigma^2(t)}} \exp - \frac{(Q - \bar{Q}(t))^2}{2\sigma^2(t)} \quad (2.4.1)$$

At low temperatures and low driving current conditions imposed above, the tails of the gaussian charge packet outside the range (-e/2, e/2) will be small and may be neglected. The tunnelling terms in equation (2.3.4) can be set equal to zero. In the Coulomb-blockade region the Master Equation can then be written as:

$$\frac{\partial s}{\partial t} = \frac{\partial}{\partial Q} \left\{ \left(\frac{Q}{\tau_s} - I_o \right) s + \frac{Ck_B T}{\tau_s} \frac{\partial s}{\partial Q} \right\} \quad (2.4.2)$$

This is the continuity equation for the density function in the Coulomb-blockade region. At $t=\infty$ both $I(t)$, the current through the junction, and $\frac{\partial s}{\partial t}$ are equal to zero. Equation (2.4.2) gives

$$(Q - \tau_s I_o) s + Ck_B T \frac{\partial s}{\partial Q} = 0 \quad (2.4.3)$$

The steady-state fluctuations of the charge σ_{ss}^2 , the average total charge and hence the distribution function may be obtained by direct substitution of (2.4.1) in (2.4.3), giving:

$$\bar{Q}_{ss} = \tau_s I_o \quad (2.4.4)$$

$$\sigma_{ss}^2 = C k_B T \quad (2.4.5)$$

Clearly, the steady-state average charge is the total charge delivered to the junction from the source. The quantity σ_{ss}^2 is the charge fluctuation around the mean value. It is identical to the expression used by Averin and Likharev (1985,1990). It will be shown in chapter (6) that the fluctuations used here correspond to the fluctuations induced in a single junction that is coupled to an external source via a line of infinitely large impedance (a condition explicitly imposed when deriving the Master Equation).

It is also possible to study the time dependence of the fluctuations. The charge packet is assumed to be gaussian at any time. Direct substitution of this gaussian charge packet, equation (2.4.1), into the Master Equation for the Coulomb-blockade case, and subsequent equating of the coefficients of equal powers of Q on both sides of the resulting relation gives,

$$\frac{d\bar{Q}}{dt} = I(t) \quad (2.4.6)$$

$$\sigma^2(t) = k_B T C - (k_B T C - \sigma_0^2) e^{-2t/\tau_s} \quad (2.4.7)$$

Relation (2.4.7) shows that the width of the charge packet changes due to the diffusion process. The significance of (2.4.7) may be shown as follows: let the junction be initially held at temperature T_1 , the uncertainty in Q will then be $k_B T_1 C$. If, at $t=0$, the temperature is changed to T , the uncertainty in the charge level will evolve with time according to equation (2.4.7) and the steady-state spread will be $k_B T C$. Connection or removal of a capacitor in series or in parallel with the tunnel junction gives rise to similar evolution of the fluctuations. Following a tunnel event or a charge measurement the fluctuations will grow with $\sigma_0^2 = 0$.

The drift process of the charge packet is summarised in relation (2.4.6). It defines the charging curve of a conventional capacitor fed by a voltage or current

source, stressing the fact that the charge is continuously delivered to the junction.

The solution of (2.4.6) is:

$$\bar{Q}(t) = \left(Q_o - I_o R_s C \right) e^{-\frac{t}{R_s C}} + I_o R_s C \quad (2.4.8)$$

Looking back at equation (2.3.7) suggested by Ben-Jacob et al (1988) and using the same gaussian charge packet in a Coulomb-blockade regime, i.e. $\frac{\partial s}{\partial t} = -I_o \frac{\partial s}{\partial Q}$, it is easy to show that the fluctuations are not described by this equation; the solution of which is given by:

$$s(Q,t) = \delta(Q - \bar{Q}(t))$$

2.4.2 Single-Electron Tunnelling:

SET events can take place, at $k_B T \ll e^2/2C$, when the total average charge exceeds $e/2$, i.e. $I_o > e/2\tau_s$. The energy change associated with the tunnelling of a single electron blocks other electrons from tunnelling until the junction recharges to the $e/2$ level. This will lead to coherent SET oscillations of the charge giving rise to a relaxation-type of oscillations (continuous charging followed by a sudden discharge) at a frequency predicted to be $f_{SET} = I_o/e$, Averin and Likharev (1986,1990), Mullen et al (1988) and Ben-Jacob et al (1988). In superconducting junctions, similar oscillations are expected to take place due to Coulomb blockade to tunnelling of Cooper pairs at a frequency $f_{Bloch} = I_o/2e$. Yoshihiro (1988) reported observation of these Bloch oscillations in superconducting granular tin films.

For a finite external resistance and high tunnel conductance, the period of oscillations, t_s , can be obtained from the relation:

$$\frac{e}{2} = \left(-\frac{e}{2} - I_o R_s C \right) \exp -\frac{t_s}{R_s C} + I_o R_s C \quad (2.4.9)$$

the solution of which gives the frequency of SET oscillations($=1/t_s$) as:

$$\dot{f}_{SET} = \left\{ R_s C \ln \left(\frac{I_o R_s C + e/2}{I_o R_s C - e/2} \right) \right\}^{-1} \quad (2.4.10)$$

Clearly, if $I_o R_s C \gg e/2$ then the frequency of SET oscillations reduces to

$\dot{f}_{SET} \approx \frac{I_o}{e} = f_{SET}$. These results do not take into account the possible thermally activated tunnelling events which will reduce the Coulomb-blockade life-time. Also the fluctuations introduced by the finite, non-zero, tunnel resistance are totally ignored.

Better insight can be achieved by solving the Master Equation for the SET case because the thermal noise and the stochastic nature of tunnelling are represented in that equation. Unfortunately, the full equation is quite complicated and an analytical solution seems very difficult. Numerical solution of the problem is sufficient to study the general features of SET oscillations.

The numerical solution given by Averin and Likharev (1986) looks at the distribution of the number of excess charges, $\{P_k(t)\}$, found on the junction. These probabilities are related by the following set of coupled equations:

$$\begin{aligned} \dot{P}_k &= \Gamma_1 P_{k+1} + \Gamma_2 P_{k-1} - (\Gamma_3 + \Gamma_4) P_k \\ \frac{d\bar{Q}}{dt} &= I(t) , Q_k(t) = \bar{Q}(t) + ek \end{aligned} \quad (2.4.11)$$

and the charge distribution function, $s(Q,t)$, is expressed in terms of $\{P_k(t)\}$ as,

$$s(Q,t) = \sum_k P_k(t) \cdot g(Q_k(t)) \quad (2.4.12)$$

where $g(Q,t)$ is a gaussian density function.

This method assumes a large driving current, $I_o \gg e/2\tau_s$, and an external resistance satisfying $R_s \gg R_t$. However, in the regimes of operation, $k_B T \ll e^2/2C$, the variance of the charge, $k_B T_C$, will be much smaller than e^2 . This implies that the set of excess (integer) electronic charges $\{ke\}$ will contain very few elements with appreciable probabilities, $\{P_k\}$; and it will be unrealistic to represent the charge density by a series of such few terms.

It was shown in the previous section that equation (2.3.7) does not account for the fluctuations. However, it contains the information necessary to run a dynamic Monte-Carlo simulation at T=0 K to trace the time evolution of the charge on the junction.

2.4.3 Numerical Solution:

In the previous sections, an analytical solution was obtained for the junction if operated entirely within the Coulomb-blockade region. A general description of the SET oscillations was also deduced. In both, the following conditions are supposed to be fulfilled:

- a. the temperature is low enough that the tails of the density function lying outside the Coulomb-blockade region could be ignored, i.e. no thermally activated tunnelling events are allowed to take place,
- b. the SET events could only take place when the total average charge just exceeds $e/2$,
- c. tunnel conductance is high and the fluctuations due to the finite conductance may be ignored.

All the above restrictions can be removed if a general method to solve the Master Equation in the Coulomb-blockade and SET regimes is developed. In this section a general numerical technique is outlined and implemented. It consists of defining a recursive discretised equation for the density function in the charge domain which will then be implemented in a computer model to propagate the charge packet into the time domain. If the charge domain is divided by equally spaced points indexed by the set of integers, $\{p\}$, the numerical solution would involve the calculation of the Q-density function at these points as time passes, provided that the initial distribution is known.

The equation to be solved, the Master Equation, can be rewritten in the following simple form:

$$\frac{\partial s}{\partial t} = Ls \quad (2.4.13)$$

where L is an operator defined as:

$$L = \frac{1}{R_s C} \frac{\partial}{\partial Q} \left(Q - R_s C I_o + C k_B T \frac{\partial}{\partial Q} \right) + \Gamma_1 E(e) + \Gamma_2 E(-e) - (\Gamma_3 + \Gamma_4) \quad (2.4.14)$$

and $E(Q)$ is a shift operator in Q -space defined by:

$$E(Q).s(Q,t) = s(Q+q,t) \quad (2.4.15)$$

Let s_p^n be the value of the charge density at point p at the n -th time step i.e. ($t=n.\Delta t$). Taylor series expansion can be used to evaluate the charge density function at the next time step, as:

$$s_p^{n+1} = \exp(\Delta t \cdot L) \cdot s_p^n \quad (2.4.16)$$

Cayley scheme can be used by first rewriting equation (2.4.16) in the following form:

$$s_p^{n+1} = \exp\left(\frac{\Delta t}{2} L\right) \cdot \exp\left(\frac{\Delta t}{2} L\right) \cdot s_p^n \quad (2.4.17)$$

then, by the application of the operator $\exp\left(-\frac{\Delta t}{2} L\right)$ to left of both sides:

$$\exp\left(-\frac{\Delta t}{2} L\right) \cdot s_p^{n+1} = \exp\left(\frac{\Delta t}{2} L\right) \cdot s_p^n \quad (2.4.18)$$

If Δt is chosen to be sufficiently small, then (2.4.18) can be expanded to lowest order in Δt and the following approximate form follows:

$$\left(1 - \frac{\Delta t}{2} L\right) \cdot s_p^{n+1} \approx \left(1 + \frac{\Delta t}{2} L\right) \cdot s_p^n \quad (2.4.19)$$

Crank-Nickolson representation of the differential operators in L allows the above relation to be expanded to the following final form:

$$A_1 s_{p-K}^{n+1} + B_1 s_{p-1}^{n+1} + C_1 s_p^{n+1} + D_1 s_{p+1}^{n+1} + E_1 s_{p+K}^{n+1} = \\ A_2 s_{p-K}^n + B_2 s_{p-1}^n + C_2 s_p^n + D_2 s_{p+1}^n + E_2 s_{p+K}^n \quad (2.4.20)$$

where $K=e/\Delta Q$. The coefficients $A_1, \dots, E_1, A_2, \dots, E_2$ are constants that can be determined from Δt and ΔQ and are independent of n , see Appendix (A). The right hand side of the relation (2.4.20) is a function of time and is to be calculated at each time step. The set of linear equations defined by equation (2.4.20) above can be recursively solved for the charge density function. Once the charge density function is known at any time, the average characteristics of the tunnel junction can be calculated, e.g. the junction will have a mean charge and average fluctuations given by:

$$\bar{Q}(t) = \sum_p Q(p) s_p^n \Delta Q \quad (2.4.21A)$$

$$\sigma^2(t) = \sum_p [Q(p) - \bar{Q}(t)]^2 s_p^n \Delta Q \quad (2.4.21B)$$

As $t \rightarrow \infty$, $s(Q,t)$ reaches a steady-state shape, which can be obtained from the relation:

$$\left. \frac{\partial s}{\partial t} \right|_{t \rightarrow \infty} = 0 \quad , \forall Q \quad (2.4.22)$$

leading to the steady-state I-V characteristics, viz.:

$$\bar{V} = \frac{1}{C} \sum_p Q(p) \cdot s_p \Delta Q \quad (2.4.23A)$$

$$\bar{I} = I_o - \bar{V} G_s \quad (2.4.23B)$$

The solution of the discretised set of linear equations (2.4.20) can be carried out using the standard relaxation techniques as the coefficient matrix is highly sparse. For the full CB problem, the tunnelling terms are identically zero; and, subsequently, $A_1=A_2=0$, $E_1=E_2=0$, and the coefficient matrix in (2.4.20) will be of the tridiagonal form. Thomas tridiagonal algorithm can then be used to calculate the density function.

2.4.4 Results of Numerical Simulations:

The simulation of the Master Equation using the discretised form (2.4.20) in the Coulomb-blockade case, figure (2.4 & 2.5), shows the excellent agreement between the numerical and analytical results. In these calculations the time step and the increment in Q are chosen to be $\Delta t=10^{-4}R_sC$ and $\Delta Q=2\times10^{-3}e$ respectively; thereby ensuring stability and convergence of the solution.

To study the SET oscillations, a current source with $I_o>e/2\tau_s$ was switched on at $t=0$ to drive a single junction that is maintained at a temperature T . At $T=0$ the noise on the junction is assumed to be represented by a gaussian distribution function. The results obtained from these simulations reflect the statistical average of an ensemble of tunnel junctions operated simultaneously. In other words, the results predict the most probable behaviour of a single junction; and this type of results tells nothing about a typical run of a real single tunnel junction.

The curves of figure (2.6) show traces of damped oscillations. The portion of the packet lying at $Q>e/2$ forms another part at the $Q'=Q-e$ due to the probability of tunnelling. This newly formed portion propagates towards the $Q=e/2$ end and mixes up with the part that was not reflected. This continuous mixing leads to a static charge packet and the loss of coherence of the tunnelling events. The steady-state average charge is related to the driving current by $\bar{Q}\propto\sqrt{I_{dc}}$. The average frequency of SET oscillations (at $T=0.05T_c$) obtained from these plots is slightly (~5%) higher than the value obtained from simple theory. This is attributed to the thermally activated tunnelling events that can take place while $\bar{Q} < e/2$. Fourier analysing the signals obtained from the model, see figure (2.7), it is clear that the SET oscillations are more coherent for small I_{dc} values than for larger driving currents, which is consistent with results obtained from other models, see next section.

The consequences of incoherence are very serious for the synchronised switching of charge in single-electronic circuits. The parallel arrangement of

identical electron sources driven by a single control voltage would become incoherent over a certain period of time, Barker et al (1992).

2.5 Distribution of Time between Tunnel Events:

The coherence of the SET oscillations in a single junction can be studied by looking at the distribution of the time between tunnel events. If a Poisson process has an average rate of occurrence equal to γ/sec , the probability that an event will take place in a small time interval, Δt , is given as $\gamma.\Delta t$ and the probability that it will not take place in that time interval is therefore $= 1-\gamma.\Delta t$.

At $T=0\text{K}$ and due to Coulomb blockade, tunnelling is completely suppressed if $Q < e/2$. The probability that a tunnel event would take place in a time interval of Δt after t can then be expressed as:

$$p(t) = \Gamma(Q(t)).\Delta t. \prod_i [1 - \Gamma(Q(t_i))\Delta t_i] \quad (2.5.1)$$

where $\Gamma(Q(t))$ is the tunnel rate when the junction holds a charge $Q(t)$. To simplify the problem, the tunnel rate, at $T \ll T_c$, may be written in the following simple form:

$$\Gamma(Q) = \begin{cases} \frac{G_t}{eC} (Q - e/2) & , Q > e/2 \\ 0 & , \text{otherwise} \end{cases} \quad (2.5.2)$$

Taking the logarithms of both sides of equation (2.5.1), and making use of the relation, $\ln(1-x) \approx -x$ if $x \rightarrow 0$, equation (2.5.1) can be rewritten as:

$$p(t) = \Gamma(Q(t)).\Delta t. \exp\left\{-\int \Gamma(Q(u)).du\right\} \quad (2.5.3)$$

The probability $p(t)$ will be identically zero when the total charge is less than $e/2$ as $\Gamma(Q < e/2) = 0$. The charge evolves classically inside the Coulomb-blockade region while the stochasticity is added once the charge becomes greater than $e/2$. It is then useful to study the distribution of the time spent above the Coulomb barrier before an electron manages to escape through the barrier. If this

distribution is known, then all the average properties of the junction can be deduced.

Let τ be the time spent above the barrier before a tunnel event occurs. The probability that a tunnel event takes place in time $\Delta\tau$ around τ is similarly given by:

$$I(t) = \Gamma(q(\tau)) \cdot \Delta\tau \cdot \exp\left\{-\int_0^\tau \Gamma(q(u)) \cdot du\right\} \quad (2.5.4)$$

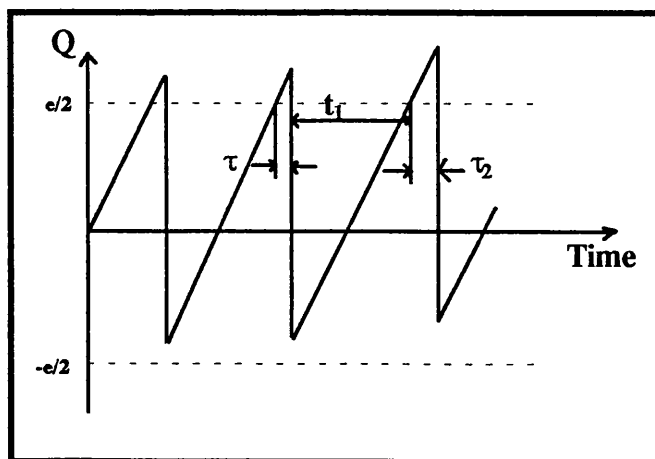
where the charge $q(\tau)$ is obtained from the charging curve and is expressed by:

$$q(\tau) = \left(\frac{e}{2} - I_o R_s C\right) e^{-\frac{\tau}{R_s C}} + I_o R_s C \quad (2.5.5)$$

Substituting (2.5.5) in (2.5.4), the distribution function of the time spent above the Coulomb barrier, $f(\tau)$, is found to be:

$$f(\tau) = \lambda \left(1 - \exp\left(-\frac{\tau}{R_s C}\right)\right) \cdot \exp\left\{-\lambda \left(\tau - R_s C \left(1 - \exp\left(-\frac{\tau}{R_s C}\right)\right)\right)\right\} \quad (2.5.6)$$

where $\lambda = (CV - e/2)/R_t e C$. Figure (2.8) shows the function $f(\tau)$ at fixed bias conditions and different R_s/R_t ratios. Low external circuit conductance will result in more time spent above the CB barrier before an electron manages to tunnel through the barrier.



Figure(2.2): Evolution of the charge with time.

Tunnelling is most likely to occur after a time τ^* above the barrier, where this time, τ^* , is obtained from $\frac{\partial f}{\partial \tau} = 0$ as:

$$\tau^* = 2R_s C \sinh^{-1} \left(\frac{1}{\sqrt{4R_s C \lambda}} \right) \quad (2.5.7)$$

The distribution function of τ has little significance on its own, but it is useful in determining the static properties of the junction and in the study of the SET oscillations.

Following a tunnel event the charge on the junction drops to $q(\tau) - e$, see figure (2.2). Let the time it takes the source to recharge the junction to $e/2$ be $t_1(\tau)$ (the dwell time). It is easy to find $t_1(\tau)$ as:

$$t_1(\tau) = R_s C \ln \left[\frac{CV + e - q(\tau)}{CV - e/2} \right] \quad (2.5.8)$$

Let the next tunnel event take place during a time interval of $\Delta\tau_2$ around τ_2 above the $e/2$ level. The time between tunnel events, t , is related to τ and τ_2 by:

$$t = t_1(\tau) + \tau_2 \quad (2.5.9)$$

The stochastic nature of tunnel events indicates that the time spent above the $e/2$ level in successive (or any) events is an independent random variable. The probability that the system stays for a time τ followed by a time τ_2 above the barrier (and the time between these events is equal to t) is given by:

$$r(t)|_{\tau, \tau_2} = f(\tau) \cdot \Delta\tau \cdot f(\tau_2) \cdot \Delta\tau_2 \quad (2.5.10)$$

The marginal distribution function of the time between tunnel events, $g(t)$, is evaluated by adding the contributions of all possible successive events characterised by τ and τ_2 and are satisfying (2.5.9). Thus the distribution of t is:

$$g(t) = \int_{\tau} f(\tau) \cdot f(t - t_1(\tau)) \cdot d\tau \quad (2.5.11)$$

The limits of integration in (2.5.11) are dependent on the applied voltage and t as well. If $V < 1.5e/C$ then any tunnel event will leave the junction at a state with $-e/2 < Q < e/2$, i.e., within the Coulomb-blockade region. On the other hand, if $V > 1.5e/C$ then any tunnel event occurring with $Q > 1.5e$ will result in a state with $Q > e/2$ and an immediate tunnel event is possible. However, these possible events, (with $t=0$) are still independent and do not violate the previous analysis. To generalise the analysis, it is possible to redefine $f(\tau)$ as $f(\tau, q_{\min})$ where q_{\min} is the minimum charge level at which the next tunnel event can occur. For $V < 1.5e/C$, q_{\min} is always equal to $e/2$. In the other case of $V > 1.5e/C$, q_{\min} can take values in the range $e/2 < q_{\min} < CV - e$.

The integration in (2.5.11) can be carried out using numerical methods. The function $g(t)$ is plotted in figure (2.9) for different R_s/R_t ratios at a fixed bias voltage. Increasing the charging time constant, R_sC , results in an increased time spent in the CB region and, consequently, the mean time between tunnel events is increased. The plots in figure (2.9) give the indication that the SET oscillations become more coherent when the conductance of the environment is high. Ueda and Yamamoto (1990) and Ueda 1990 used the ratio mean/(s.d.) of the time between tunnel events to measure the degree of coherence of the SET oscillations. This shows that the coherence is enhanced at low coupling conductance which agrees with the results obtained from the frequency domain analysis extracted from the time-evolution of the charge discussed in the previous sections.

The uncertainty in the time spent above the $e/2$ level implies a corresponding spread in the charge level at which tunnelling may occur. If $h(Q)$ is the density function of the tunnelling charge level, then:

$$h(Q).dQ = f(\tau).d\tau \quad \text{or} \quad h(Q) = f(\tau)/i(Q) \quad (2.5.12)$$

and $i(Q)$ is given from circuit analysis as $i(Q) = (V - Q)/R_s$. On substitution, $h(Q)$ turns out to be:

$$h(Q) = \frac{1}{e} \frac{R_s}{R_t} \left(\frac{Q - e/2}{CV - Q} \right) \left(\frac{CV - Q}{CV - e/2} \right)^{\frac{1}{e} \frac{R_s}{R_t} (CV - e/2)} \exp\left(\frac{1}{e} \frac{R_s}{R_t} (Q - e/2)\right) \quad (2.5.13)$$

This relation is identical to the result obtained by Ueda and Yamamoto (1989) and Ueda (1990) and was used as a basis of their calculations

2.5.1 I-V Characteristics:

At low temperatures, $T \ll T_c$, the I-V curves of the single junction can be directly calculated from the density functions derived in the previous sections. The dwell time in the Coulomb-blockade region is a continuously decreasing function of τ , and the average dwell time is calculated from

$$\bar{t}_1 = \int t_1(\tau) f(\tau) d\tau \quad (2.5.14)$$

The average time between tunnel events is given from the simple relation $\bar{t} = \bar{\tau} + \bar{t}_1$. In the case of a current biased junction the time t_1 depends linearly on τ and the average time between tunnel events is then $\bar{t} = \bar{\tau} + t_1(\bar{\tau})$. The average current through the junction is evaluated from $\bar{i} = e/\bar{t}$ and the average voltage across the junction is $\bar{v} = V - \bar{i}R_s$.

A family of I-V curves are shown in figure (2.10). For high R_s values the average voltage across the junction can be less than the threshold value, $e/2C$. Tunnelling in this regime occurs at charge levels slightly higher than $e/2$ and the system spends most of the time in the Coulomb-blockade regime; thus, the averaging process results in a small positive voltage value.

2.5.2 Voltage-biased Junction:

Let a fixed voltage bias be maintained across the single junction; a condition that can be realised by connecting the junction to a voltage source of zero internal impedance by a circuit of infinite conductance, $R_s=0$, thus,

$$f_v(\tau) = \lambda \exp(-\lambda\tau) \quad (2.5.14A)$$

$$h_v(Q) = \delta(Q - CV) \quad (2.5.14B)$$

Equation (2.5.14B) stresses the fact that tunnel events take place only at $Q=CV$ which is imposed by the fixed voltage bias condition. Equation (2.5.14A) is a negative exponential distribution with mean time equal to $1/\lambda$. The voltage bias condition implies zero dwell time. This allows the time between tunnel events to have a distribution exactly identical to that of the time spent above the $e/2$ level, i.e.

$$g_v(t) = f_v(t) = \lambda \cdot \exp(-\lambda t) \quad (2.5.15)$$

and the average time between tunnel events is $1/\lambda$. The variance of the time between the events is $1/\lambda^2$. The Ueda measure of the coherence of SET oscillations (mean/s.d.) is equal to unity, indicating a poor quality. The average current passing in this case is:

$$\bar{i} = \frac{1}{R_t} (V - e/2C) , V > e/2C \quad (2.5.16)$$

and the average voltage is $\bar{v} = V$.

2.5.3 Current-biased Junction:

In the case of a current-biased junction, the external circuit conductance is vanishingly low whereas the supply voltage level is high and the current is $I_{dc} = V/R_s$. Furthermore, let $R_s \gg R_t$. The relationship between the current and voltage representation of the supplies is shown in figure(2.3) below, $V = I_{dc} \cdot R_s$.

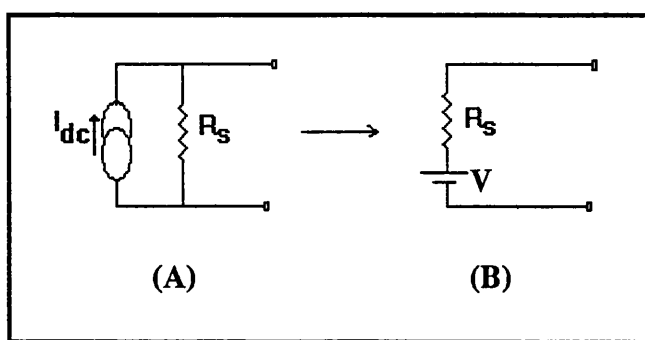


Figure (2.3):Relationship between current and voltage sources.

The distribution function $f_c(\tau)$ then reduces to:

$$f_c(\tau) = \frac{I_{dc}}{eR_t C} \tau \exp\left(-\frac{I_{dc}}{2eR_t C} \tau^2\right) \quad (2.5.17)$$

which still satisfies, $\int f_c(\tau) d\tau = 1$. The average time spent above the $e/2$ level before tunnelling is:

$$\bar{\tau} = \left(\frac{\pi e R_t C}{I_{dc}} \right)^{1/2} \quad (2.5.18)$$

and the average time between tunnel events is then found to be:

$$\bar{t} = \frac{e}{I_{dc}} \exp\left(-\frac{\bar{\tau}}{R_s C}\right) \quad (2.5.19)$$

The average voltage across the current-biased junction turns out to be:

$$\bar{v} = \left(\frac{\pi e R_t I_{dc}}{2C} \right)^{1/2} \cdot \left[1 + \frac{e}{2CR_s I_{dc}} \right] \quad (2.5.20)$$

The first term in (2.5.20) is identical to the result obtained by Averin and Likharev (1987) and Mullen et al (1988). The second term is a correction term due to the finite impedance of the external circuit. The correlated SET events causes oscillations at a more or less fixed frequency that can be readily obtained as:

$$\bar{f} = \frac{I_{dc}}{e} \exp\left(-\frac{\bar{\tau}}{R_s C}\right) \quad (2.5.21)$$

and is clearly less than the value obtained from the 'orthodox' theory. The discrepancy is, again, due to the finiteness of the external circuit resistance.

It is also straight-forward to show that:

$$h_c(Q) = \frac{(Q - e/2)}{eR_t C I_{dc}} \cdot \exp\left(-\frac{(Q - e/2)^2}{2eR_t C I_{dc}}\right) u(Q - e/2) \quad (2.5.22)$$

where $u(x)$ is the unit step function. Equation (2.5.22) is an important relation in describing the SET oscillations in a current biased junction. The charge level at which tunnelling may occur has a dispersion:

$$\sigma_Q^2 = eR_t C I_{dc} \cdot \left(2 - \frac{\pi}{2}\right) \quad (2.5.23)$$

from which it is deduced that the uncertainty is minimised at low driving currents. In the limit $I_{dc}=0$, tunnelling takes place exclusively at $Q=e/2$ i.e.

$$h_c(Q) \rightarrow \delta\left(Q - \frac{e}{2}\right) \quad (2.5.24)$$

The uncertainty in the time between tunnel events is derivable from $f_c(\tau)$ defined in equation (2.5.17) and is found to be:

$$\sigma_\tau^2 = \frac{eR_t C}{I_{dc}} (4 - \pi) \quad (2.5.25)$$

Equations (2.5.25) and (2.5.23) seem contradictory regarding the coherence of SET oscillations. Reducing the uncertainty in the level at which the event is expected to take place would increase the uncertainty in the timing of the event and, consequently, will increase the time between tunnel events. This is summarised in the uncertainty relation,

$$\sigma_Q \cdot \sigma_\tau = \frac{eR_t C}{\sqrt{2}} \cdot (4 - \pi) \quad (2.5.26)$$

Furthermore, if a single junction is used in a circuit and a single tunnel event is required to cause some effect in the rest of the circuit, it will then be important to wait for some minimum time to ensure that the event occurs during that time. The stochastic nature of the process makes it impossible to ensure this to occur; however, if the event is required to occur with a probability, p , then the minimum time for this, in case of a current-biased junction, is:

$$t = \left[\frac{2eR_t C}{I_{dc}} \log \frac{1}{1-p} \right]^{1/2} \quad (2.5.27)$$

The time to elapse before a given certainty is reached will be less in case of larger currents.

2.5.4 Q-factor of SET Oscillations:

The quality of oscillations caused by the correlated SET events may be described in terms of the deviation of the frequency of oscillations from the central frequency. Let σ_t be the standard deviation of the time between tunnel events. The bandwidth of the SET oscillations is then estimated as:

$$\Delta f = (\bar{t} - \sigma_t)^{-1} - (\bar{t} + \sigma_t)^{-1} \quad (2.5.28)$$

and the Q-factor is evaluated as:

$$Q_f = \frac{\bar{f}}{\Delta f}$$

For a voltage-biased junction, Q_f has its minimum value of zero. The Q-factor for the current-biased junction is

$$Q_{fc} = \frac{e - R_t C I_{dc} (4 - \pi)}{2\sqrt{e R_t C I_{dc} (4 - \pi)}} \quad (2.5.29)$$

The Q-factor of SET oscillations is enhanced if the driving current satisfies $I_{dc} \ll e/R_t C$. Figure (2.11) shows the variations of Q_f with the applied voltage for different values of R_s . For a specific value of R_s the coherence may be increased by a proper selection of the applied voltage bias.

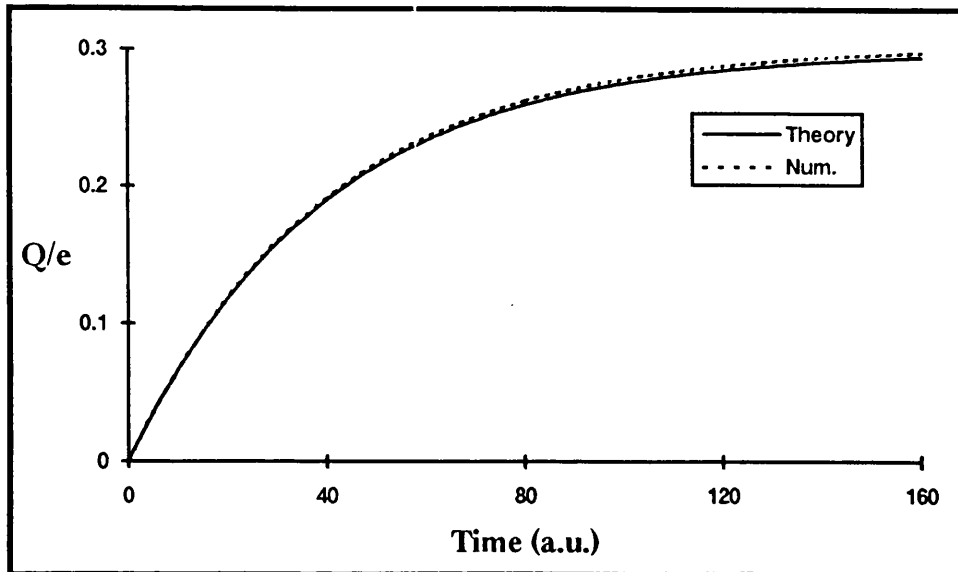
Each tunnel event is accompanied by an uncertainty in time equals to σ_τ^2 . Consecutive tunnel events will increase this uncertainty; after N tunnel events the uncertainty will be $N\sigma_\tau^2$. The uncertainty becomes of the order of the time between tunnel event after N' events where $N' \approx \bar{t}^2 / \sigma_\tau^2$. For a current-biased junction: if $I_{dc} = 0.01e/R_t C$ then $N' \approx 100$.

Time evolution of the voltage across the junction obtained from the simulation of the Master Equation supports the above mentioned loss of coherence as time passes. This is indicated in figure (2.6) by the decaying oscillations and

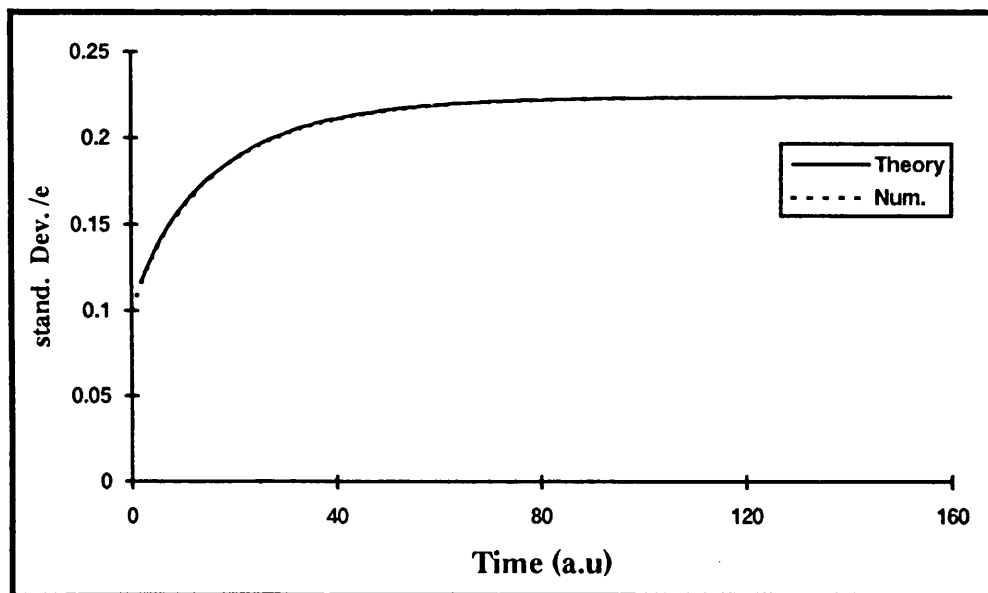
the tendency to attain a constant average (expected) charge level and also in figure (2.7) where the spread in the frequency spectrum reflects the decaying oscillations.

Summary:

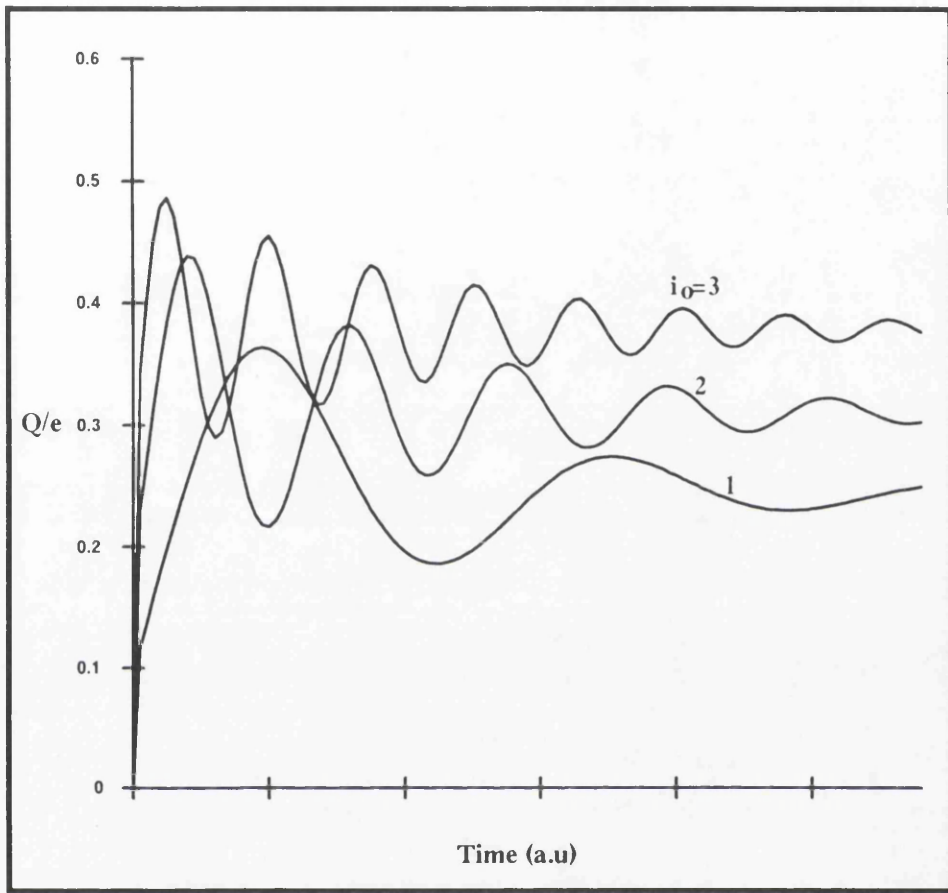
In this chapter three models were used to study the properties of the single normal tunnel junction. Tunnelling phenomenon across the junction was investigated using a semiclassical method. The total tunnel rate was derived and shown to include a small correction term that is attributed to the distribution of wave-vectors of the incident electrons in the longitudinal and transverse directions. Numerical solution of the Master Equation was implemented to study the evolution of the charge on the junction with time. This was then used to inspect the coherence of the SET oscillations in the frequency domain. The coherence of the SET oscillations obtained from the current and voltage-biased junctions was studied via the distribution of time between tunnel events. This method was also used to derive the I-V characteristics of the single junction.



Figure(2.4): Variation of the average charge on the single junction with time, calculated from the numerical solution and from the conventional charging curve.
 $I_0=0.3e/(R_s C)$, $k_B T C=0.05e^2$.



Figure(2.5): Standard dev. of the charge variable as a function of time calculated using the analytical and numerical solutions of the Master Equation in the Coulomb-blockade region. $I_0=0.3e/(R_s C)$, $k_B T C=0.05e^2$.



Figure(2.6): Evolution of the charge on a single tunnel junction with time: $T=0.05T_c$, $R_s/R_t=30$, $i_0=I_0/(e/R_tC)=1, 2 \& 3$.

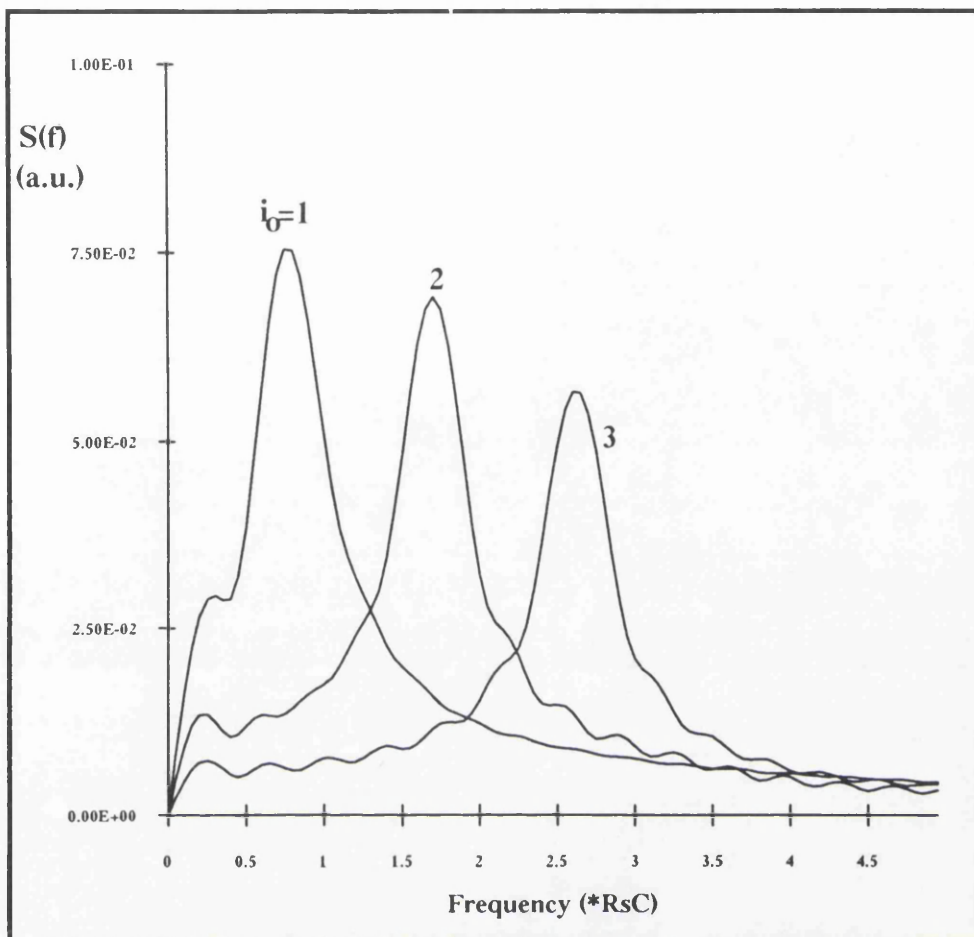


Figure (2.7): Frequency spectrum of the SET Oscillations. The parameters are:
 $T=0.05$ T_c , $R_s/R_t=30$, $i_o=I_o/(e/R_sC)=1,2$ and 3 .

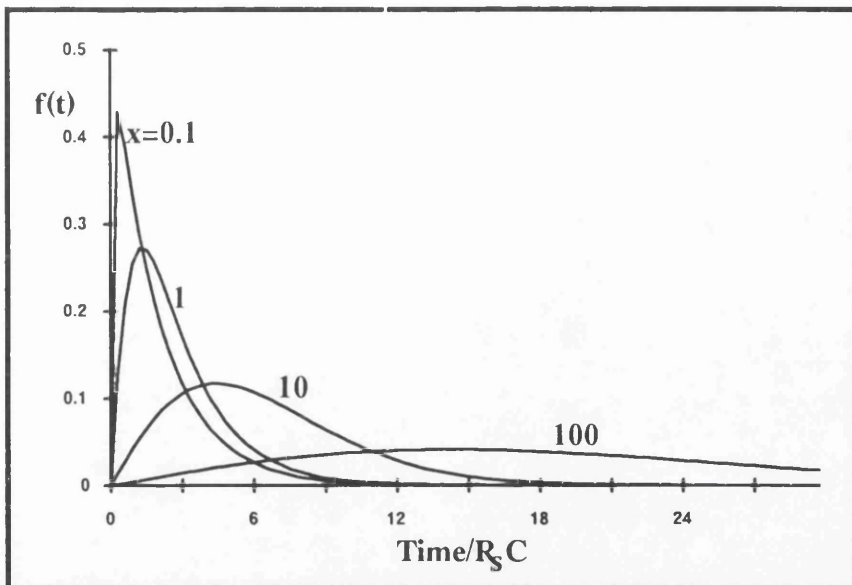


Figure (2.8): Distribution of the time spent above the $e/2$ charge level in a single junction-system before the tunnel event takes place, $V=e/C$, $x=R_s/R_t=0.1, 1, 10, 100$.

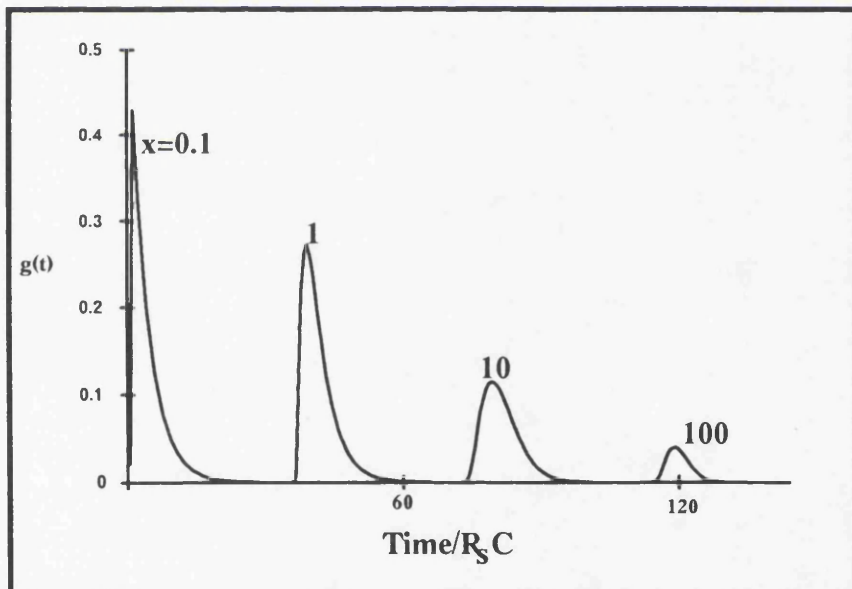
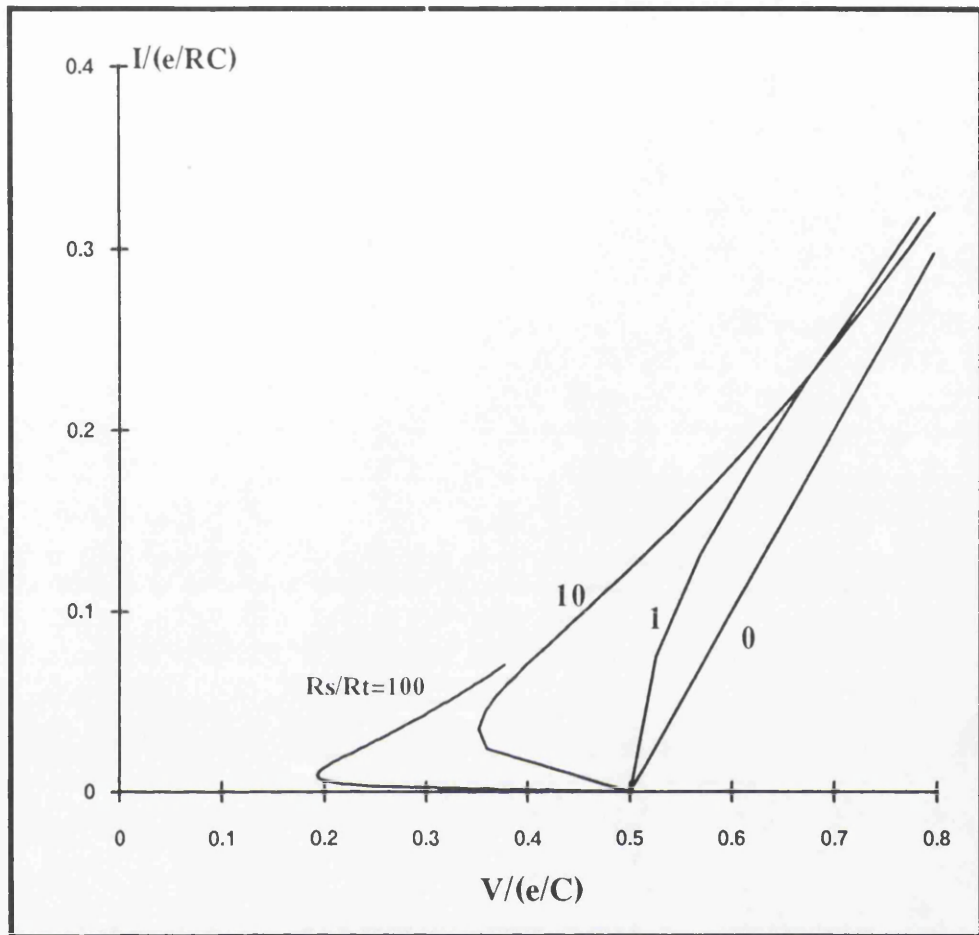


Figure (2.9): Distribution of the time between successive tunnel events across a single tunnel junction; parameters: $V=e/C$, $x=0.1, 1, 10 \& 100$.



Figure(2.10): I-V characteristics of the single junction calculated from the distribution of time between tunnel events.

Plots correspond to $R_s/R_t=1, 10$ and 100.

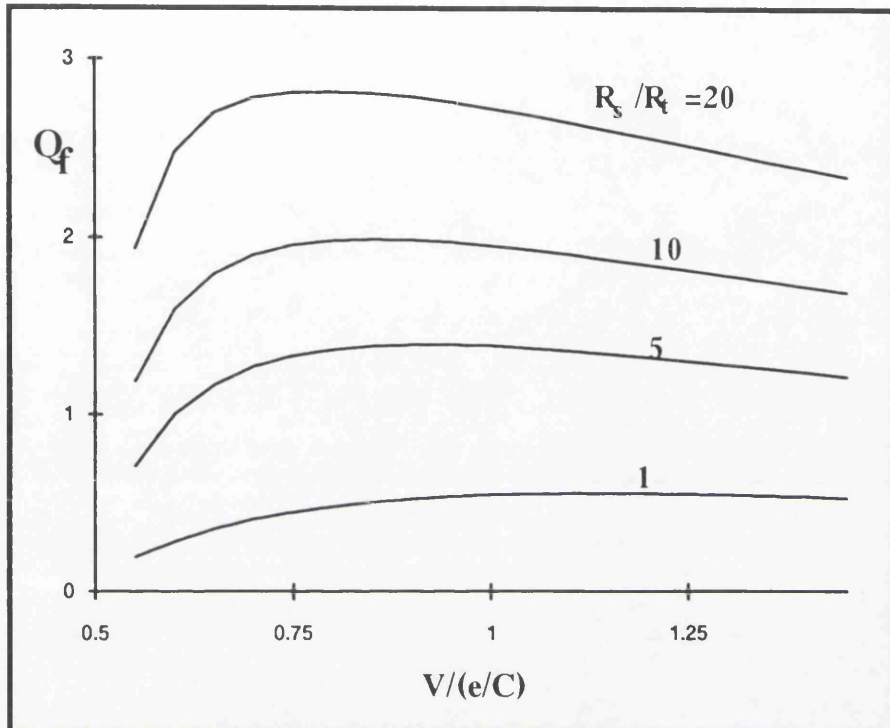


Figure (2.11): Quality factor of the oscillations resulting from the tunnelling of single electrons, curves correspond to: $R_s/R_t=1,5,10,20$

Chapter (3)

The Double-Junction System

3.1 Introduction:

The theory of Coulomb blockade and single-electron tunnelling has been presented in the previous chapters. It was shown that the flow of discrete carriers through the single junction can be controlled only by the driving source. This is a disadvantage, as in electric circuits the bias source is normally fixed and the variation of the bias level may cause unwanted transients in the circuit.

A first step towards the use of tunnel junctions in single-electronic circuits is the gated double-junction structure, termed the turnstile, the simplest circuit of which is shown in figure (3.1). Two tunnel junctions are connected in series and gating is accomplished by coupling the central electrode to the control gate voltage, V_g .

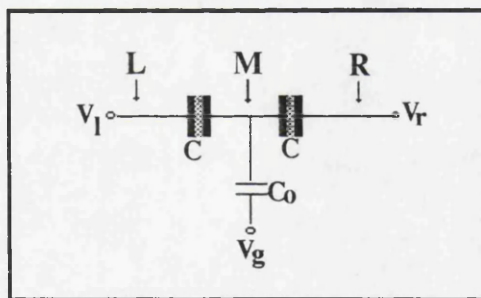


Figure (3.1):The Double-junction System (The Turnstile).

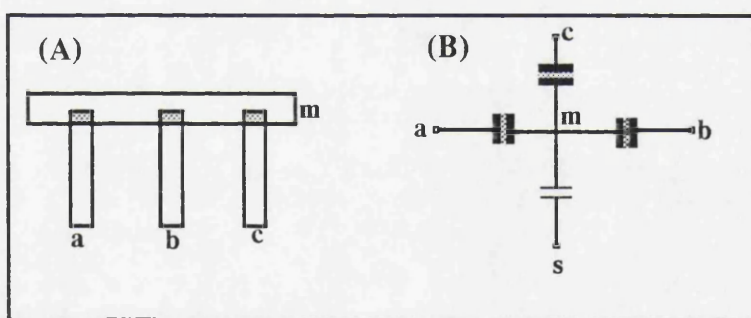
3.2 Experimental Structures:

In the following sections some experimental structures used by different groups to achieve the turnstiling action are briefly described. These structures were operated as single-electron transistors. Several experiments had been conducted to demonstrate the possibility to control the flow of single electrons

through the turnstile of a modified version of the structure of figure (3.1), see e.g. Geerligs and Mooij (1990).

a. Fulton's Structure: (Fulton and Dolan (1987))

This is basically a two-junction configuration, figure (3.2). It consists of three adjacent electrodes (a,b and c) sharing the same central electrode (m). Two electrodes are used to pass the current and the third to monitor the potential at the central point. The Al-Al junctions are typically $(0.03\mu\text{m})^2$ and the central electrode is $0.05 \times 0.8(\mu\text{m})^2$. These junctions have a tunnel resistance of the order of $40 \text{ k}\Omega$. The substrate is an oxidised silicon wafer with oxide thickness of $0.44 \mu\text{m}$. Gating is accomplished by an Au-Cr film on the other side of the substrate (point s in figure (3.2.B)). It is to be emphasised that all electrodes are metallic and such structures are important to study the basic theory of Coulomb blockade and single-electron tunnelling.



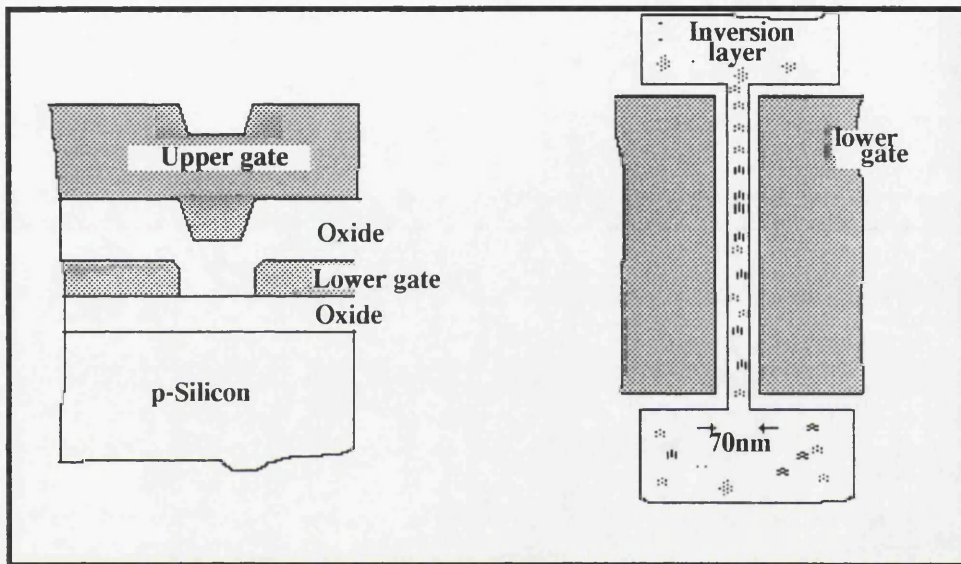
Figure(3.2) A: Fulton's Structure, B: Equivalent circuit.

b. Scott-Thomas's Structure:(Scott-Thomas et al (1989))

First direct observation of the conductance oscillations of a confined 1-DEG channel with the charge density were reported on these structures. The lower metallic gate, see figure (3.3), confines an inversion layer (25nm wide and 1-10 μm long) to the region beneath the gap. The upper gate overlaps the source

and drain n⁺ pads; and contact to the narrow channel is made by wide 2-DEG regions. The upper gate provides the lateral control field to the 1-DEG.

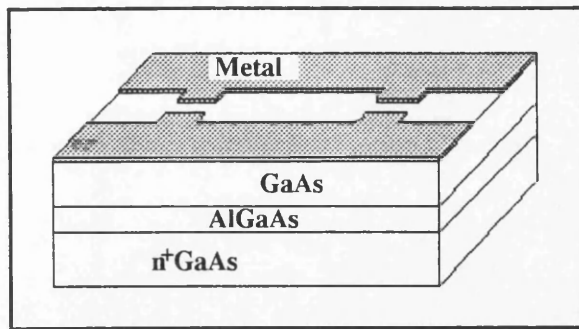
This structure contains no clearly defined potential barriers to induce tunnel effects. Trapped charges at the Si-SiO₂ interface create potential barriers along the length of the channel; thus forming a double-junction configuration or a multi-junction structure. For the dimensions of this structure and typical density of trapped states, 10¹⁰/cm², two potential barriers are most likely to be created and the structure will, therefore, be a double-junction structure.



Figure(3.3):Scott-Thomas Structure.

c. Meirav's Structure:(Meirav et al (1990))

Metal electrodes with two constrictions are deposited on a GaAs-AlGaAs heterostructure, figure(3.4). The gap between the two electrodes defines the channel and the two constrictions in the gap define the isolated segment of the channel which corresponds to the central electrode of the turnstile.



Figure(3.4): Meirav's structure.

d. Pasqueir's Structure:(Pasqueir et al (1993))

This structure is similar to Meirav's structure. The confinement formed here figure (3.5), is a 2-DEG rather than the 1-DEG in Meirav's structure. The heights of the tunnel barriers, and hence the tunnel conductance of either junction, can be controlled by varying V_1 or V_2 while V_o controls the size of the 2-DEG and the middle electrode serve as a gate electrode, see figure (3.5.B).

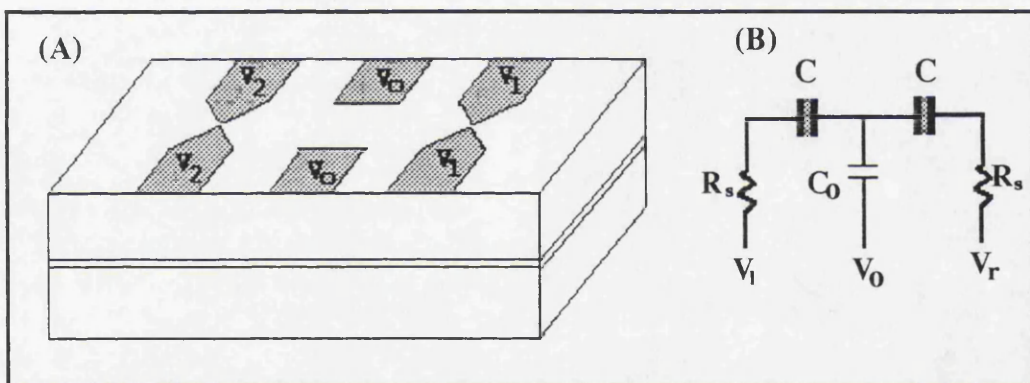


Figure (3.5):A: Pasqueir's structure, B: Equivalent circuit.

3.3 Semiclassical Model:

The basic idea of single-electronic circuits is the Coulomb blockade of tunnelling and the correlated single-electron tunnelling. Correlation of tunnel events manifests itself in two ways:

- (a) *Time correlation:* where a tunnel event will block other events until some charge is redelivered to that junction. In other words, if the exact

timing of the event is known, it is possible to know -roughly- the time the next event, this has been discussed in the previous chapter.

(b) *Space correlation*: in this case a tunnel event across a junction will induce charges on other junctions; thus affecting the tunnelling probabilities in the all junctions of the system.

It is important to know exactly the type of effects induced by a single tunnel act across any junction of the system. This is crucial to the understanding of the operation of single-electronic systems.

Geerligs (1991) and Kastner (1992) explained the Coulomb blockade in a structure consisting of a metal particle imbedded in the insulating gap between two metallic electrodes in terms of an energy gap in the tunnelling density of states of the particle. This succeeds in describing the onset of tunnelling into the metallic island but does not account for the subsequent behaviour.

Functioning of the double-junction system may be studied by investigating the potential profile of the device and the effects caused by single tunnelling acts. Tunnelling of electrons into and out from the central island changes the relative positions of the Fermi levels of the electrodes. This is due to the change in the electrostatic energy of the circuit due to the addition/removal of the charge to/from the electron gas. Let the turnstile of figure (3.1) be biased such that $V_r - V_l = V$. It is assumed that the circuit has no resistive components in any of its paths. The potential profile is shown in figure (3.6.A) for an arbitrary gate voltage. V_1 and V_2 are the potential drops across the two junctions. If n excess electrons are assumed to occupy the central electrode, then:

$$V_1(n) = \frac{1}{C_T} \{ CV_r - (C + C_o)V_l + C_o V_g - ne \} \quad (3.3.1A)$$

$$V_2(n) = \frac{1}{C_T} \{ (C + C_o)V_r - CV_l - C_o V_g + ne \} \quad (3.3.1B)$$

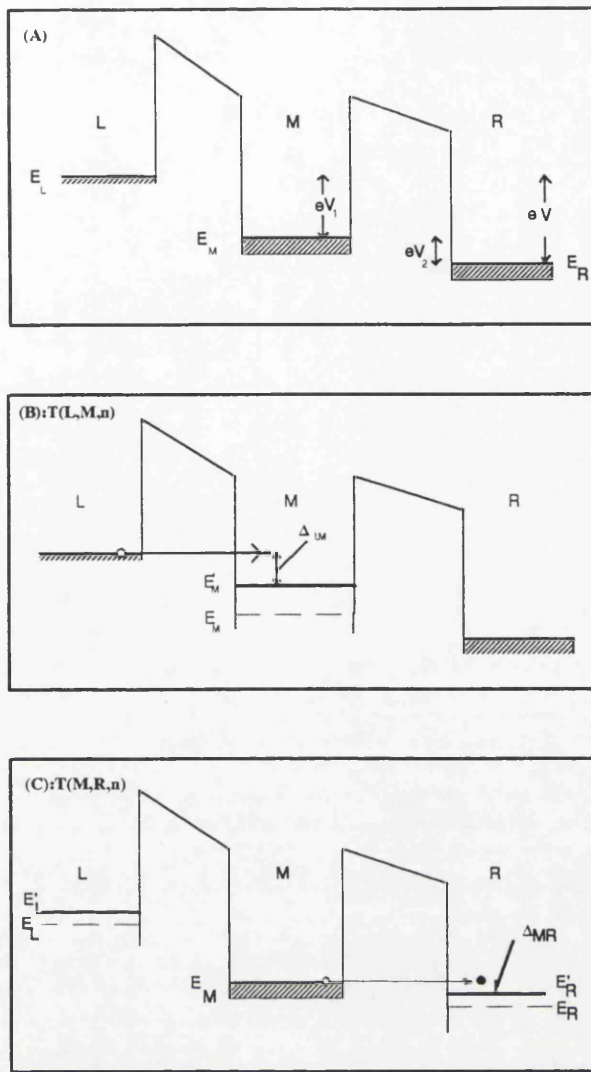


Figure (3.6): Potential Profile of a Double-junction System.

Now, consider the tunnel events that may take place across the junctions of the double-barrier structure:

$T(L,M,n)$: (tunnelling of an electron from L to M when there are exactly n excess electrons at M before the event) the additional electron on the central electrode will be accommodated on a total capacitance of $C_T=2C+C_0$; and the Fermi level at M will increase by $e^2/2C_T$, figure (3.6.B). The electron performing this event should find an empty energy state at M; this can happen at $T=0K$ when:

$$\Delta_{LM}(n) = eV_1(n) - \frac{e^2}{2C_T} > 0 \quad (3.3.2A)$$

and the event will, therefore, be completely blocked if $\Delta_{LM}(n) < 0$.

$T(M,R,n)$: this event will lower the electron energy levels of the central electrode by $e^2/2C_T$. The energy levels of the left electrode will be lifted by the same amount while the energy difference between the Fermi levels in the left and right electrodes is still eV, figure (3.6.C). The event $T(M,R,n)$ will be possible if:

$$\Delta_{MR}(n) = eV_2(n) - \frac{e^2}{2C_T} > 0 \quad (3.3.2B)$$

The conditions leading to the occurrence or suppression of the events $T(M,L,n)$ and $T(R,M,n)$ can also be obtained.

The tunnel rate is obtained from the quantum golden rule and is found to be similar to equation (2.2.9) with Δ defined as:

$$\Delta = \pm eV_i(n) - \frac{e^2}{2C_T}, \quad i=1,2 \quad (3.3.3)$$

The general case of a tunnel junction in a capacitive circuit was studied by Esteve (reported by Geerligs (1990)). The same arguments given above show that a minimum charge -termed the critical charge- should build on the tunnel junction before the event can take place.

Considering the initial and final energy levels participating in a single tunnel act across a junction in a system of tunnel and non-tunnel junctions, it can be shown that the critical charge is given as: (Geerligs (1990))

$$q_c = \frac{e}{2} \left(1 + \frac{C_e}{C} \right)^{-1} \quad (3.3.4)$$

where C_e is the total shunt capacitance seen by the tunnel junction. This assumes that the charge relaxation time, τ_r , is much smaller than the tunnelling time. The changes that will take place in the circuit immediately after the tunnel event will therefore affect the event. This is the non-local limit considered by Amman et al (1989). Resistive components in the circuit increase the relaxation time, at least for some junctions, and a tunnelling electron will sense changes taking place in a segment of the circuit around the junction. In the local limit, the tunnelling electron senses variations in the potential of the junction across which the event is taking place. The critical charge is then:

$$q_c(\text{local})=e/2 > q_c(\text{non-local})$$

For fixed bias voltages, V_r and V_l , the number of excess electrons in the central electrode can be controlled by varying the gate voltage. From equations (3.3.2) it follows that the charge on the central electrode changes by $\pm e$ as a result of a change in the gate voltage of:

$$|\Delta V_g| = e/C_0 \quad (3.3.5)$$

a value that is independent of the parameters of the tunnel junctions. The periodic increase of the excess charge on the central electrode with the gate voltage results in periodic oscillations of the line conductance of the turnstile. In other words, the small signal transfer conductance, $\partial I / \partial V_g$, is a periodic function of the gate voltage. These oscillations were first observed by Scott-Thomas et al (1989) in the conductance of a one dimensional electron gas using Si structures. Meirav et al (1990) also observed these oscillations in a GaAs transistor with narrow constricted channel. The oscillations were identified to correspond to the addition of an exact electronic charge to the central electron gas. Similar oscillations were observed by Meurer et al (1992) on arrays of confined quantum dots in AlGaAs-GaAs heterostructure. Fulton's structures, Fulton and Dolan (1987), revealed well-defined and persistent conductance oscillations that are in accord with the basic theory. The experiments carried out by Pasqueir et al (1993) on the structures of figure (3.5) also showed clear $G-V_g$ oscillations indicating a stable 2-DEG island size in the given range of operation. The regular variation of the value of the conductance peaks is due to the modulation of the barriers by the adjacent gate potential, Pasqueir et al (1993)

3.4 Finite-State Machine Model:

The voltage levels applied to the turnstile play a crucial role in guiding the overall behaviour of the device; ranging from complete Coulomb blockade to continuous random SET events. The Linear Programming (LP) method, Roy et al (1993), is a powerful tool in defining the voltage levels required to cause the pre-

defined transitions in simple single-electronic circuits. However, once the circuit gets complicated, the legal states of the system become more inter-related through the transition probabilities and extra care is needed when using the Linear-Programming technique.

If all transitions in the system are caused by externally controlled inputs, it will be desirable to model the effects of these inputs on the state of the system. It is to be mentioned that the same input may cause different effects on the system depending on the current state of the system. Studying such systems, one must consider all possible inputs and all possible legal states.

The Finite-State Machine (FSM) provides a frame-work in which such State-Input-Transition relationship can be studied with a good level of controlling the complexity of the system under consideration. The FSM has been widely used in designing digital circuits and communication systems, Mead and Conway (1980).

The FSM assumes that any input sensed by the system will invoke an action. This action may be taken by the system itself or by another system. Following this action the system changes its state, or the state is changed, accordingly. The transition from a state to another may be a physical transition or conceptual transition, e.g. to keep record of the history of events. Thus, the system must have a finite and well-defined set of states. The digital single-electronic systems, including the turnstile, may be modelled within the FSM. The FSM together with the LP methods form a powerful combination in designing single-electronic circuits.

The simple turnstile is suggested to provide a means of controlled flow of single electrons in a circuit, e.g. Geerligs and Mooij (1990) and Likharev (1988). A controlled gate voltage is first tuned to V_{g1} ; this allows only one electron to tunnel from the left, L, to the central island, M. The excess electron will stay at M as long as the voltage is held at V_{g1} . When the gate voltage is later switched to V_{g2} , the electron will pop out through the other junction and no other event is to

take place afterwards, until the voltage is switched back to V_{g1} . In this mode of operation V_r and V_1 are kept constant. These performance specifications can be transformed into the FSM model as shown in figure (3.7).

In this model, the state of the turnstile is defined by the number of excess electrons at the central electrode. The inputs -the voltages- cause transitions from one state to another, or may not cause a transition, depending on the state of the device and the input level.

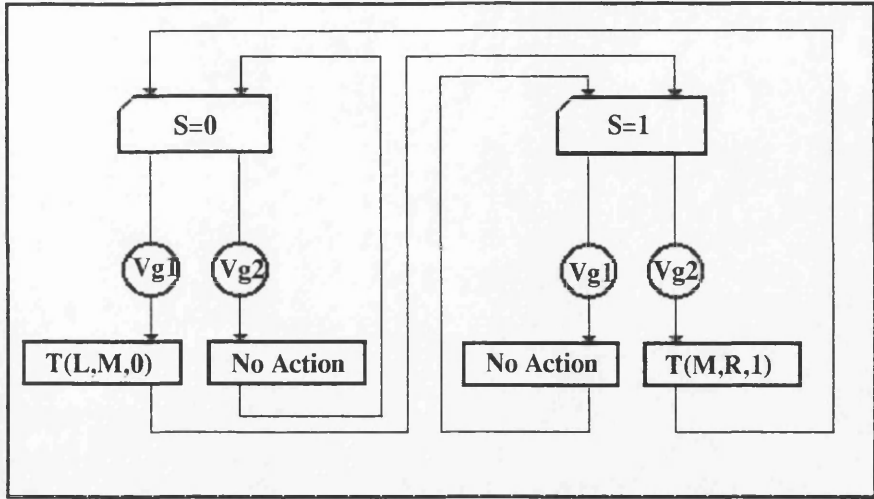
To simplify the LP manipulations, the following transformation can be used:

$$\begin{aligned} V_1(n) &= u - \frac{ne}{C_T} \\ V_2(n) &= v + \frac{ne}{C_T} \end{aligned} \quad (3.4.1)$$

where u and v are functions of the voltage levels and are defined according to equation (3.3.1). The full set of relations obtained from the LP method based on the FSM model are given in Appendix (B).

Clocking-Phase I: In figure (3.8.A), one can identify two possible bias regions in which the number of unwanted, but possible, events is minimum. In these regions, beside the desired tunnel event, $T(L,M,0)$, there is a possibility of occurrence of another unwanted event. In the area labelled A1 in figure (3.8.A), the event $T(R,M,0)$ may occur before $T(L,M,0)$, while in A2 the excess electron may tunnel through the RHS junction giving rise to the event $T(M,R,1)$.

Clocking-Phase II: In phase II, B1 and B2 areas in the $u-v$ space are similar to A1 and A2 in phase I. In B1, the event $T(M,L,1)$ is possible, i.e. the electron may pop in the wrong direction. In B2, the event, $T(L,M,0)$ may take place after the required event, $T(M,R,1)$, has taken place. Thus, a continuous sequence of the events $T(L,M,0)-T(M,R,1)$ will be observed if the turnstile is biased at any point in B2.



Figure(3.7): Finite State Machine for the turnstile action.

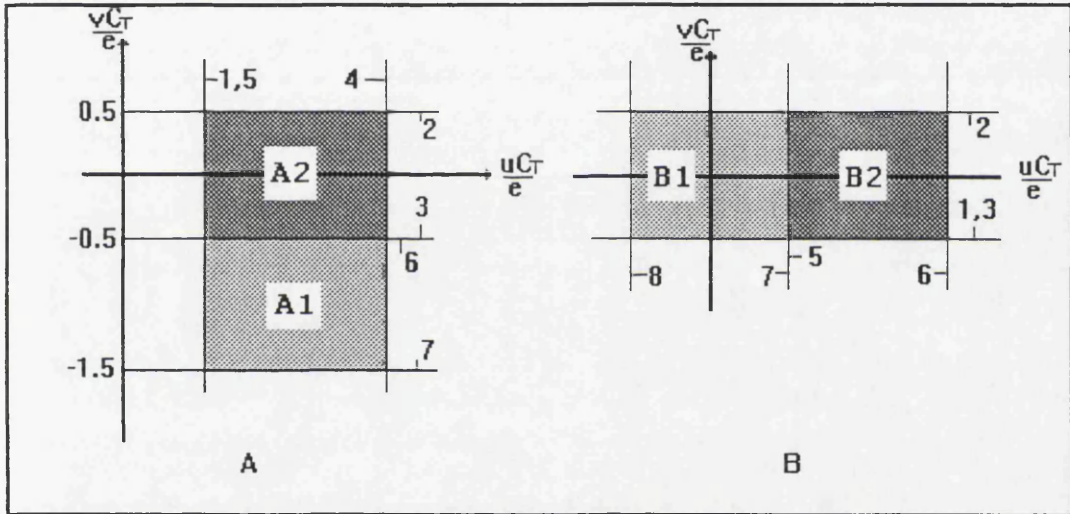


Figure (3.8) A: Clocking-In Phase, B: Clocking-out Phase.

The above analysis reveals the types of problems facing the single-electronic circuit designer. Choosing the border line between A1 and A2 (or B1 and B2) does not guarantee zero tunnelling rates for the two possible unwanted events; because these events will then be easily thermally activated. On the other hand, biasing the device away from these areas would lead to an enhanced controllability over the events.

The addition of resistive and/or reactive components to the turnstile circuit dampens down the junctions' charging/discharging process, hopefully, in favour of the required tunnel event. For clocking-phase I, the device may be biased at A1 and the damping elements chosen to force the charging process in favour of the event T(L,M,0); while in the clocking-phase II the circuit is biased at B1 and the process is forced to favour the event T(M,R,1).

A multi-level phased gate input, together with the damping elements, is an effective means of controlling the tunnel events. In the clocking-phase I, the turnstile may be biased first at a point in A2 and the damping elements are chosen to lead the charging process fast in favour of the event T(L,M,0). The condition for the unwanted event, T(M,R,1), is initially unsatisfied as the system is still found at the state S=0. Following the tunnel event, T(L,M,0), the condition for T(M,R,1) should not be satisfied until the bias point is switched to A1, which is the steady state point. In this area, the event T(R,M,0) is no longer a problem because the system has already changed its state.

3.5 Static Monte-Carlo Method:

Monte-Carlo methods have been widely used in studying the double-junction structure. Other single-electronic systems studied using the Monte-Carlo methods include the triple-junction system (the electric pump) and the long homogeneous arrays of tunnel junctions, e.g. Mullen et al (1988 A&B) and Amman et al (1989). The static MC method implemented by Mullen and Amman assumes that the circuit will relax to its steady state following a tunnel event in a time negligibly shorter than the time till the next tunnel event. This assumes, in principle, zero resistance and inductance in the circuit.

Tunnelling process is assumed to be a Poisson point process; and only one tunnel event is, therefore, allowed to take place at a time, e.g. Levine (1976). This allows the state of the system, $S(t)$, after an infinitesimal time interval Δt to be written as, see e.g. Mullen et al (1988) and Amman (1989) :

$$S(t + \Delta t) = \begin{cases} n+1 & , p_+ = [\Gamma(R, M, n) + \Gamma(L, M, n)].\Delta t \\ n-1 & , p_- = [\Gamma(M, R, n) + \Gamma(M, L, n)].\Delta t \\ n & , p_o = 1 - (p_+ + p_-) \end{cases} \quad (3.5.1)$$

Relation (3.5.1) represents three mutually exclusive events; viz. the charge at the central island may change by $+e$, change by $-e$ or stay unchanged. Clearly, the probabilities satisfy: $p_+ + p_- + p_o = 1$. The Monte-Carlo model will determine which of the three events is to take place during the time interval Δt and then modify the state of the turnstile accordingly (note: *system stays unchanged* is assumed to be an event).

Let the turnstile circuit have infinitely large conductances in all its paths and zero inductance. The tunnel rates will be constant during the system's visit to any state and the probability of occurrence of any tunnel event during an infinitesimally small time interval, Δt , is equal to $(\text{rate} \times \Delta t)$. It is this assumption and the assumption that the traversal time for tunnelling is negligibly small which allow the use of a negative exponential distribution to represent the time between tunnel events (and hence the Poisson nature of tunnel events). The latter assumption may be put differently as: the whole system is assumed to be frozen while a tunnel event is taking place until this event is completed.

For a Poisson point process that occurs at a fixed mean rate of λ , the probability that the event takes place in a time interval t is given by:

$$r = 1 - \exp(-\lambda t).$$

Let the four tunnel rates appearing in equation (3.5.1) be denoted by $\lambda_1, \dots, \lambda_4$. In a Monte-Carlo simulation the event that is most likely to occur is selected and the state of the system is changed accordingly. Let the random numbers chosen from negative exponential distributions with means $1/\lambda_i$, $i=1, \dots, 4$, be $\{t_i; i=1, \dots, 4\}$. The system then changes its state after a time τ where:

$$\tau = \min \{t_i; i=1, \dots, 4\} \quad (3.5.2)$$

The Poisson processes have the property of being completely memoryless, e.g. Beaumont (1983). This implies that the expected behaviour in the future will not be affected by the history of events. It is therefore justified to reset the whole system following any event and start a fresh observation.

The process described above should be iterated for a time long enough to allow the average properties of the device to be determined -with high degree of confidence- from the collected data. The simulation method described above uses the fact that each tunnelling process is independent of all other processes. The main function of the simulator is, therefore, to monitor the competition between the different processes and to select the event that is scheduled to occur first.

An equivalent approach is to combine all processes in a single process having an equivalent rate of occurrence, Hockney (1988). Let the double-junction system be in the state $S=n$ at $t=0$; the probability that the system will remain in that state for a time t is:

$$\begin{aligned} p\{S(t)=n\} &= \exp(-\lambda_1 t) \times \exp(-\lambda_2 t) \times \exp(-\lambda_3 t) \times \exp(-\lambda_4 t) \\ &= \exp(-[\lambda_1 + \lambda_2 + \lambda_3 + \lambda_4]t) \\ &= \exp(-\lambda_T(n)t) \end{aligned} \quad (3.5.3)$$

This simply tells the fact that the system, when in any state, will decay at a rate that is equivalent to the sum of the individual tunnel rates and the whole decay process will be another Poisson point process. Within this equivalent system, the i -th process has a probability of occurrence that is proportional to its tunnel rate.

The I-V curves of a double-junction structure calculated from the static Monte-Carlo methods described above are shown in figure (3.11) which reveal a sharp discontinuity at the critical voltage. The increased capacitance to ground, C_o , reduces the critical voltage. The capacitance to ground plays an important role in the turnstiling action as the single electrons will be partially accommodated on this junction. Figure (3.12) displays the conductance oscillations as a function of the gate voltage at fixed terminal voltage. Each period corresponds to the addition of an electron to the central electrode; a fact that is revealed in figure (3.13).

Static Monte-Carlo simulations have shown that the turnstile specifications, listed in section (3.4), can be met if the critical charges are increased above their non-local limit. This will create a zone in the u-v space ($V_r-V_1-V_g$ spaces) in which the only condition satisfied is that of the required event. In figure (3.10) two areas in the u-v space are shown: in the area labelled X there is a possibility of occurrence of the event $T(L,M,0)$ and all other events are blocked provided that the system was initially at the state $S=0$. In the area labelled Y in figure (3.10), the event $T(M,R,1)$ is allowed at the state $S=1$ and all other events are blocked. The strict local limit (critical charge= $e/2$ for both junctions) is applicable.

3.6 Dynamic Monte-Carlo Simulation:

It was shown in the previous section that some performance uncertainties will arise when the undamped turnstile is operated as a memory element. This is attributed to the fast relaxation process following any event. Resistive and inductive components can be used to regulate the charge/discharge process in such a way that the probability of occurrence of certain event at a particular state-input combination is enhanced, while other events become less likely to occur. This will, in effect, enhance the reliability of such devices. It is therefore important to study the behaviour of the device in real time and try to select the combination of damping components that ensure the required behaviour. Figure (3.9) shows a simple turnstile circuit in which damping is provided by two equal external resistors. This circuit models the structure used by Pasqueir et al (1993) and is shown in figure (3.5). To simplify the analysis further, the circuit is supposed to be symmetrically biased, such that $V_r=-V_1=V$.

At any time, the total charge accumulated on any junction is equal to the sum of the charges due to the voltage sources (q_i) and the charge (δ_i) due to any excess charge at the central electrode. The two charging processes -as seen by each junction- are independent. Thus the superposition theorem can be used to determine the total charges on the different junctions.

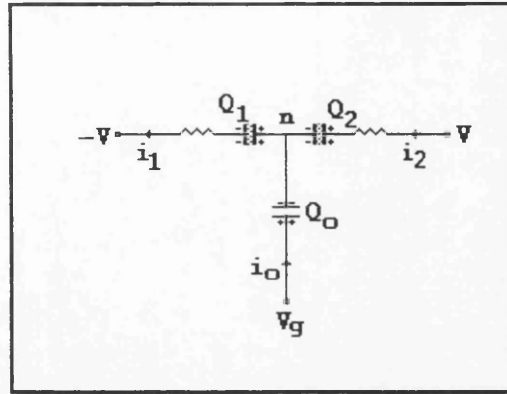


Figure (3.9): Damped Double-junction System.

Let a tunnel event take place. The tunnelling electron first causes changes in the state of the junction through which it is tunnelling; whereas, other junctions will sense this event later. In other words, the local limit is to be used.

The differential equations modelling the charging process due to the sources only have the solution:

$$q_i(t) = A_i \cdot \exp\left(-\frac{t}{RC}\right) + B_i \cdot \exp\left(-\frac{C_T t}{RCC_o}\right) + q_{is} \quad , i=0,1,2. \quad (3.6.1)$$

where A_i 's, B_i 's are constants and q_{is} 's are the steady-state charges. If the initial charges on the junctions are $\{q_{io}, i=0,1,2\}$, the initial currents can be obtained from:

$$\begin{aligned} V + V_g &= \frac{q_{1o}}{C} + \frac{q_{2o}}{C_o} + RI_{1o} \\ 2V &= (q_{1o} + q_{2o})/C + R(I_{1o} + I_{2o}) \end{aligned} \quad (3.6.2)$$

The currents also satisfy the boundary conditions, $I_{ks}=0$, $k=0,1,2$. This allows the constants A_i 's and B_i 's to be determined.

For the other process (the redistribution of the excess charge at M following a tunnel event), the charges are obtained by solving the following set of differential equations:

$$\begin{aligned}
 R \frac{d\delta_1}{dt} + \frac{\delta_1}{C} + \frac{\delta_o}{C_o} &= 0 \\
 R \frac{d\delta_2}{dt} + \frac{\delta_2}{C} - \frac{\delta_o}{C_o} &= 0 \\
 \delta_o - \delta_1 + \delta_2 &= ne
 \end{aligned} \tag{3.6.3}$$

and these charges are subject to the following steady-state conditions: $\delta_{1s} = \delta_{2s} = eC/C_T$ and $\delta_{os} = eC_o/C_T$, for each additional electron.

The evolution of the charges, δ_i 's, is found to be similar to that of q_i 's; the only difference being in the boundary conditions. The two processes can, therefore, be described by one curve, similar to equation (3.6.1), provided that the boundary conditions are properly defined.

Let n excess electrons exist at M . The charging curves are given by $Q_i(t,n)$, where t is the time since the last tunnel event, or measurement. Let the event $T(L,M,n)$ take place at time t . This event will modify the initial conditions to: $Q_{1o} \rightarrow Q_1(t,n) + e$, $Q_{2o} \rightarrow Q_2(t,n)$ and $Q_{oo} \rightarrow Q_o(t,n)$. The steady-state conditions become, $Q_{os} \rightarrow q_{os} + (n+1)\delta_{os}$, $Q_{1s} \rightarrow q_{1s} - (n+1)\delta_{1s}$ and $Q_{2s} \rightarrow q_{2s} + (n+1)\delta_{2s}$.

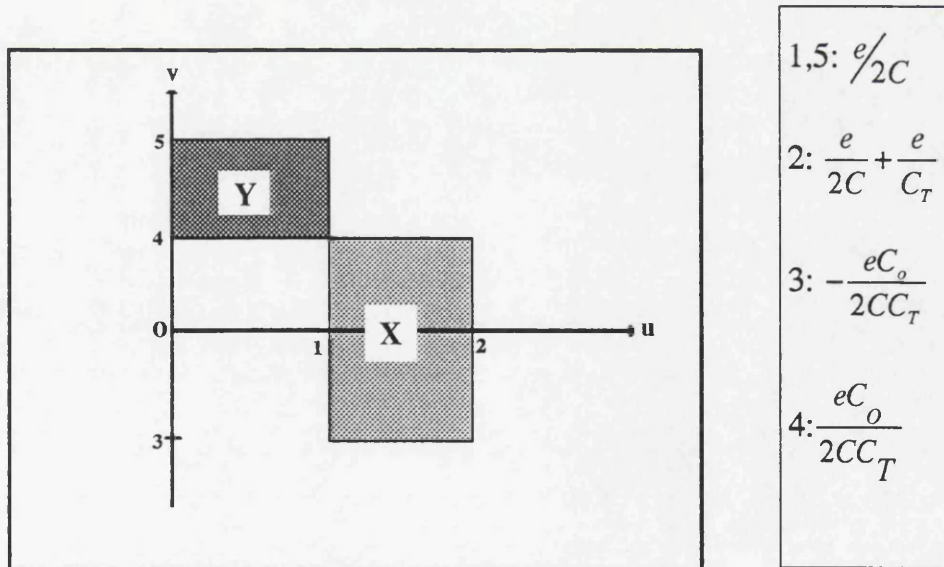


Figure (3.10): Operational areas for the damped circuit. See Appendix (C).

Following a change of the bias conditions (from a point in X to a point in Y of figure (3.10) or vice versa), the time spent before a tunnel event becomes probable -the dwell time- is a deterministic variable and can be obtained by solving for the dwell time, t , in equation (3.6.1). Following this time, the charge level on that junction becomes a stochastic variable due to the uncertainties introduced by the tunnelling probability. The distribution of time spent above the critical charge before an event occurs can be obtained following the same steps used for the single junction case. It follows that the distribution of the time that elapses before the event takes place is:

$$f(t) = \Gamma(q_i(t)).\exp\left[-\int_0^t \Gamma(q_i(\tau)).d\tau\right] \quad (3.6.4)$$

The function $f(t)$ together with a sample obtained from a dynamic Monte-Carlo simulation for a double-junction system are shown in figures (3.14 & 3.15). In this case the junction was initially biased at a point in X and a steady state is assumed to exist. The steady state ensures the presence of an excess single electron at M and the state is therefore $S(0)=1$. At $t=0$, the bias conditions are changed to a point in Y. Figure (3.14) shows the evolution of the charges on the junctions with time. The event taking place is $T(M,R,1)$. Following the event, the charges will be described by the same set of equations, but with different boundary conditions. It is important to notice that the steady-state total charges on each tunnel junction will be less than the critical charges for the junctions, i.e. no other tunnel event will take place and the system will relax at the new steady state at Y which is $S=0$.

Let the system be found at the state $S(0)=0$ and the system be initially biased at Y. If the conditions are changed to a point in X, the charges will evolve according to equation (3.6.1). Figure (3.16) shows a typical behaviour of the charges. The event taking place is $T(L,M,0)$. No other event is expected to take

place, as the charging curves following the event will be confined to the region below the critical charges of each junction.

These curves indicate that the turnstiling action can be achieved by adding the resistive components to the bare turnstile circuit. The disadvantage of the resistive components in the circuit will be the a reduction in the operational frequency.

Figures (3.15 and 3.17) show the distribution of the time that elapses before the event $T(M,R,1)$ or $T(L,M,0)$ occurs. Such functions are important in designing and assessing the performance and reliability of SEE circuits. For the turnstile action, a square wave may be applied at the gate (alternates between X and Y). It is important to set a minimum period for these pulses to ensure a certain error rate (r per pulse). The error rate is related to the distribution function by,

$$1 - r_i = \int_0^{T_o} f_i(\tau) d\tau \quad (3.6.5)$$

where T_o is the duration of the pulse. If $R \gg R_t$ and C_o is of the same order as C , then:

$$f_i(t) \approx z \cdot t \cdot \exp\left(-\frac{z}{2}t^2\right) \quad (3.6.6)$$

where $z = -\frac{1}{RR_tC^2} \left(A + \frac{BC_T}{C_o} \right)$, A and B are the constants of equation (3.6.1).

Then equation (3.6.6) reduces to the form:

$$r_i = \exp\left(-\frac{z}{2}t_o^2\right), \quad t_o \ll RC \quad (3.6.7)$$

where t_o is the time spent above the Coulomb barrier.

3.7 Master Equation:

The models described so far in this chapter are applicable at zero temperature. These models do not take into account the thermal fluctuations of the

charge. The charge fluctuations of possible thermally activated events can be taken into account by previous models if the distributions of charges at different junctions are known. Likharev (1987) suggested a general equation to represent the state of any single-electronic system. The model relates the state of the system to the other states through the transition rates and the density of other states.

The Master-Equation model used to describe the single junction in the previous chapter can be extended to cover the double-junction and multi-junction systems.

Let the turnstile be coupled to the sources by external resistances satisfying the relations:

$$R_1, R_2 \gg R_Q$$

and let the tunnel resistances be high, $R_t \gg R_Q$. Under these conditions the charges on each junction will evolve slowly with time and can be regarded as well-defined variables. Let $s_i(Q, t)$ be the distribution of the charge at any time on the i -th junction. Each junction can be regarded as a single isolated junction and can then be described by the Master Equation:

$$\frac{\partial s_i}{\partial t} = \frac{s_i}{RC} + \left(\frac{Q}{RC} - I_i(t) \right) \frac{\partial s_i}{\partial Q} + D_i \frac{\partial^2 s_i}{\partial t^2} + F_{Ti} \quad , i=0,1,2 \quad (3.7.1)$$

At any time t , the total average charges on the junctions are given by:

$$\bar{Q}_i(t) = \int Q s_i \cdot dQ \quad (3.7.2)$$

Simple circuit analysis gives:

$$\begin{aligned} I_1(t) &= \left(V + V_s - \frac{\bar{Q}_1}{C_o} - \frac{\bar{Q}_2}{C} \right) / R \\ I_2(t) &= \frac{1}{R} (2V - (\bar{Q}_1 + \bar{Q}_2) / C) - I_1 \\ I_o(t) &= I_1 - I_2 \end{aligned} \quad (3.7.3)$$

These currents imply that the three equations (3.7.1) are coupled differential equations. The tunnelling terms, F_{Ti} , are similar to the single junction terms.

3.7.1 Charge Fluctuations:

The quantity D_i in equation (3.7.1) is the steady-state variance of the charge at (junction i) around its mean value. The quantum Langevin approach can be used to determine these fluctuations. Let the inductance of each arm of the double-junction system shown in figure (3.9) be equal to L. Let i_0, i_1 and i_2 be the instantaneous currents due to the noise generated in the resistive elements. Then:

$$-v_{nl}(t) = L\ddot{q} + R\dot{q}_1 + \frac{q_1}{C} + \frac{q_0}{C_0} \quad (3.7.4)$$

$$v_{n2}(t) = L\ddot{q}_2 + R\dot{q}_2 + \frac{q_2}{C} - \frac{q_0}{C_0} \quad (3.7.5)$$

where $v_{n1}(t)$ and $v_{n2}(t)$ are the instantaneous noise voltages. The two noise sources are independent and may be treated separately. Fourier transforming the above equations and ignoring the inductive elements, the total charge fluctuations are found to be equal to:

$$\begin{aligned} \langle q_{1,2}^2 \rangle &= \int_0^\infty \frac{C^4 S_v(\omega) d\omega}{(1+C^2 R^2 \omega^2)(C_T^2 + C^2 C_o^2 R^2 \omega^2)} + \\ &\quad \int_0^\infty \frac{C^2 \{(C+C_o)^2 + C^2 C_o^2 R^2 \omega^2\} S(\omega) d\omega}{(1+C^2 R^2 \omega^2)(C_T^2 + C C_o^2 R^2 \omega^2)} \end{aligned} \quad (3.7.6)$$

where $S_v(\omega)$ is the noise power spectral density of a single source, given by:

$$S_v(\omega) = \hbar \omega R \times \coth(\hbar \omega / 2k_B T) / \pi$$

If the external resistances are high and satisfy the relation:

$$\hbar/RC \ll k_B T$$

then the integral in (3.7.6) can be evaluated by contour integration in the complex domains. It is approximately given by,

$$\langle q_{1,2}^2 \rangle = \frac{\hbar}{8R(1+\beta)} \left[(2+\beta) \cot\left(\frac{\hbar}{2k_B T R C}\right) + (2+3\beta) \cot\left(\frac{\hbar(1+2\beta)}{2k_B T R C}\right) \right] \quad (3.7.7)$$

where $\beta = C/C_o$. In the classical high temperature limit, the charge fluctuations will reduce to:

$$\langle q_{1,2}^2 \rangle \approx k_B T C \frac{1+\beta}{1+2\beta} \quad (3.7.8)$$

Clearly, the fluctuations of the charge variable in the tunnel junctions of the double-junction system are less than the fluctuations in the single junction case ($k_B T C$). In the limit $\beta \rightarrow \infty$ corresponding to two series-connected tunnel junctions and no capacitance to ground, $C_0=0$, equation (3.7.8) gives $D=k_B T C / 2$.

Summary:

The transistor action has been demonstrated using the double-junction system. Problems will arise if the double-junction structure is to be used as a memory element. Resistive elements in the circuit will help solve some of these problems, at the cost of additional delay and lowered operational frequency.

The Finite-State Machine model has been presented and suggested to model the State-Input-Transition relationships in digital single-electronic systems.

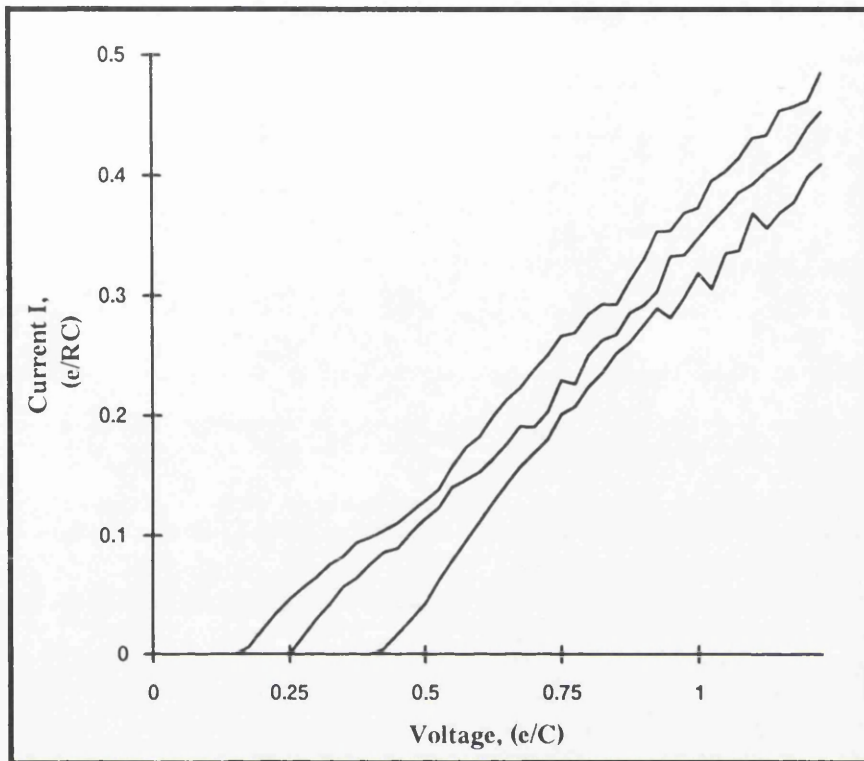
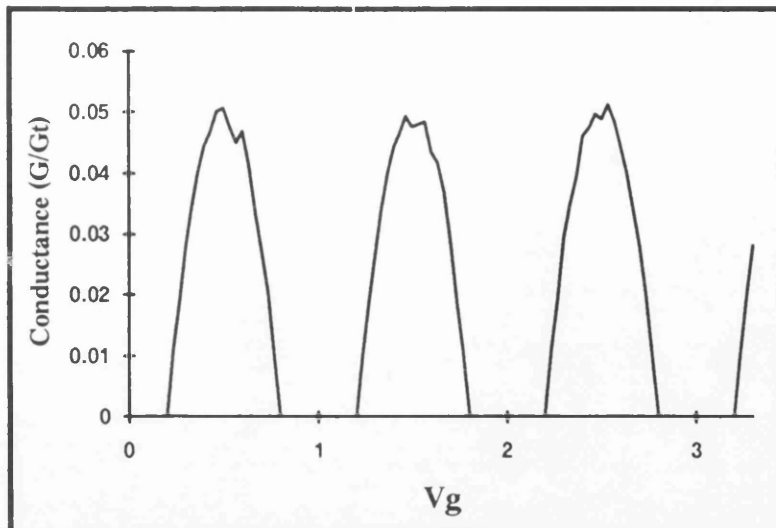
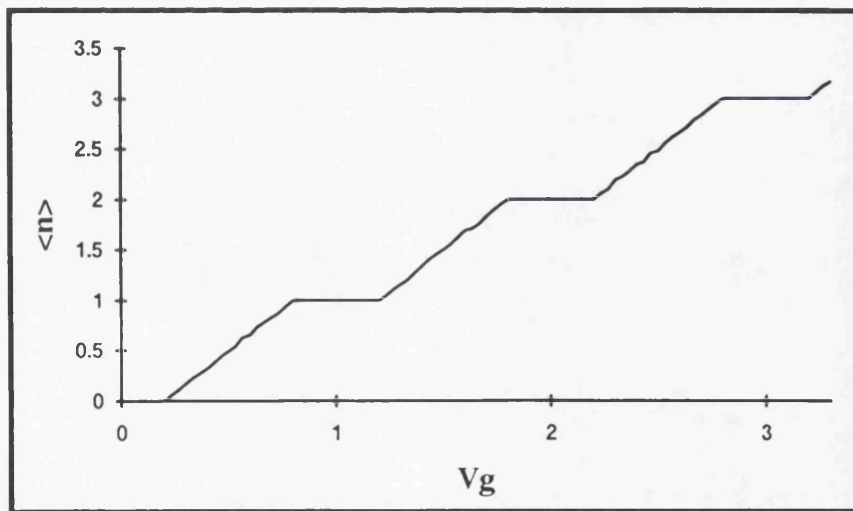


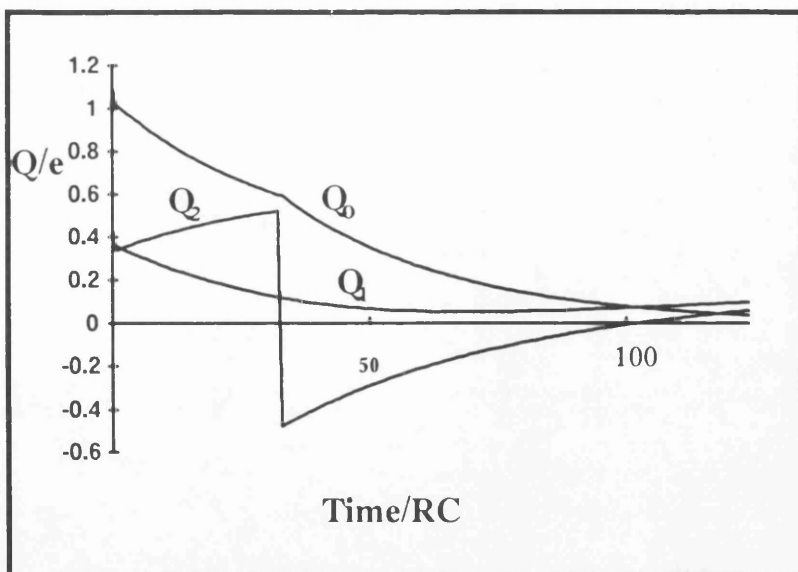
Figure (3.11):I-V characteristics of a double-junction system obtained from static Monte Carlo simulations. No. of electrons allowed to exit = 500, curves upwards correspond to $C/C_o=5,1,0.5$.



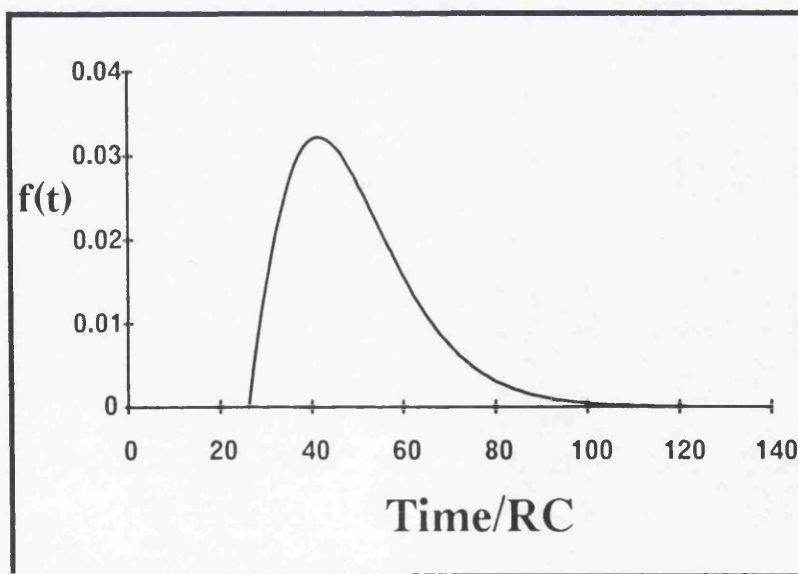
Figure(3.12):Oscillation of the line conductance of a double-junction system with gate voltage, parameters are: $C/C_0=1$, $V=0.1 e/C$



Figure(3.13):Average number of excess electrons at the central electrode of a double-junction system: $C=C_0$, $V=0.1 e/C$.



Figure(3.14): Evolution of charges with time. The event taking place is $T(M,R,1)$, when bias voltages change from a point in X to a point in Y. Parameters are: $(C/C_o=1, R_s/R_t=100)$



Figure(3.15): Distribution of the time that elapses before the event $T(M,R,1)$

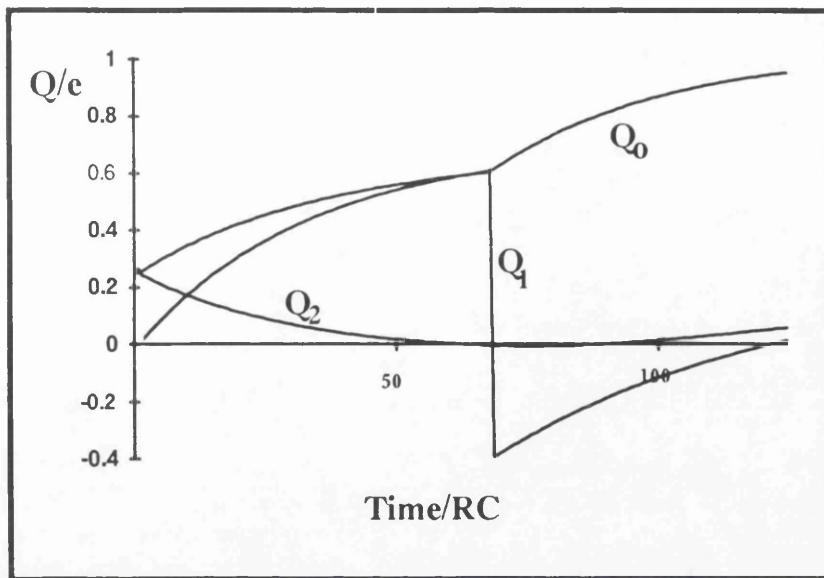
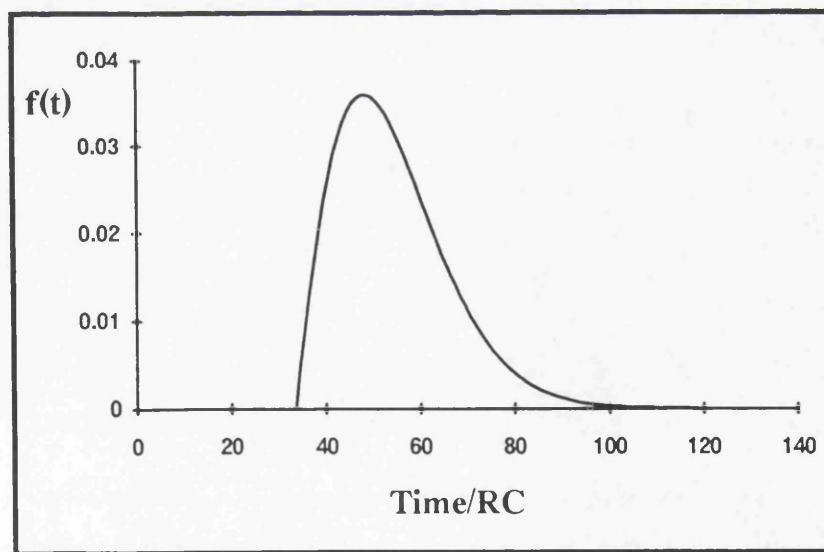


Figure (3.16): Evolution of charges with time when the bias point is changed from a point in Y to a point in X. The event taking place is $T(L, M, 0)$. Parameters are $(C/C_0=1, R_s/R_t=100)$.



Figure(3.17):Distribution of the time elapsing before the event $T(L, M, 0)$.

Chapter (4)

Single-Electronic Systems

4.1 Introduction:

This chapter is intended to be an extended introduction to the next chapter where an exact solution of some of the problems addressed will be presented. In the following sections, some multi-junction systems are described and the conventional techniques used to model these systems are briefly outlined. Some modelling techniques have already been described and applied to the double-junction structure.

4.2 The Single-Electron Pump:

It was shown in the previous chapter that the double-junction system may be operated as a switching device and can also be used as a memory element in digital systems. The problems arising when clocking electrons in and out of the central electrode may be eliminated by adding a third tunnel junction to the double-junction structure. The electric pump is basically a shift register where the clocking of electrons through the device is achieved by two coupled gate voltages operated in a controlled sequence.

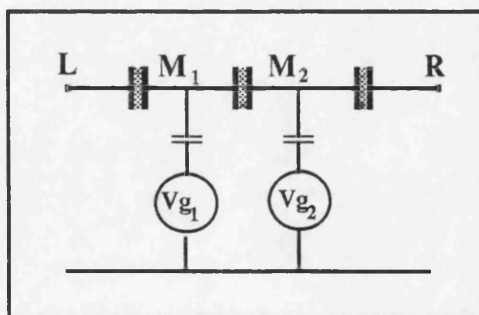


Figure (4.1): The Single-Electron Pump

Starting with the device at the state $(0,0)$, where the integers correspond to the number of excess electrons at M_1 and M_2 respectively, the voltage levels at V_{g1} and V_{g2} are first selected such that the condition for the event $T(L, M_1, (0,0))$ is

satisfied while all other events are blocked. In phase II of the 'pumping' action the system will force the event $T(M_1, M_2, (1,0))$ and in the final stage the electron will pop out at R as a result of the event $T(M_2, R, (0,1))$. Repetition of this sequence gives rise to a stream of electrons at node R at a rate that is determined from the controlled sequence. The $V_{g1}-V_{g2}-V$ areas of the proper pumping action and the error rates were studied by Barker et al (1993) using the standard Linear Programming methods and the Monte-Carlo techniques. This three-phase device was shown to have a high frequency advantage compared to the two-phase device (turnstile), but it has smaller area of legal operation.

Geerligs (1990) achieved the shift-register action by applying a rf signal (4-20MHz) to the central island of a four-junction array. A current of $I=ef$ was observed indicating that exactly one electron per rf cycle passes through the structure. Kouwenhoven et al (1991) fabricated a structure in which a single quantum dot is coupled to a 2-DEG by two tunnel barriers. The structure is effectively a double-junction system. The turnstiling action was achieved by modulating the heights of the barriers using two phase-shifted rf signals (5-20MHz). It was demonstrated that an integer number of electrons pass through the dot in each rf cycle, depending on the applied voltage level.

A four-junction shift register has been proposed by Barker et al (1992). This device is a three-phase register in which the electron will be localised at the inner three electrodes before it is finally received at the other side of the device.

4.3 Arrays of Tunnel Junctions:

A linear array of series connected tunnel junctions has features which are similar to a double-junction system in that the flow of charges through the array can be controlled by a single gate point. These arrays are of special interest because the circuit equations can be exactly solved in the limit of long homogeneous arrays.

The Coulomb blockade of tunnelling was first observed in thin granular metal films which are characterised by a random distribution of tunnel junctions. Sheng et al (1973) used a linear array of tunnel junctions to model such granular structures. It was argued that the optimum conduction path through the film may be deduced from the grain dimensions and the ambient temperature. It was shown that the film resistance increases exponentially with $T^{-0.5}$.

In the last few years it has become possible to fabricate tunnel junctions with well-defined dimensions. Overlap tunnel junctions having sizes down to $0.06(\mu\text{m})^2$ and 20-25 Å thick were fabricated by Delsing (1990) by evaporating aluminium at two different angles through a lift-off stencil defined by electron-beam lithography and a double-layer resist. The junctions have capacitances of the order of 10^{-16} - 10^{-15} F. This technique is limited to relatively large junction capacitance and consequently low operating temperatures ($T_c < 10$ K).

Recently, Schottky islands and dot arrays have been fabricated at Glasgow (Barker et al (1992)). These new structures have ultra-small capacitances ($< 10^{-17}$ F) with critical temperatures in excess of 60 K and scalable to much larger than the room temperature.

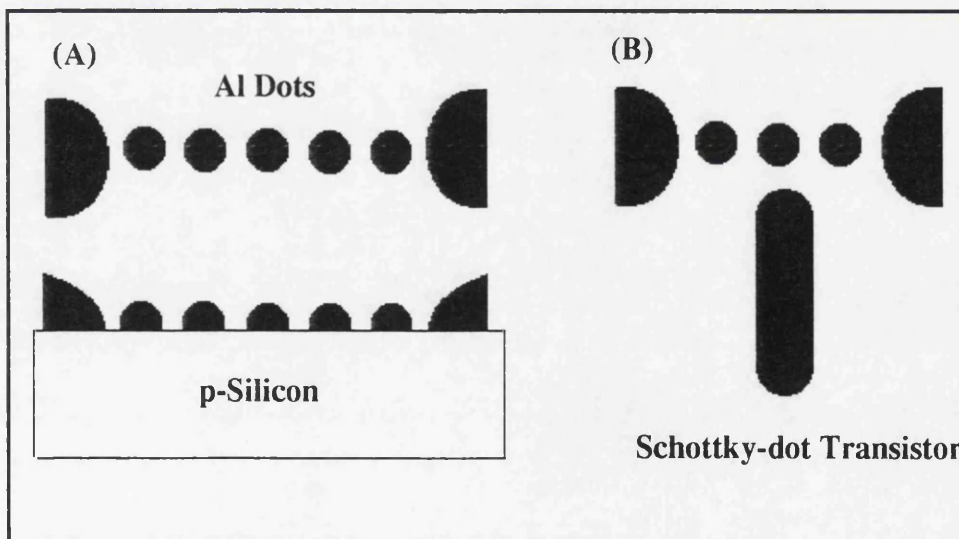


Figure (4.2): Schottky-dot structures

Figure (4.2.A) shows a schematic representation of a 40nm diameter line of Al dots grown on a p-Si substrate and having an inter-dot separation of 12-15nm. Multiple arrays of Schottky dots of similar dimensions have also been fabricated. This technology is expected to provide a means of building a vast range of single-electronic devices and systems. Figure (4.2.B) shows a possible arrangement to achieve the transistor action. Other applications including the turnstile, inverter and other simple logic gates have been suggested as well, Barker (1993).

4.4 Modelling the Multi-Junction Systems:

The devices investigated so far (single junction, turnstile and the pump) are relatively simple, yet they are sensitive to variations of the parameters of the junctions and operating conditions, e.g. ambient temperature, bias levels and charges trapped in the vicinity of the junctions. Increasing the complexity of the systems at hand, e.g. by adding more junctions or modifying the connectivity of these devices, results in new devices or systems with different characteristics. These features of the general class of the single-electronic systems impose the need of a unified frame-work within which all such systems can be studied.

The development of single-electronic systems requires the proper design of the junctions in order to achieve the desired capacitance values. The direct measurement of the ultra-small capacitances involved in these systems is very difficult. Asenov (1993) used a parallelised 3-D Poisson solver to estimate the parameters of the Schottky structures shown in figure (4.2), see also Roy et al (1993).

4.5 Single-Electron Solitons:

The dynamics of electron transfer in a single-electronic system are studied here with reference to the long array of tunnel junctions, the equivalent circuit of which is shown in figure (4.3). The array is assumed to be homogeneous and infinitely long. Let $\{\phi\}$ denotes the set of potential values at the nodes of the

array. The nodal-voltage equations in the presence of the excess charges at some nodes can be written as:

$$\phi_1 = V_L \quad (4.5.1A)$$

$$\phi_{N+1} = V_R \quad (4.5.1B)$$

$$-C(\phi_{i+1} - \phi_i) + C_o\phi_i + C(\phi_i - \phi_{i-1}) = Q_i \quad (4.5.1C)$$

where Q_i is the total excess charge at the i -th node.

The set of equations (4.5.1) is valid for long as well as short homogeneous arrays of tunnel junctions. The inhomogeneous arrays can be described by a similar set of equations, see e.g. Amman et al (1989).

Consider a long array fed at one end, e.g. $V_R=0$, and $V_L \neq 0$. The potential profile along the array at any state is obtained by solving (4.5.1). Equivalently, the potential at any node due to a single source can be evaluated, then the superposition theorem is used to find the total potential distribution (sources include the excess charges at different nodes and the bias sources). Let a single unit electronic charge ($\pm e$) be located at the node $i=k$ that lies away from the edges of the array. Equations (4.5.1) can now be written as:

$$C(\phi_{i+1} + \phi_{i-1} - 2\phi_i) - C_o\phi_i = \pm e\delta_{ik} \quad (4.5.2)$$

This is a discretised form of the following differential equation:

$$C(\Delta x)^2 \frac{\partial^2 \phi}{\partial x^2} - C_o\phi = \pm e\delta(x - x_k) \quad (4.5.3)$$

where Δx is the step size, $x=i\Delta x$. It is not difficult to show that the solution of the differential equation (4.5.2) is:

$$\phi_i^{(k)} = \pm \frac{e}{2Cs \sinh \lambda} \exp(-\lambda|i-k|) \quad (4.5.4)$$

$$\text{where: } \lambda = \cosh^{-1} \left(1 + \frac{C_o}{2C} \right).$$

From (4.5.3) and (4.5.4) it is clear that the excess charge at $i=k$ represents a soliton with length λ (in units of number of junctions) with total charge of $\pm e$. The centre of the soliton is located at $i=k$. The soliton causes a substantial polarisation

of the junctions that lie within λ away from the centre. It is also straight-forward to show that the total energy of the single soliton is given by: (see e.g. Bakhvalov (1989))

$$E_{ss} = \frac{e^2}{2C_{eff}}, \quad C_{eff} = (C_o^2 + 4CC_o)^{1/2} \quad (4.5.5)$$

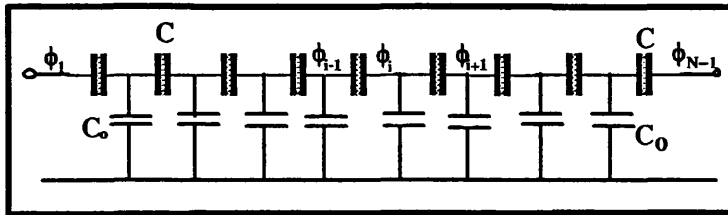


Figure (4.3): Equivalent circuit of the multi-junction array

The potential induced at any node due to the voltage source can also be obtained as:

$$\phi_i^{(source)} = V_L \exp(-\lambda i) \quad (4.5.6)$$

and the total potential at any node in the presence of any soliton distribution is evaluated as:

$$\phi_i = \phi_i^{(source)} + \sum_k n_k \phi_i^{(k)} \quad (4.5.7)$$

where n_k is the number of solitons or anti-solitons at node k (assumed positive for solitons and negative for anti-solitons if $\phi_i^{(k)}$ is evaluated for a soliton), and k is assumed to lie far away from the edges of the array.

From the above analysis it becomes clear that a soliton or anti-soliton at any node will be affected by all other solitons and anti-solitons together with the applied voltages; and therefore, the tunnelling events will depend on all these factors. The tunnelling rate from node i to node $i\pm 1$ can be obtained using the quantum golden rule as:

$$\Gamma_{i,i\pm 1} = \frac{G}{e^2} \frac{\Delta}{1 - \exp(-\Delta/k_B T)} u(\Delta) \quad (4.5.8)$$

where $\Delta = eV_{i,i\pm 1} - \frac{e^2}{2C_{i,i\pm 1}}$, $V_{i,i\pm 1} = \phi_{i\pm 1} - \phi_i$, $u(x)$ is the unit step function, G is the tunnel conductance of the junction and $C_{i,i\pm 1}$ is the total capacitance between the neighbouring nodes i and $i\pm 1$.

Successive injection of electrons into the array is achieved for voltages greater than a threshold value which is determined from the relation:

$e|V_{1,2}| - \frac{e^2}{2C_{1,2}} > 0$. This assumes an array with an initial soliton distribution of $\{n\} = \{0\}$ and thus the threshold voltage is:

$$V_{th} = \frac{e}{2C} (\exp(\lambda) - 1)^{-1} \quad (4.5.9)$$

Relation (4.5.9) was found to be in excellent agreement with the threshold voltage obtained from (3.3.4) for long arrays ($N > 10$). The agreement is quite reasonable (within less than 10%) for arrays with N as small as five junctions.

4.6 Monte-Carlo Modelling:

It was shown in the previous section that it is possible to analytically describe (approximately) the homogeneous long array of tunnel junction by a set of differential equations, which are exactly solvable. This is, in general, not possible for inhomogeneous arrays and other configurations, and the Monte-Carlo techniques offer the obvious route to model such structures. In this section, a brief description of the Monte-Carlo method is given and some of the results obtained from such simulations will be discussed. Full description of the Monte-Carlo model as applied to a linear array of junctions is given by Amman et al (1989) and Bakhvalov (1989). The main features are:

- the state of the particular system under study at any time is represented by the set of integers, $\{n\}$, corresponding to the number of excess electronic charges at all nodes,
- the nodal voltages, $\{\phi\}$, are determined from the circuit equations,
- the tunnel rates of all possible events are calculated using (4.5.8),
- the time that elapses before the next tunnel event is determined from the tunnel rates; exploiting the exponential distribution of the time between events and the memoryless property of the system,
- the soliton distribution, $\{n\}$, is modified following any event, and
- the whole process is repeated for a time long enough to allow the steady-state properties to be extracted from the collected statistics.

Figure (4.4) shows the I-V curves of a homogeneous 8-junction array for different C/C_o ratios at $T=0$ K. The observed critical voltages are in good agreement with relation (4.5.9). In figure (4.5), the transfer characteristics of a 3-junction system are shown. The plots of the average number of excess electrons observed at the 'internal' nodes indicate that the oscillations correspond to the addition of exactly two electrons to the system. Monte-Carlo simulations have also shown that linear arrays with N tunnel junctions will exhibit a V_g period that corresponds to the addition/removal of exactly $(N-1)$ electrons to/from the system. For a long homogeneous array, the change in the potential in a typical period is given as:

$$|\Delta\phi| = \frac{e}{C_{eff}} \sum_{i=-\infty}^{\infty} \exp(-\lambda|i|) = \frac{e}{C_{eff}} \coth\left(\frac{\lambda}{2}\right) \quad (4.6.1)$$

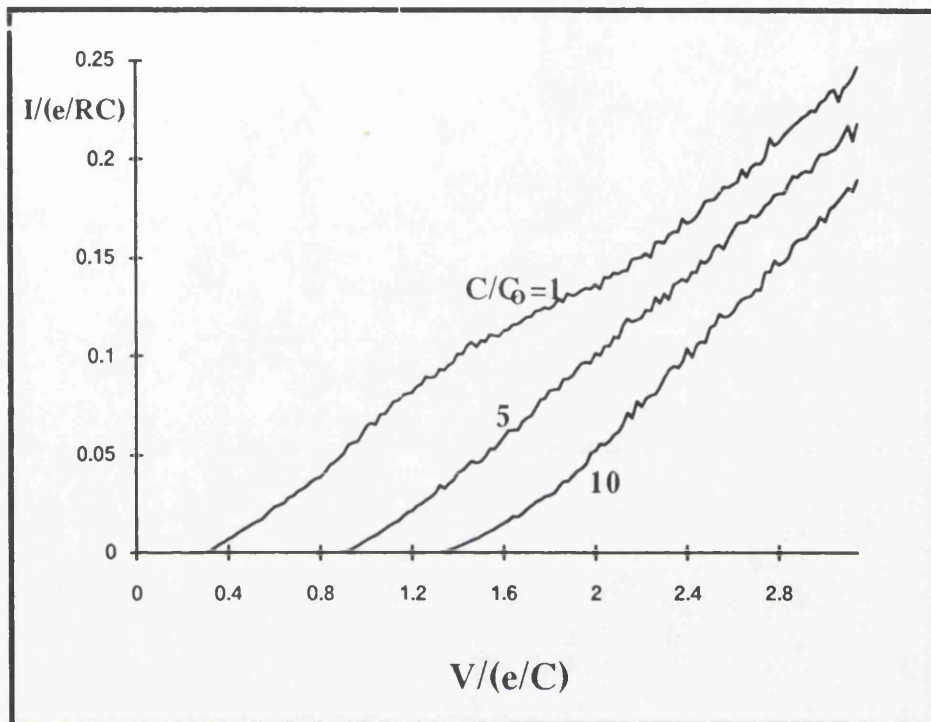
and this value is equal to the change of the gate voltage in that period. Substituting the value of λ defined in (4.5.4) in (4.6.1), it follows that:

$$|\Delta V_g| = e/C_o \quad (4.6.2)$$

Monte-Carlo simulations have also shown that the soliton structures are normally formed and destroyed in some regular patterns; at more or less regular time intervals. This gives rise to regular voltage patterns across each junction.

Summary:

Soliton states do exist in single-electronic systems. Elements of the capacitance matrices representing such systems should be properly estimated and the full 3-D Poisson solvers are needed in most cases. Exact analytical solutions exist for a limited class of systems and Monte-Carlo methods have been extensively used to model the single-electronic systems.



Figure(4.4): I-V characteristics of an 8-junction array calculated using the static Monte-Carlo methods: $V_g=0$, $C/C_0=1,5,10$.

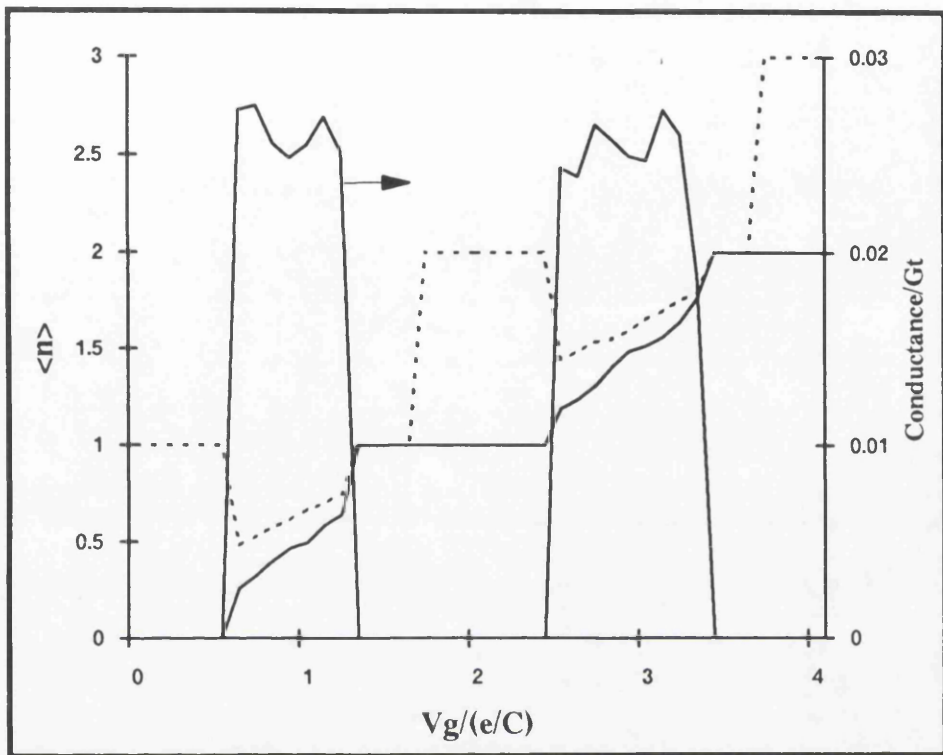


Figure (4.5): Dependence of the average number of excess charges at the inner electrodes of a three-junction array and the variation of the line conductance with the gate voltage.

Chapter (5)

Traffic Theory

5.1 Introduction:

The Monte-Carlo simulation method described in chapter (4), as applied to simulating the single-electronic systems, monitors the behaviour of the stochastic tunnel events and traces the evolution of the whole system. The data obtained from long observations is then used to produce representative measures for the behaviour of the system.

Monte-Carlo simulations have revealed that the conduction process through a single-electronic system passes through a finite set of soliton states. These soliton states and the relationships between them are strongly dependent on the bias conditions together with the parameters of the system at hand. It was also observed that the stationary properties of the single-electronic system can be determined if the densities of the different soliton states that occur during the conduction process are known. It is an easy task to list the set of active states from a Monte-Carlo simulation and to trace the relationship between the different states as well.

The objective of this chapter is to look into some analytical routes to determine the distribution of the states without resorting to the Monte-Carlo methods. Some applications are given to show the efficiency of the new technique.

5.2 Traffic Model for Tunnelling Dynamics:

The system studied in this chapter is a network of tunnel junctions; which can be a double-junction structure, a linear array of tunnel junctions, a two-dimensional array of tunnel junctions or any other combination of tunnel and non-tunnel junctions, see figure (5.1).

The state of the system at any time may be described by the set of nodal voltages $\{V_i(t); i=1,2,\dots,N_n\}$ where N_n is the number of physical nodes in the

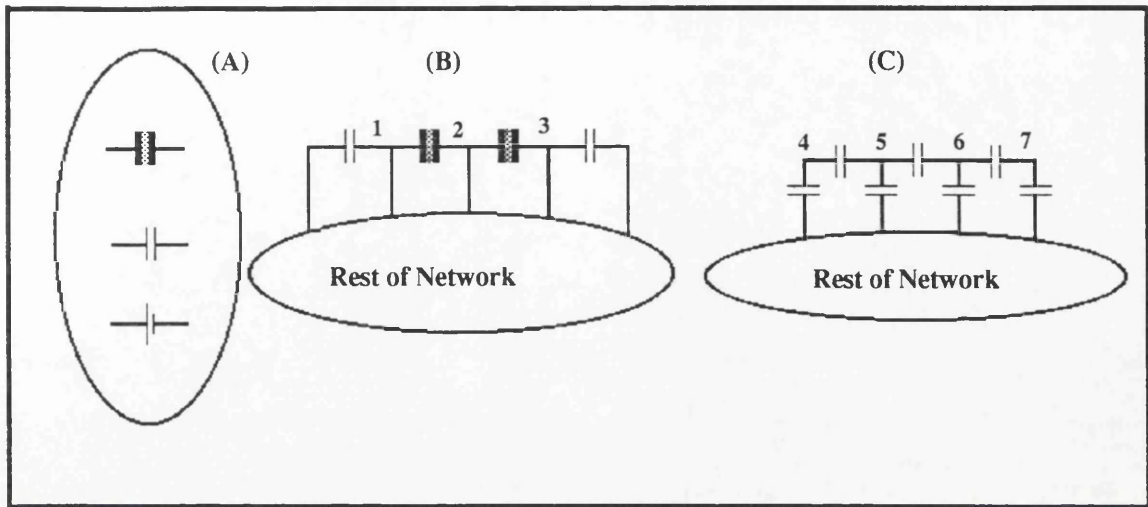


Figure (5.1): Single Electronic Circuits: A: Circuit elements, B: Examples of tunnel nodes (1,2,3) & C: Examples of non-tunnel nodes (4,5,6,7).

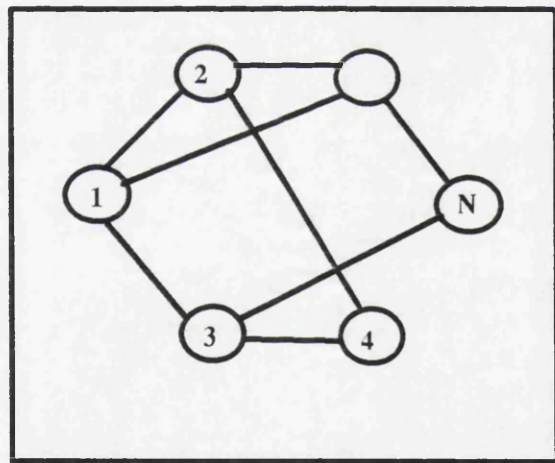


Figure (5.2): Traffic Model for the flow of electrons between tunnel nodes: Circles represent tunnel nodes and lines are bilateral.

system. Alternatively, the state of the system may be represented by a state-vector corresponding to the set of the number of excess electrons present at the nodes at the specified time:

$$\psi(t)=\underline{n}=\{n_i(t); i=1,2,\dots,N\}, n_i(t) = \text{integer} \quad (5.2.1)$$

where N is the number of nodes capable of accommodating excess electrons. Let the set of nodes through which electrons can tunnel be denoted by D . A node in the network is considered to be a tunnel node if at least one tunnel junction is connected to that node. Thus, the node will be able to accommodate excess charge, i.e. the total charge at that node (at some time during the steady-state behaviour under some bias conditions) may be different from zero. It is clear that the set D is essentially a subset of the physical nodes in the system and therefore, $N \leq N_n$.

The two ways of representing the state of the system are equivalent, because the nodal voltages are linearly related to the bias voltages and excess charges at the tunnel nodes. This is clearly reflected from the analysis given in the previous chapter in connection with the linear array of tunnel junctions, see in particular equation (4.5.7).

The Monte-Carlo method assumes that the charge relaxes to the (new) steady state in a short period of time, $\tau_r < \tau_b$; where τ_b is the time to the next tunnel event. The relaxation time depends on the low-frequency impedance of the circuit. Let the total impedance seen by a single junction in a multi-junction system be $Z(\omega)$. The relaxation process will be fast if $Z(\omega)$ is small for $\omega < eV/\hbar$ where V is the p.d. across the junction just before the tunnel event. The charges on the junctions and the various tunnel rates will be constant as long as the system is found at the state \underline{n} .

The tunnelling conductances of all junctions are taken to be small such that the system will relax to the steady state well before any tunnel event may take place. It implies that there is no correlation between successive tunnel events.

During any period of time, while the system is at $\psi=\underline{n}$, electrons may tunnel (with some probability that can be equal to zero) from the i-th tunnel node to the j-th tunnel node if there is a single tunnel junction between the two nodes (this condition will be relaxed when the charge-macroscopic quantum tunnelling is taken into account). Tunnelling can occur between the nearest neighbouring nodes (elements of the set D).

It is convenient to treat all tunnel and non-tunnel nodes in a unified way. This can be achieved by defining the $(N_n \times N_n)$ node connection matrix ,X, such that:

$$x_{ij} = \begin{cases} 1 & ; \text{node}_i \& \text{node}_j \text{ are connected via a tunnel jn} \\ 0 & ; \text{otherwise} \end{cases} \quad (5.2.2)$$

In a single-electronic system with the connectivity as defined in (5.2.2), electrons can tunnel from node i to j, or vice versa, if these nodes are connected via a single tunnel junction. This is mathematically represented by the relation:

$$x_{ij}=x_{ji} \quad (5.2.3)$$

Given the node connection matrix, the tunnel nodes are those satisfying the following condition:

If $\exists j$ such that $x_{ij}=1$ then node i is a tunnel node, and relation (5.2.3) implies that node j is a tunnel node too.

In figure (5.2), each tunnel node is represented by a circle. Two nodes are joined by a line if the connection matrix element, x_{ij} , is equal to unity; indicating that electrons may tunnel between these nodes. Each line connecting two nodes is a bilateral line due to the property (5.2.3) above.

Let a tunnel event takes place from node i to some other tunnel node in the system. The probability that the electron is destined to node j is given by:

$$p_{ij}(\underline{n}) = \frac{\Gamma(i, j, \underline{n})}{\Gamma_i(\underline{n}_i)} \quad (5.2.4)$$

where

$$\Gamma_i(\underline{n}) = \sum_{k:x_{ik}=1} \Gamma(i, k, \underline{n}).$$

Relation (5.2.4) is an important relation that is extensively used by the Monte-Carlo simulators. It was shown in chapter (3) that the *collective* tunnelling process is a Poisson point process, having a total rate of occurrence -at any state- that is equal to the sum of the individual tunnel rates at that state. The quantity $\Gamma_i(\underline{n})$ is the throughput at the node at the given soliton state and represents the outgoing traffic from node i at that state. On the other hand, the same node -at $\psi = \underline{n}_i$ - receives incoming traffic given by the sum of all traffic destined to this node, i.e.

$$\Lambda_i(\underline{n}) = \sum_{k:x_{ik}=1} \Gamma(k, i, \underline{n}) \quad (5.2.5)$$

The model described above is similar to a typical Traffic Model, having the following general features:

- a. the entities -electrons- move stochastically between a finite set of centres, which are the tunnel nodes of the system,
- b. on arriving at a node, the entities join a queue and wait for some sort of service,
- c. the tunnel nodes serve as service centres, at which the electrons receive some service; which in effect delays the movement of these electrons,
- d. number of electrons is large and conserved,
- e. no external entities are allowed to join the activities,
- f. service is provided to entities in a random way.

In the conventional Traffic Models, entities may depart from a node only if that entity has arrived to that node some time in the past; i.e. empty nodes will not contribute to the departure process in any way. In contrast, the tunnel nodes always contain a large number of conduction electrons, any of which can contribute to the 'Traffic' process. This implies that the queues are always 'full'

even if that node has already 'served' n electrons and is left with a total charge of $+ne$. The departure process at a node is affected by the varying 'service rate' (the tunnel rate from a node to another) which is a function of the state of the whole system. Most systems that are represented by Traffic Models have 'service rates' at the nodes that are load-dependent and are not affected by loads at other nodes. For the model under study, the departure rate at a node is dependent on the load at all nodes in the system.

The nodes do not distinguish between the electrons in the 'queue', i.e. the system has no way of keeping a record of the history of the electrons that arrive at that particular node. Thus, a random selection queue discipline is used to provide service to the incoming electrons, Schwartz (1977).

At any state $\psi = \underline{n}$, the arrival process -as seen by any node- is a Poisson point process; and the service time (time between tunnel events) at that node has a negative exponential distribution. This statement assumes that any departure or arrival event will not affect the two processes in any way. This is not true for the systems under study because any event will change the state of the system and will modify all tunnel rates in the system. However, if the system is kept frozen at a particular state, then the arrival and departure processes will be of the Poisson nature.

In Traffic Theory, the traffic intensity factor defined as $a_i = \Lambda_i / \Gamma_i$ represents a measure of stability at node i . Stability is attained at node i during the steady-state behaviour if the condition $a_i < 1$ is satisfied while the queue size will grow without limit if $a_i > 1$. For the model under consideration this factor has a different role: $a_i(\underline{n}) > 1$ indicates that an electron is more likely to tunnel into this node because electrons are arriving at this node at a rate that is greater than their departure rate. The other case, $a_i(\underline{n}) < 1$, implies the tendency of the node to lose an electron to some other node in the system.

The above analysis assumes that the system is stationary at a state, \underline{n} , and the properties of the system do no change with the flow of traffic. In fact, any

tunnel event will change the state of the system and all state-dependent variables, e.g. Γ 's, will be affected. This is analogous to the adaptive routing policy in communication systems where the state of any node is (frequently) distributed to all other nodes and the routing policy is changed accordingly, Schwartz (1977).

So far, only electrons are assumed to exist, as jobs, in the network. In fact, electrons and holes coexist inside the network. If there are n_e electrons in the network at time t , then there must be the same number of holes in the network to maintain charge neutrality, i.e. $n_h = n_e$. Theoretically speaking, the system can sustain an infinite number of electrons and the same number of holes. One then speaks about a system of two classes of jobs; the traffic dynamics of the two types of entities are correlated; created or annihilated depending on the sort of event undertaken. Strangely, the two classes of jobs are created within the network, and destroyed by simple collision inside the network too. Tackling the traffic problem via this route seemed confusing and leading to more problems and questions than to simplifications and solutions.

Looking back at the simple model for system dynamics, it is reiterated that the occurrence of any tunnel event, while the system is found at state ψ will terminate that state and will give birth to a new one. This implies that the system will be described by a different state-vector each time a tunnel event occurs. Energy considerations show that the set of state-vectors is a finite set, which can be represented by:

$$\{\psi\} = \{n_1, n_2, \dots, n_M\} \quad (5.2.6)$$

and M is the number of legal stationary soliton states ($M \geq 1$).

The finite number of states and, furthermore, the regular state patterns formed during a conduction process in a single-electronic system was observed in a Monte-Carlo simulator. The set of active states and the relationship between these states is primarily dependent on the bias conditions applied to the system. If the bias conditions change while the system is occupying the state ψ_{init} , the system will then pass through some transient states $\{\psi_{\text{tr}}\}$ not all of which may be

attainable during the subsequent steady-state behaviour. The new bias conditions may also lead to a static state; and the system will therefore stay forever in that static state. It is therefore important to discover the intermediate states together with the stationary states (if these states do exist). A unified algorithm will be discussed in section (5.8).

Define the occupancy (density) of a state to be the proportion of time this state is occupied. It then defines the probability of finding the system at that state. Let the occupancy of the legal soliton state ψ_i be denoted by P_i . All stationary properties of the network can be calculated in terms of the occupancy vector $\{P\}$. The current passing between the tunnel nodes labelled ℓ and m is given as the sum of the contributions of all legal states, i.e.

$$I_{lm} = e \sum_{i=1}^M P_i \{ \Gamma(l, m, \psi_i) - \Gamma(m, l, \psi_i) \} \quad , x_{\ell m} = 1 \quad (5.2.7)$$

The average number of excess electrons at node ℓ is given by:

$$\langle n_\ell \rangle = \sum_{i=1}^M P_i n_i \cdot u_\ell \quad , \text{node } \ell \in D \quad (5.2.8)$$

where u_ℓ is a unit vector in the direction of node ℓ (dot product is performed). Other steady-state properties, e.g. differential conductance, may similarly be evaluated.

Relation (5.2.7) is similar to the equation used by Beenakker (1991) in the study of the properties of a single quantum dot. Odintsov et al (1991) used the above equation to describe the tunnelling dynamics in a generalised system. They applied it to the evaluation of the conductance of a double-junction system. Each junction was treated independently and assumed to be connected to an equivalent impedance.

Thus far, the problem has reduced to that of determining the set of active states and the density of each active state; which are the subjects of the following sections.

5.3 Density of Soliton States:

In equations (5.2.7 & 5.2.8), the state-dependent variables, Γ 's, can be easily calculated from the knowledge of the junctions' parameters and the changes in the free energy, see equation (4.5.8). It still remains a problem to discover the set of legal stationary states, $\{\Psi\}$, and the density of each soliton state, P_i .

The problems encountered when dealing with the Traffic Model suggested to represent the tunnelling dynamics are eliminated in the following model. The inconveniences introduced by the different classes of jobs and the theoretically unlimited number of jobs involved are removed.

During the steady-state behaviour, the system is known to form a finite set of soliton structures. The dynamics of formation and destruction of these soliton states can be described by another Traffic Model.

The soliton structures may be thought of as service centres that provide some sort of service to the system; and the system will spend some time at the state each time that state is visited. The system itself is represented by a particle or a job that travels stochastically between the service centres (states) and receives service (delay) at these nodes.

The mechanism of the conduction process via the tunnelling events leads to the formation of the soliton state ψ_i at an average rate λ_i . On the other hand, the system would emerge from the particular state, ψ_i , at a rate that is equal to the rate of entering that state, Kleinrock (1976). On leaving this state, the system may form (enter) any other soliton state. This is quite abstract; as it is known that a single tunnel event is responsible for the transition and this will limit the possible end soliton structures to a finite subset of the universal set of soliton states. Figure (5.3) shows a diagrammatic representation of the relationship between the soliton states. Each line in the diagram represents a unidirectional relationship, i.e. the legality of the transition $\psi_i \rightarrow \psi_j$ does not necessarily imply the possibility of transition in the reverse direction.

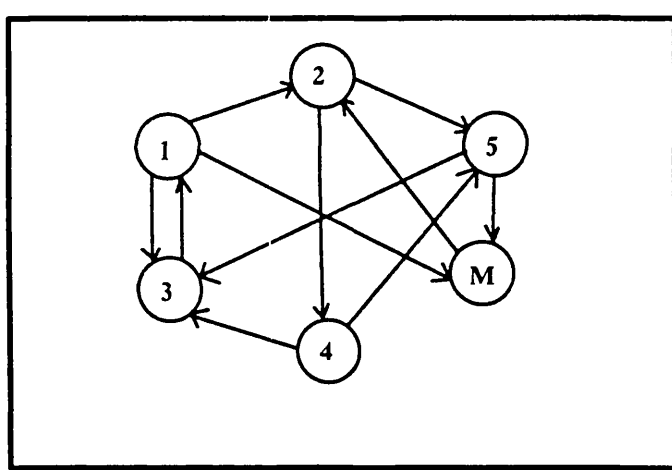


Figure (5.3): Soliton States in a Single-Electronic System. Circles represent the states and the unidirectional lines indicate the direction of possible transition.

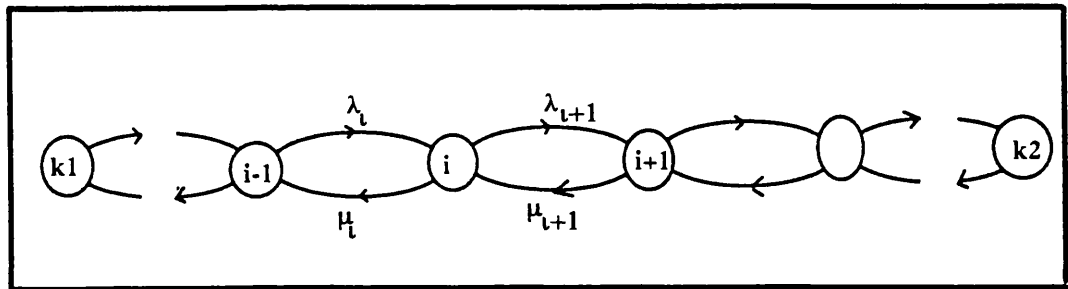


Figure (5.4): Soliton States in a Double-Junction System (The Birth-Death Model). Transition rates are shown here.

In fact, the academic infinite number of soliton states corresponds to the academic infinite number of electrons and holes mentioned in connection with the model for electron-tunnelling dynamics. The advantage of the current model over the previous one is that the dynamics of state transitions are well-understood and can be easily modelled; unlike the dynamics of a system with two correlated classes of jobs.

Let the system be found at the state ψ_i , the system will be described by this state-vector until a tunnel event takes place and the system will then be described by another state-vector. Let a single tunnel event from the tunnel node k to node ℓ be responsible for the transition from the soliton state $\psi_i = n_i$ to the state $\psi_j = n_j$. Looking at the soliton states as service centres, the departure rate from state ψ_i to state ψ_j when the system occupies state ψ_i is defined as:

$$\mu_{ij} = \Gamma(k, \ell, \psi_i) \quad , \quad x_{k\ell}=1 \quad (5.3.1)$$

which is a state-dependent variable that can be obtained from equation (4.5.8). In the spirit of (5.3.1) and exploiting the Poisson nature of tunnelling events (as being responsible for the transitions between states), the total departure rate (service rate at state ψ_i) is therefore given by the sum of the departure rates from this node (state) to all other service nodes:

$$\mu_i = \sum_{\substack{j=1 \\ j \neq i}}^M \mu_{ij} \quad (5.3.2)$$

As a result of this finite service rate at the state, the system will spend an average time of $1/\mu_i$ at ψ_i each time it visits that state. This residence time has no direct implication on the rate at which this state is visited.

The transition probability from node ψ_i to node ψ_j is obtained similar to (5.2.4) as:

$$r_{ij} = \frac{\mu_{ij}}{\mu_i} \quad i,j=1,2,\dots,M, i \neq j \quad (5.3.3)$$

provided that the system is already found at ψ_i . Again, r_{ij} is state-dependent and can be calculated from the system's parameters and the soliton structures. These transition probabilities can be collected into a single ($M \times M$) routing matrix \underline{R} .

Now that the routing probabilities are known, the input traffic, λ_i , to node i is calculated as the superposition of the proportion of each departure stream from all other nodes. This allows the arrival rate to node i to be expressed in terms of other arrival rates as:

$$\lambda_i = \sum_j \lambda_j \cdot r_{ji} \quad (5.3.4A)$$

and in matrix form, this set of equations can be written as

$$\underline{\lambda} \cdot (\underline{I} - \underline{R}) = \underline{0} \quad (5.3.4B)$$

where $\underline{\lambda}$ is the row vector $(\lambda_1, \lambda_2, \dots, \lambda_M)$ and \underline{I} is the unit $M \times M$ identity matrix. On writing equation (5.3.4) it should be recalled that the steady-state incoming traffic to a node is equal to the total outgoing traffic from that node. This is necessary to ensure stability. The set of equations (5.3.4) above is called the *traffic equations*; the solution of which gives the average traffic entering and leaving each centre.

The occupancy, P_i , of the soliton structure, ψ_i , is given by the following simple relation:

$$P_i = \text{visit rate to this state} \times \text{residence time per visit} = \lambda_i / \mu_i.$$

Unfortunately, the matrix $(\underline{I} - \underline{R})$ has a zero-valued determinant and the set of traffic equations will have an infinite number of solutions, Lipschutz (1981).

In the following part, the conventional route used in Traffic Theory to tackle this type of problems is followed. It is also possible to arrive at the same conclusions making use of the definition of the density of states given above and any of the solutions of the traffic equations.

The network forms a closed network of servers in which there is exactly one job trapped inside. At any time, the job (system) will be found somewhere in the network. This single job is not allowed to leave the network and, obviously, there are no exogenous arrivals.

Define the vector $\underline{m}(t)=(m_1, m_2, \dots, m_M)$ where $m_i(t)$ is the number of jobs (systems) found at state ψ_i at time t . It is clear that:

$$m_i(t) = \begin{cases} 1 & ; \text{system found in } \psi_i \\ 0 & ; \text{otherwise.} \end{cases} \quad (5.3.5A)$$

and, as there is exactly one system -job- travelling inside the network, it becomes clear that the elements of $\underline{m}(t)$ will satisfy:

$$\sum_{i=1}^M m_i(t) = 1 \quad (5.3.5B)$$

In summary, the Traffic Model described above for soliton states in single-electronic systems has the following general properties:

- a. service completion time (delay) that is state-dependent (load-dependent) and has a negative exponential distribution (for a particular state),
- b. number of jobs found in the network is fixed (equal to unity),
- c. routing is random and can be described in terms of well-defined probabilities (R).

It was shown by Jackson (1959) that, for systems satisfying the above conditions, the joint probability distribution of $\underline{m}(t)$ for the network in equilibrium is separable. Baskett et al (1975) extended the theorem and showed that systems with a number of selection policies, including the First-In-First-Out policy applicable to this model, are still separable.

In general, the joint probability distribution is given by:

$$P(\underline{m}) = \frac{1}{G} \alpha_1(m_1) \alpha_2(m_2) \dots \alpha_M(m_M) \quad (5.3.6)$$

where G is a normalisation constant and α_i depends on the traffic properties at node i .

Let $\lambda^* = (\lambda_1^*, \lambda_2^*, \dots, \lambda_M^*)$ be some non-zero solution of the traffic equations.

For this solution, the functions $\alpha_i(j)$ for the system under study are defined as:

$$\alpha_i(0) = 1, \quad \alpha_i(1) = \frac{\lambda_i^*}{\mu_i} \quad (5.3.7)$$

and the normalisation factor, G , is selected such that the sum of the densities of states defined in (5.3.6) should sum to unity. It is, hence, calculated as:

$$G = \sum_{\{m\}} \prod_{i=1}^M \alpha_i(m_i) \quad (5.3.8)$$

where the summation is realised over all possible sets $\{m\}$ satisfying (5.3.5).

For a closed network of queues with exactly K jobs being trapped inside, the normalisation constant is normally calculated using a convolution algorithm of a recursive nature, e.g. Eade (1987). However, the system under study forms a simple version of the general class of closed networks, as $K=1$ here. Using the definition (5.3.7) and the condition (5.3.5B), the following expression for G is obtained:

$$G = \sum_{j=1}^M \frac{\lambda_j^*}{\mu_j} \quad (5.3.9)$$

It is to be noticed that if $m_i=1$ then $m_j=0$ for all $j \neq i$, i.e. $m_j=\delta_{ij}$.

It is then easy to show that probability of finding the system at the soliton state ψ_i is given as;

$$P_i = \frac{1}{G} \frac{\lambda_i^*}{\mu_i} \quad (5.3.10)$$

which is the key result of this section and it is an important result in studying the steady-state characteristics of the single-electronic systems.

The technique makes no assumption about the tunnel rates apart from the Poisson nature of all tunnel events. This allows the model to be used in a wide range of applications, provided that the various tunnel rates can be determined from the knowledge of the tunnel characteristics.

5.4 Birth-Death Model:

It was shown in chapter (3) that the flow of electrons through a turnstile or a single quantum dot system can be controlled by an external gate electrode. The classical theory presented in chapter (3) ignores the discreteness of energy spectrum in the confined region, an assumption that is valid in the case of large metallic dots. In the 2-DEG of an inversion layer or heterostructure the energy level separation may be comparable to the charging energy and the continuum approximation is no longer valid. Kulik and Shekhter (1975) studied the conductance oscillations using the Gibbs distribution function to evaluate the equilibrium distribution of the number of excess electrons at the central island. Beenakker (1991) investigated the distribution of electrons among the available energy levels together with the distribution of excess electrons on the dot. The equilibrium distribution was calculated via the Gibbs function. For the non-equilibrium ($V \neq 0$) distribution the detailed balance equations were used. Linear response theory was then used to estimate the non-equilibrium distribution from the known equilibrium values. This technique is accurate for small values of applied voltages and can be used to determine the low-bias characteristics, e.g. the zero-bias conductance.

The Traffic Theory presented in the previous section provides an exact analytical solution to the problem of current flow in a double-junction system and other systems as well. It was shown in the previous section that the steady-state characteristics of the single-electronic systems can be evaluated from the densities of legal soliton states.

In this section a modified version of the theory is applied to the double-junction system and then extended to investigate the effects of the discrete energy spectrum of a single quantum dot.

The state of the double-junction system can be described by $\psi(t)=n$, where n is the number of excess electrons occupying the central node at time t . Let the system be found at the soliton state $\psi=n$ at time t . Following the same line of reasoning used in developing the general Traffic Model, one can find all traffic parameters for the two-junction system and then determine all steady-state characteristics of this system. Instead, analogy is established between this model and the conventional Birth-Death model (a model that has been extensively studied). The occupancies of states are then determined from the resulting model.

In the double-junction system, each state is related to, at most, two soliton states. Leaving state $\psi=n$ the system can enter (form) either $\psi=n-1$ or $\psi=n+1$. The process is therefore a Markovian Birth-Death process in which the stochastic variable, n , can either increase or decrease by unity. Let λ_n be the transition rate from state $\psi=n-1$ to state $\psi=n$ when the system is found at $\psi=n-1$:

$$\lambda_n = \Gamma(L, M, n-1) + \Gamma(R, M, n-1) \quad (5.4.1)$$

and λ_n corresponds to the birth coefficient of $\psi=n$. It represents the rate at which the system will try to increase the population at the central electrode by unity provided that there are already $(n-1)$ electrons at that electrode. The death coefficient, μ_n , is similarly defined as:

$$\mu_n = \Gamma(M, L, n) + \Gamma(M, R, n) \quad (5.4.2)$$

and again, this is the rate of losing an electron when there are exactly n electrons inhabiting the central electrode. A birth or a death event at a particular state will terminate that state and will leave the system in a new state.

In the conventional Birth-Death processes the stochastic variable can acquire only non-negative integer values. In contrast, the number of excess electrons at the central node, M , may assume both positive and negative values. Nevertheless, the process possesses the properties of the Birth-Death processes

and the standard solutions are applicable. Figure (5.4) shows a diagrammatic representation of the Birth-Death process and the relationship between the various soliton states.

Before proceeding to seek a solution, it is important to determine the set of active states that will be created and annihilated during the conduction process. In the double-junction case, the active states are discovered according to the following simple rule:

if $\lambda_n > 0$ and $\mu_n > 0$ then both ψ_{n-1} and ψ_n are legal active states

The set of active states can be discovered using this criterion if at least one state is known to be active. A general algorithm to discover the set of active states in a single-electronic system will be discussed in section (5.8).

Now, let k_1 and k_2 be respectively the minimum and maximum number of excess electrons that can be accommodated on the central electrode during the steady-state behaviour. Detailed-balance equations of states show that the occupancy of the state $\psi=n$ is given by: (see e.g. Schwartz (1977))

$$P_n = \begin{cases} G^{-1} & , n = k_1 \\ G^{-1} \prod_{i=1+k_1}^n \frac{\lambda_i}{\mu_i} & , k_1 < n \leq k_2 \end{cases} \quad (5.4.3)$$

where G is a normalisation factor given by:

$$G = 1 + \sum_{n=k_1+1}^{k_2} \prod_{i=k_1+1}^n \frac{\lambda_i}{\mu_i} \quad (5.4.4)$$

Equations (5.4.3 & 5.4.4) are the key results of this section. To use this model, the active soliton states should first be discovered and the Birth-Death coefficients are then calculated according to the nature of the problem at hand. The static characteristics of the double-junction system can be obtained once the occupancies of all states are known.

The average current passing through the double-junction structure is evaluated from:

$$I = e \sum_{n=k_1}^{k_2} P_n \{ \Gamma(L, M, n) - \Gamma(M, L, n) \} \quad (5.4.5A)$$

and currents satisfy:

$$\text{current through the left junction} = \text{current through right junction}$$

The dc and the differential conductances of the double-junction system can be calculated from (5.4.5A).

The average excess charge on the charge dot is:

$$\bar{q}_{ex} = e \sum_{k_1}^{k_2} n \cdot P_n \quad (5.4.5B)$$

The I-V characteristics of a symmetrical double-junction were investigated in chapter (3) using Monte-Carlo simulations. The curves were found to exhibit a well-defined discontinuity corresponding to the onset of conduction at the critical voltage. At higher voltages the line conductance approaches the limiting value $G=G_t/2$. For a symmetrically-biased double junction, $V_r=-V_\ell=V$ and $V_g=0$, the number of legal states is always an odd number. At $\psi=0$ the events $T(L,M,0)$ and $T(M,R,0)$ are equally likely to occur. The densities are then related by: $P_n=P_{-n}$. The average excess charge at M is zero. The application of a gate voltage disturbs the symmetry of states and, as a result, both odd and even total number of states are attainable at different bias conditions. With the application of a gate voltage of $V_g=ke/C_o$, where k is an integer, the average excess charge will be $= \pm ke$ and the states will be related by: $P_n=P_{n+k}$.

The Birth-Death model gives an exact solution to the double-junction system and the details of the I-V curves are easily obtained. For a symmetrical double junction, $C_1=C_2=C$ & $R_{t1}=R_{t2}$, the differential line conductance ($\partial I/\partial V$) exhibits peaked structures; the largest peak is located at the critical voltage, figure

(5.6.A). Examining another system with $R_{t2} \gg R_{t1}$ & $C_1 = C_2$, the peaks of the differential conductance are more clearly observed and the I-V curve exhibits a step-like shape. The peaks correspond to the onset of new soliton states and the addition of new paths to the conduction process. Let the maximum number of soliton states, at a certain step, be equal to n . The creation of a new soliton state, $\psi = n+1$, requires $\Gamma(L, M, n) > 0$. The three states $\{n-1, n, n+1\}$ will be potentially active in the transitional regime between the two steps. The system may be modelled by a three-state Birth-Death model with the following coefficients: (backward tunnel events not allowed)

$$\begin{aligned}\lambda_1 &= \Gamma(L, M, n-1), & \lambda_2 &= \Gamma(L, M, n) \\ \mu_1 &= \Gamma(M, R, n) & \mu_2 &= \Gamma(M, R, n+1)\end{aligned}$$

Using the relation (5.4.5), the dc current passing through the double-junction system is found to be:

$$I = e \frac{\lambda_1 \mu_1 \mu_2 + \lambda_1 \lambda_2 \mu_2}{\mu_1 \mu_2 + \lambda_1 \mu_2 + \lambda_1 \lambda_2} ; R_2 C_2 \gg R_1 C_1 \quad (5.4.6)$$

If λ_1 and λ_2 are much greater than μ_1 and μ_2 , the current will be approximated by $I \approx e \mu_2$. The differential conductance obtained from the above equation was found to be in excellent agreement with the results of the general model where all legal active states are taken into consideration.

For the symmetrical-bias conditions assumed here, the state $\text{Max}\{\psi\} = n$ would persist for a voltage $\Delta V(n)$ given by, (see equation (3.3.1)),

$$\Delta V(n) = \frac{e}{C_T} \quad (5.4.7)$$

For structures with $R_2 C_2 \gg R_1 C_1$ the density of soliton states will be highly localised at the state $\text{Max}\{\psi\}$. This is clearly reflected by the integer-valued step-like shape of the average number of excess electrons given in figure (5.6.B). The current though the device will be mainly determined by the junction that has the larger R_C value; J_2 in this example, and it forms the bottle-neck in the path of the

charge. Following the increase of the charge by $+e$ at M, the potential difference across the junction J2 changes by:

$$\Delta V_2 = \frac{e}{C_T} \quad (5.4.8)$$

This causes a change in the total current of:

$$\Delta I = \frac{e}{R_2 C_T} \quad (5.4.9)$$

The step size of the current obtained by Amman et al (1988) is similar to (5.4.9) with the capacitance (C_1+C_2) replacing C_T . The tunnelling rate across the junction J2 becomes larger at higher voltages and the density of soliton states becomes distributed between a number of states. This smears out the steps and reduces the value of the conductance peaks.

The plots of figure (5.7) show the excellent agreement between the transfer characteristics obtained from the Traffic Theory and those obtained using the usual Monte-Carlo techniques. The superiority of the Traffic Model appears in the approximate 1/300 ratio of CPU execution time of the two methods. This is the ratio when the Monte-Carlo simulation monitors the departure of 750 particles.

Inspecting the transfer characteristics, it is easy to identify the oscillations in the dc conductance with the gate voltage at fixed terminal voltages. These oscillations are in accord with the classical theory in the low bias regime where transport is always achieved through the same number of soliton states. Transport in the first segment of figure (5.7.A) forms the states {0,1} while the second segment creates the set of states {1,2} and the third segment will then form the states {2,3} and so on. In the regime $V < V_{th}$ the average charge at the central electrode at $V_g=0$ is always zero. An average of an integer number of electronic charges will be observed at the central electrode for $V_g=ne/C_0$ where n is an integer. The conductance peaks occur at $V_g=(n+1)e/2C_0$. At higher terminal voltages, e.g. the case of $V=0.5e/C$ shown in figure (5.7.B), more states can be generated leading to the splitting of the segments. In this example, the soliton

states formed during the conduction process in the first, second, third and forth segments are respectively: {0,1}, {0,1,2}, {1,2} and {1,2,3}. In figure (5.7.C), the segments of the curve correspond respectively to: {-1,0,1,2}, {0,1,2,3} and {1,2,3,4}. At $V_g=0$ the terminal voltage $V=e/C$ will lead to an average charge of $e/2$ at the central electrode, which is the condition for maximum dc conductance where the Coulomb blockade effects are minimum. The other peaks are observed at $V_g=ne/C_o$, $n=\pm 1, \pm 2, \pm 3$ etc. The maximum of the conductance peaks increases with the applied voltage while the maximum to minimum decreases. At $V>>V_{th}$ the conductance approaches a constant value given by $G_\infty \approx G_0/2$.

Recently, Shikhin et al (1993) studied the I-V-V_g relationship for the double-junction system using an approximate iterative relation to calculate the density of states (suggested by Kulik and Scheckter (1975) from the Gibbs distribution function). Their results show a similar I-V_g phase relationship, but the technique is valid for small V and V_g values.

The structures studied by Thomas et al (1989), and shown in figure (3.3), revealed a conductance peak corresponding to the critical voltage. The tunnel barriers in this structure are randomly formed by the electrostatic potential due to single trapped charges. However, their data corresponds to the case $C_1R_{t1} \approx C_2R_{t2}$. Concrete evidence of the differential conductance oscillations was reported for the first time by Barner and Ruggiero (1987). Their structures consisted of Ag granules embedded in Al₂O₃ between Ag films. Steps in the I-V curves were also observed by Wilkins et al (1989) on a double-junction structure formed using a Scanning Tunnelling Microscope probing a 10nm diameter In droplet deposited on an oxidised metal substrate.

5.5 The Quantum Dot:

A metallic dot of 10nm diameter has approximately 40×10^4 conduction electrons with an average energy spacing between the levels of 10^{-4} eV. The energy spectrum can be considered as a continuum of levels, and the occupancy

of these levels is approximated by the Fermi-Dirac distribution function. Decreasing the size of the dot increases the energy separation, Δ , and decreases the total number, N_0 , of conduction electrons on the dot. With few electrons on the dot, the Fermi-Dirac distribution can no longer model the occupancy of the discrete levels.

At $T=0$ K, the levels on the isolated dot will be occupied up to some maximum energy level just below the Fermi level and all other levels will be empty. It will be assumed that the conduction process would take place entirely within the unoccupied levels of the dot. This assumption suggests that at $\psi=0$ only the events $T(L,M,0)$ or $T(R,M,0)$ are to be expected; whereas, at this state, the events $T(M,L,0)$ and $T(M,R,0)$ can never occur. In other words, the excess number of electrons on the dot will always satisfy $n \geq 0$. This simplifies the analysis of transport through the dot.

The Birth-Death model described in the previous section is a general and efficient method in studying the stationary properties of double-junction systems. The application to metallic structures is straight-forward as the tunnel rates can be directly evaluated from the free energy and the tunnel resistance. The discrete energy levels of the quantum dots restrict the active levels that may contribute to the tunnelling process. Figure (5.5) shows a diagrammatic representation of the energy spectrum in the quantum dot and the contact reservoirs. Such structures were studied by Averin and Korothov (1990) and Beenakker (1991). Transport through the double-junction system with discrete energy levels is treated here in a way reminiscent to the sequential resonant tunnelling process in a semiconductor double-barrier structure, e.g. Chang et al (1974). The dot has energy levels labelled E_p ($p=1,2,..$) measured from the bottom of the well. Conservation of energy constraints predicts that for the event $T(L,p,n)$ the tunnelling electron must have emanated from an initial level on the left reservoir given by,

$$T(L,p,n) \rightarrow E_i^L(n) = E_p + E_x + \frac{e^2}{2C_T} + eV_1(n) \quad (5.5.1)$$

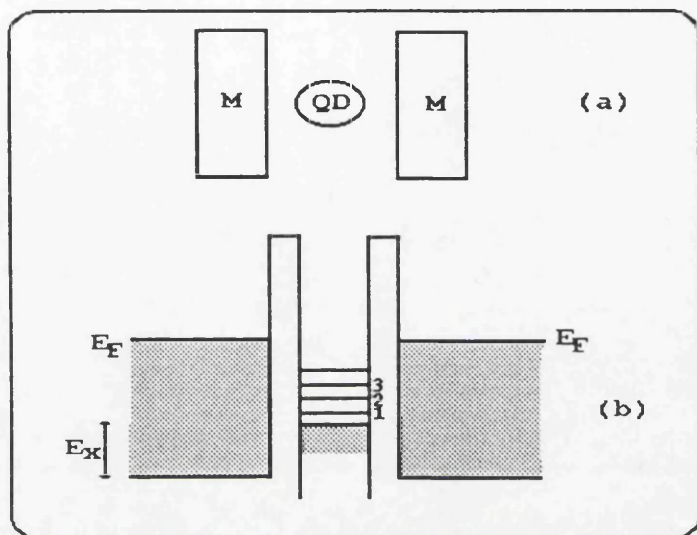


Figure (5.5): (a) Single Quantum dot imbedded in the insulating layer between metallic electrodes.
 (b) Energy spectrum of the electrodes and the dot at equilibrium.

where E_x is the maximum filled level of the isolated dot, E_x and E_i^L are measured with respect to the bottom of the conduction band of the metallic reservoir. Although this model assumes a symmetric structure, systems with dissimilar metals may be investigated in a similar fashion. Similarly, the initial and final energies on the left and right electrodes participating in tunnel events are given by:

$$T(p, L, n) \rightarrow E_f^L(n) = E_p + E_x - e^2/2C_T - eV_1(n) \quad (5.5.2)$$

$$T(p, R, n) \rightarrow E_f^R(n) = E_p + E_x - e^2/2C_T - eV_2(n) \quad (5.5.3)$$

$$T(R, p, n) \rightarrow E_i^R = E_p + E_x + e^2/2C_T + eV_2(n) \quad (5.5.4)$$

Equations describing resonant tunnelling in semiconductor double-barrier structures may be retrieved from the above set of equations if the charging energy term, $e^2/2C_T$, is set equal to zero. Consider a tunnel event $T(L, p, n)$ and let the incident electrons have wave-vectors confined to the longitudinal direction. Using the quantum golden rule, the tunnel rate may be approximated by:

$$\Gamma(L, p, n) = \gamma \cdot \left\{ 1 + \exp\left(\frac{E_i^L - E_F}{k_B T}\right) \right\}^{-1} \cdot (1 - f_p^n) \quad (5.5.5)$$

where γ depends on the elastic transmission coefficient and density of states, and f_p^n is the probability that level p is occupied if the dot is inhabited by n electrons. Energy considerations show that the event $T(L, p, n)$ will be blocked, at $T=0$ while the p -th level is empty, if

$$E_p > E_F - eV_1(n) - e^2/2C_T \quad (5.5.6)$$

The average tunnel rate at a certain state, $\psi=n$, can be evaluated once the occupancies of the energy levels on the dot are known, e.g.

$$\Gamma(L, M, n) = \sum_p \Gamma(L, p, n) \quad (5.5.7)$$

The state $\psi=n+1$ with the p-th level occupied can be constructed from the state $\psi=n$ with this level empty and then adding an electron to the p-th level. The difference between the energies of the two states is:

$$\Delta_p^n = \frac{(n+1)^2 e^2}{2C_T} - \frac{(ne)^2}{2C_T} + E_p \quad (5.5.8)$$

The occupation factors of the energy levels are related by: (e.g. Ashcroft and Mermin 1976),

$$f_p^{n+1} = (1 - f_p^n) \cdot \exp\left(-\frac{\Delta_p^n - \mu(n+1)}{k_B T}\right) \quad (5.5.9)$$

where $\mu(n)$ is the chemical potential of the dot when occupied by n excess electrons. The general solution of (5.5.9) gives the Gibbs grand canonical distribution which was used by Beenakker (1991) to evaluate f_p^n . The disadvantage of the Gibbs formulation is that a record of all possible combinations is required before the occupancy of a certain state may be calculated. This is not the case when using (5.5.9). For bulk metals, the number of conduction electrons is very large, of the order of $10^{22}/\text{cm}^3$, and the addition or removal of a single electron will not alter the distribution, i.e. $f_p^{n+1} = f_p^n = f(E_p)$ which gives rise to the Fermi-Dirac distribution. In quantum dots, the number of electrons is small and hence the chemical potential varies significantly with n. The relation (5.5.9), together with the following relations, can be recursively used to calculate the occupation numbers

$$\begin{aligned} f_p^0 &= 0 \quad , \forall p \\ \sum_i f_i^{n+1} &= n+1 \end{aligned} \quad (5.5.10)$$

The solution of the second equation of (5.5.10) gives the chemical potential of the dot, $\mu(n+1)$.

At equilibrium, with no voltage applied across the double-junction, electrons can flow into empty levels on the dot. Each additional electron modifies

the positions of the Fermi levels with respect to the vacuum level. This process accumulates a maximum charge, $e n_0$, on the dot such that the addition/removal of one electron to/from the dot will increase the total free energy of the system. In equilibrium, the Fermi levels will be closest to alignment but there may be some difference. The resulting voltage difference between the dot and the metallic reservoirs will be accounted for in the solution of the circuit equations. Tunnelling into or out from the dot with no voltage applied to the system is not only determined by the closest alignment of the Fermi levels but also by energy considerations for the individual tunnel events, starting with a neutral dot. The equilibrium number of excess electrons on the dot is the largest integer ($n \geq 0$) satisfying the following relations,

$$\begin{aligned} \Gamma(L, M, n-1) &> 0, \\ \Gamma(L, M, n) &= 0 \quad \& \\ \Gamma(M, L, n) &= 0 \end{aligned} \tag{5.5.11}$$

The previous arguments are also true for the case of a dot having a continuum of energy levels. Following the exchange of electrons between the metallic reservoir and the dot, the Fermi levels need not be in full alignment. The reason for this is that the addition/removal of a single electron to/from the dot causes a shift in the relative positions of the Fermi levels in the dot and the reservoirs of a discrete amount equals to e^2/C_T , (provided that the conditions for tunnelling are fulfilled in the first place).

To examine the effects of the discrete energy levels on the I-V curves the following hypothetical parameters are assumed: $E_F = 7E_c$, $E_x = 3E_c$, $C/C_0 = 1$ and Δ is taken to be of the same order as E_c . The equilibrium number obtained from (5.5.11) is $n_0 = 2$; and these electrons occupy the levels $p=1$ and $p=2$. Figure (5.8) shows the I-V characteristics of this quantum dot structure. In the region of the first step, a, an electron first tunnels from the left into the first empty level in the dot, i.e. there are two possible events, due to spin degeneracy, viz. $T(L, 3, 2)$ or

$T(L,4,2)$. This event is then followed by either $T(3,R,3)$ or $T(4,R,3)$. The levels involved in the conduction process in this regime are $p=3,4$.

As the applied voltage is increased, more single electron levels on the dot become accessible to the conduction process giving rise to the step like structure shown in figure (5.8). In the second step, b, the first energy level becomes available and contributes to the conduction mechanism. In this regime, electrons may tunnel from the left electrode into the first empty energy level, giving rise to the event $T(L,3,2)$ or $T(L,4,2)$. The electrons monitored at the right electrode may emerge through one of the following set of events: $T(1,R,3)$, $T(2,R,3)$, $T(3,R,3)$ or $T(4,R,3)$. Thermodynamic equilibrium will be regained following the event $T(M,R,3)$. In the regimes a & b, the state of the dot oscillates between $\psi=2$ and $\psi=3$. In the third step, c, the state $\psi=4$ becomes accessible and this would increase the set of possible tunnel paths.

On the experimental side, transport through semiconducting quantum dots was examined by Reed et al (1988). Their structure consisted of an InGaAs quantum dot embedded between n+ GaAs contacts. Reed and co-workers explained the observed step-wise structure, similar to the curve in figure (5.8), in terms of resonant tunnelling and used these I-V characteristics to infer the density of states of the quantum dot.

The classical theory predicts oscillations in the line conductance of the double-junction structure. The dynamics of the conduction process via discrete energy levels are complicated, even in simple structures. For the quantum dot, the discrete energy spectrum changes the shape of the transfer characteristics and the periodicity of oscillations, figure (5.9). Let the dot initially host n excess electrons at a gate voltage = V_g . The levels up to the n-th level will be occupied. Changing the gate voltage to $V_g + \Delta V_g(n)$ increases n by one and the additional electron will be accommodated in the (n+1)-st level. The period of conductance oscillations then satisfies the following relation:

$$E_{n+1} - E_n = e \left\{ V_1(n-1, V_g) - V_1(n, V_g + \Delta V_g(n)) \right\} \quad (5.5.12)$$

from which the period is obtained as:

$$\Delta V_g(n) = \frac{C_T}{C_o} \left\{ \frac{e}{C_T} + \frac{E_{n+1} - E_n}{e} \right\} \quad (5.5.13)$$

A double junction with large central electrode has $E_{n+1} \approx E_n$ and the above relation gives the classical periodicity of $|\Delta V_g| = e/C_o$. Recently, Foxman et al (1993) studied the transfer characteristics of a semiconductor double-barrier system. The energy separation between the levels in their structure is $\Delta = 0.4E_c$ and the system has shown a well-defined step-like structure in the V_g -G relationship that is similar to the relation shown in figure (5.9).

The differential conductance deduced from the model described here forms a series of delta functions located at the points of discontinuities. However, the thermal fluctuations tend to broaden these conductance peaks. Lorentzian line shape has been suggested and shown to fit the conductance peaks in semiconductor double-barrier structures, see e.g. Meirav et al (1990), Beenakker (1991) and Foxman (1993).

5.6 Multi-Junction Systems:

Increasing the complexity of a single-electronic system, e.g. by adding more tunnel junctions, will increase the set of possible states that will contribute to conduction and will generate new paths through which charge can travel from a point to another. The interaction between the various soliton states affects the characteristics of the system. This is investigated here by adding another tunnel junction to the double-junction system studied in the previous sections.

In this 3-junction system, the tunnel junctions are taken to be identical; each with a value C. The capacitances to ground are also identical and have a value C_o . Let $V_r=0$ and $V_l=-V$. The I-V characteristics obtained from the Traffic Model are shown in figure (5.10). The total dc conductance, in the case of

identical tunnel resistances, approaches the classical series conductance at high bias voltages. However, the differential conductance at low bias voltages oscillates in a manner similar to the oscillations observed for the double-junction case. The magnitudes of the conductance peaks are enhanced if one of the junctions has a dominant $R_t C$ value. Figure (5.11) corresponds to a system with $R_{t3} \gg R_{t1}, R_{t2}$. In the region (a) of figure (5.11), conduction passes through the following set of states $\{\Psi_a\} = \{(0,0), (1,0), (0,1)\}$ and the system is found to stay most of the time at the state (0,1). In this region a maximum of one electron can be found inside the system. The number of electrons is then: $\{n_a\} = \{0,1\}$.

In the second region, labelled (b) in figure (5.11), the system has a total number of states equals to 4,5,6 or 7; increasing with the increase of applied voltage. The transition from a set to another, e.g. 5 to 6, is smooth and no changes in current or in conductance are observed. The number of excess electrons in the system here forms the set: $\{n_b\} = \{0,1,2\}$. The dominant state is (1,1). Eleven states contribute to the conduction process in region (c) with the dominant state being (1,2). The spectrum of the number of electrons expected is $\{n_c\} = \{0,1,2,3\}$. Finally, in the region (d) twelve states are observed with the state (1,2) still being dominant and a set of $\{n_d\} = \{-1,0,1,2,3\}$.

It is concluded from this analysis that the conductance peaks each time the system becomes able to accommodate one more electron or hole, and the additional electron/hole need not be permanently hosted in the system. The size of current rise, if a bottle-neck exists in the circuit, can be found using the changes of the dominant state as found for the double-junction case.

5.6 Time Evolution of States:

The general Queuing Theory applied so far describes the steady-state behaviour of the system; the densities of states obtained from by (5.3.10) correspond to the densities at $t=\infty$ viz. $P_i(\infty)$. Let a measurement be made at time $t=0$ and the system be at the state $\psi=\psi_k$, then the densities can be written as:

$$P_i(0) = \begin{cases} 1 & , i = k \\ 0 & , i \neq k \end{cases} \quad (5.6.1)$$

At a later time the state of the system will be a mixture of all possible legal states, each with a density $P_i(t)$. Take a small time interval Δt around t . The probability of finding the system at the state ψ_i then satisfies:

$$P_i(t + \Delta t) = P_i(t) \left\{ 1 - \sum_{j \neq i} \mu_{ij}(t) \cdot \Delta t \right\} + \sum_{j \neq i} P_j(t) \mu_{ji}(t) \cdot \Delta t \quad (5.6.2)$$

where μ_{ij} is the departure rate from state ψ_i to state ψ_j defined in (5.3.1). In the limit $\Delta t \rightarrow 0$, the above relation reduces to the following partial differential equation:

$$\frac{\partial P_i}{\partial t} = \sum_{j \neq i} P_j \mu_{ji} - P_i \mu_i \quad (5.6.3)$$

and the densities should sum to unity at any time. The first term in the RHS of the above relation is the rate at which other states are entering the state ψ_i at time t ; while the other term is the rate of leaving this state. At $t \rightarrow \infty$ all derivatives are equal to zero and the set of equations (5.6.3) reduces to the set of traffic equations

given by (5.3.4), $\{ P_j \mu_{ji} = P_j \mu_j \cdot \frac{\mu_{ji}}{\mu_j} = \lambda_j \cdot r_{ji}; P_j \mu_j = \lambda_j \}$.

The relation (5.6.3) derived above is an interesting result. Its solution can be used to determine the most probable evolution of the variables of the single-electronic system with time.

Let the conduction mechanism through a single quantum dot be described by two soliton states, $\{\psi\} = \{n, n+1\}$, with the birth and death coefficients being λ and μ respectively. If the system is known to occupy the state $\psi=n$ at $t=0$ then the solution of the differential equations (5.6.3) will show that the density of the two soliton states will evolve according to:

$$P_n(t) = \frac{1}{\lambda + \mu} \left\{ \mu + \lambda \cdot \exp[-(\lambda + \mu)t] \right\} \quad (5.6.4A)$$

$$P_{n+1}(t) = \frac{\lambda}{\lambda + \mu} \{1 - \exp[-(\lambda + \mu)t]\} \quad (5.6.4B)$$

and in the limit $t \rightarrow \infty$, the densities approach the values:

$$P_n = \mu / (\lambda + \mu) \quad \text{and}$$

$$P_{n+1} = \lambda / (\lambda + \mu)$$

coinciding with the results obtained from the Birth-Death model.

5.7 Algorithm to discover the Active States:

The technique described in this chapter assumes that the set of states contributing to the conduction process is known or can be discovered. A simple algorithm to list the active states for the double-junction was mentioned in section (5.5). For a complicated system, the most popular states can be spotted from a Monte-Carlo simulation running for a relatively short time.

A simple way is to choose a large set, Ψ , such that the active states are guaranteed to be contained in this set. The solution of the traffic equations for these states will then help enumerate the list of active states according to:

$$P(\text{active state}) > 0 \text{ while } P(\text{redundant state}) = 0.$$

The disadvantage of this method is that a large set is to be chosen in the first place, which is not an easy guess as it may appear. Besides, one should also trace the relationship between these states.

The algorithm used in this study dynamically allocates memory space to states and links the states together as these states are discovered. The main data structure is a list of state records with the following data types:

State_Record =

```

ψ      : State_Vector;
Aux    : ^Auxiliary_Record ;
P      : Real ;           { Density }
Next   : ^State_Record   ;{ Next state in list }
```

end;

The Auxiliary_Record list is another data structure of the states linked to this state via the tunnelling probabilities. It has the following data types:

Auxiliary_Record =

```

State    : ^State_Record ;
μ       : Real ;           {Transition rate}
Next    : ^Auxiliary_Record ;

```

end;

The algorithm starts by any initial state and determines the states of the Auxiliary_Record from the conditions of tunnelling. Any state discovered in the auxiliary list must have its own record in the State_Record list. The list of records builds this way. It is to be noticed that some states discovered in the State_Record list using this algorithm may not be active during the conduction process. This depends on the initial state, i.e. if the initial state is an active state then all states in the list will be active while choosing an inactive initial state will lead to the accumulation of some inactive states in the list. This suggests that choosing any state from a Monte-Carlo simulation running in its steady state will guarantee the accumulation of only active states in the list.

If the bias conditions do not lead to current flow, the system will pass through some transient states and eventually remain in a static state, ψ_{static} , which can be discovered from the list using,

(i) *If \exists State: State^.Aux=nil then $\text{State} \in \{\psi_{\text{static}}\}$.*

Finally, the set of active states can be determined from:

(ii) *If state ψ_a is known to be active, then all states in the Auxiliary_Record related to this state are necessarily active.*

It is therefore sufficient to determine, at least, one active state and then the above rule can be used to discover all other active states. This can be done by first making sure that the system is conducting, i.e. there are no static states in the list.

Let the algorithm be started with an initial state = ψ_{init} . Using the above data structures, it is possible to find the states that may be active during the steady-

state behaviour. If the system is known to be conducting (by checking (i)) then it will be known that the last state discovered in the list will -definitely- be active. This is the state satisfying $State^.Next=nil$. Starting with this state as a *first_active_state*, and using rule (ii) mentioned above, it is possible to determine set of all active states.

Summary:

In this chapter an exact and efficient technique for modelling the single-electronic systems has been presented. A version of the technique is applied to the double-junction system and has proved high efficiency compared with the conventional Monte-Carlo methods. The Birth-Death model was applied to a quantum dot structure with discrete energy spectrum. The CPU time reduction was found to be of the order of 1/400 against the Monte-Carlo model that monitors the passage of 1000 particles. The efficiency increases fast with increased system complexity.

An efficient algorithm that determines the set of active states during the conduction process and the relationship between these states has been implemented. The technique is quite general and extendible to include thermal and quantum fluctuations, macroscopic quantum tunnelling and charge trapping/detrapping effects.

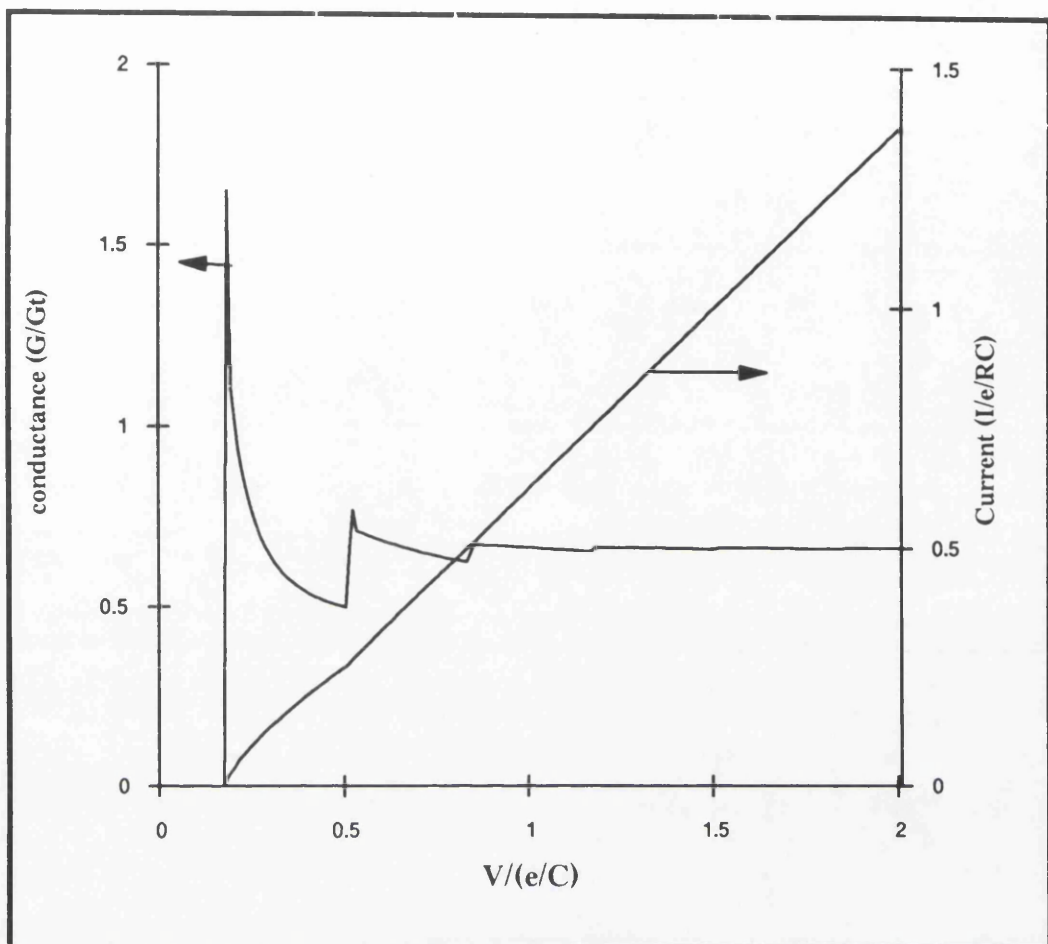


Figure (5.6.A): I-V characteristics of a symmetrical double-junction structure. Shown also the conductance. The limiting value of the line conductance is $G=G_t/2$. The current approaches a linear relationship ($I \propto (V - V_{th})$).

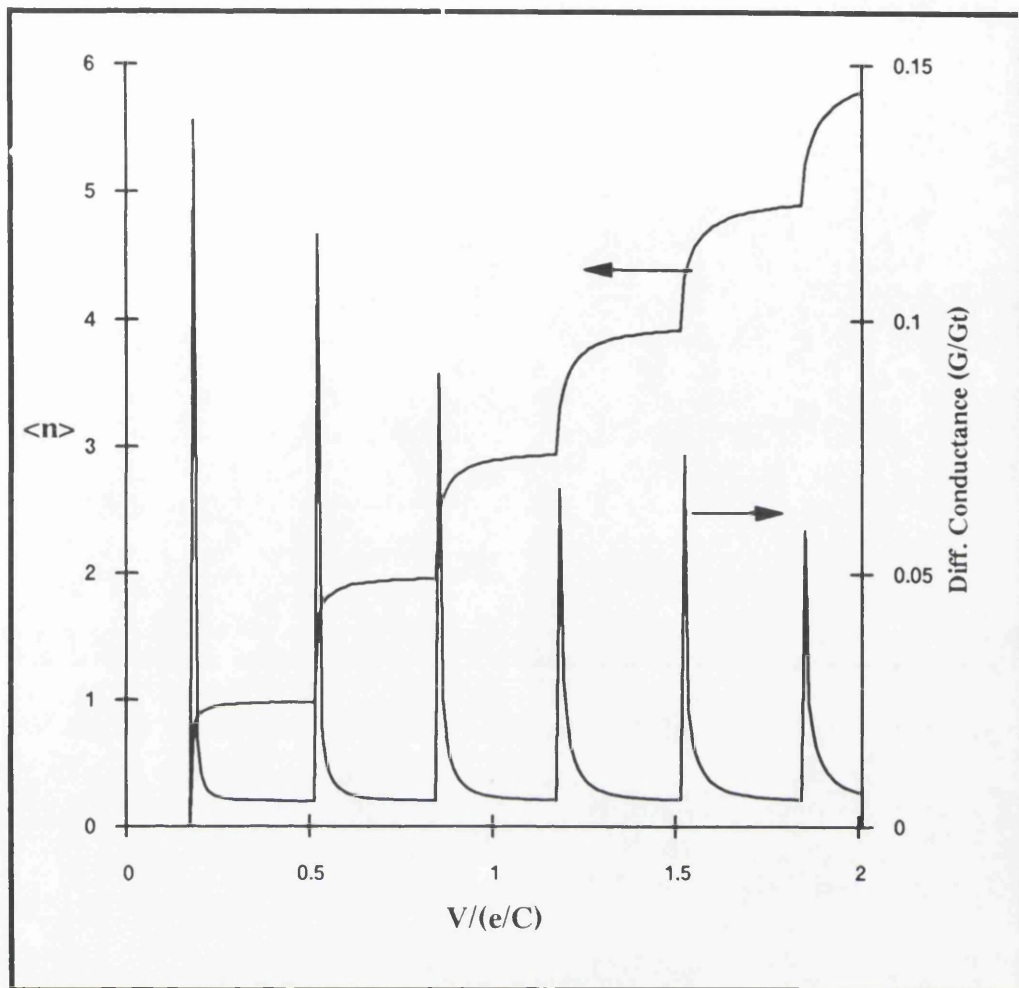
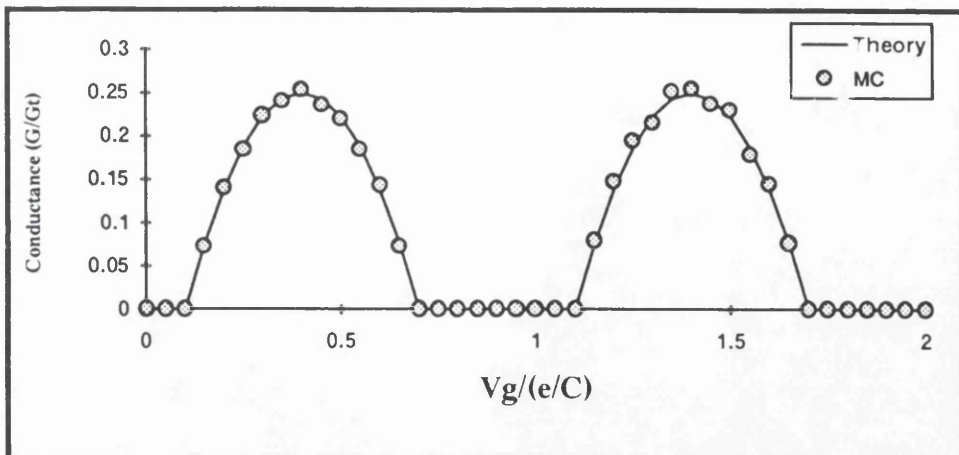
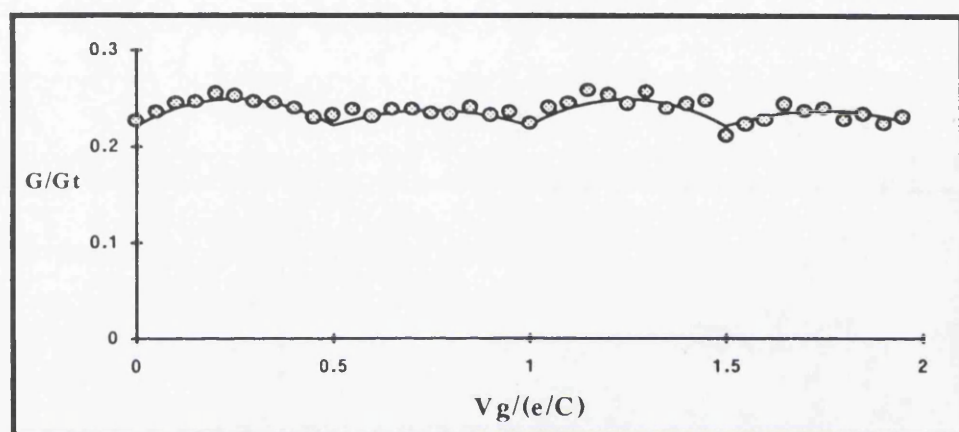


Figure (5.6.B): The differential line conductance and average number of excess electrons at the central electrode of an asymmetrical double-junction structure:

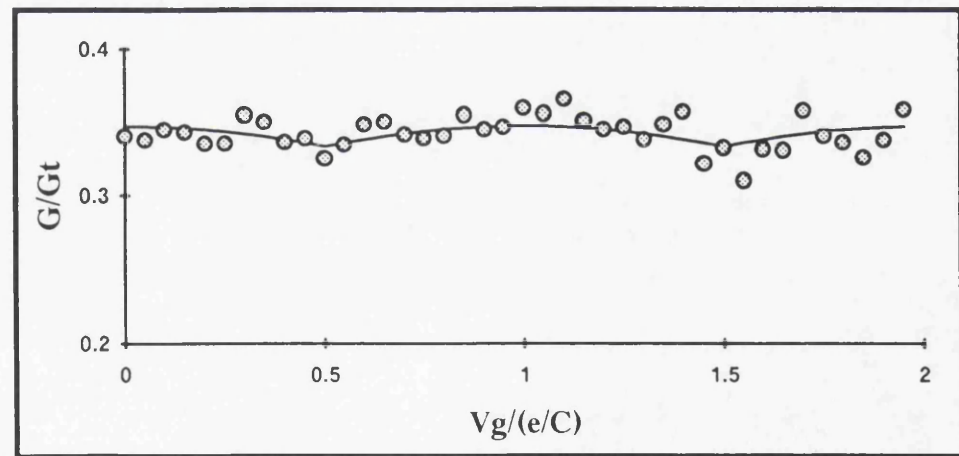
$$R_{t2} \gg R_{t1}, C_1 = C_2.$$



(A): $V=0.2e/C$

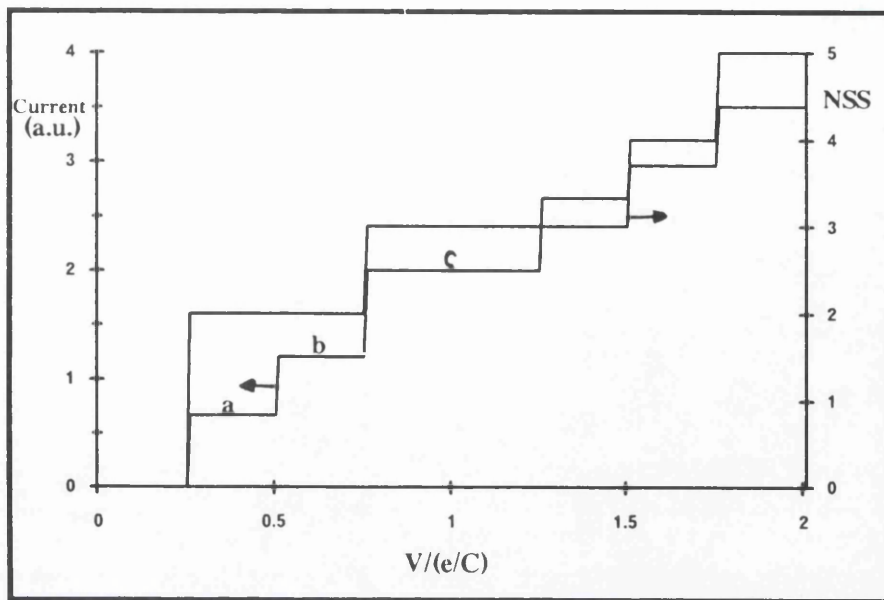


(B): $V=0.5e/C$

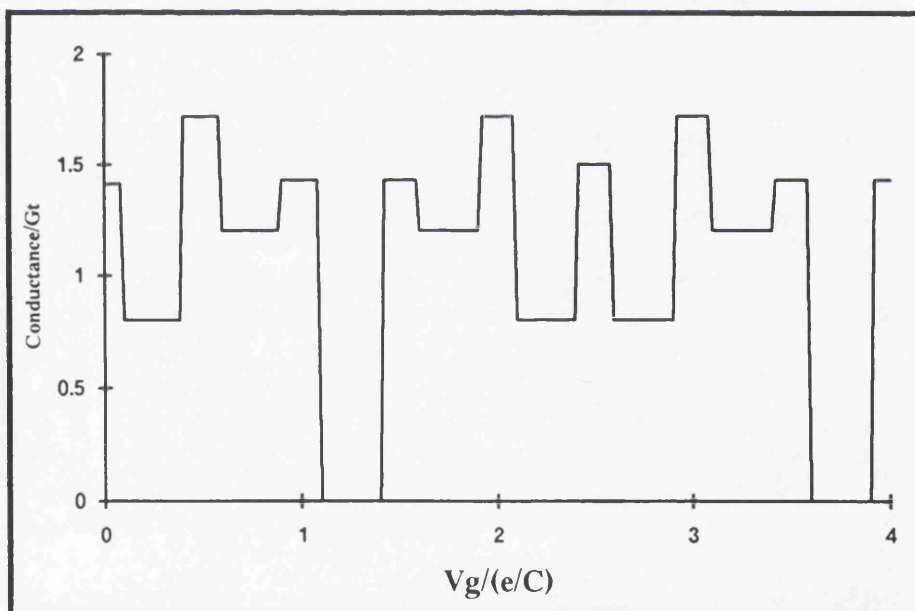


(A): $V=e/C$

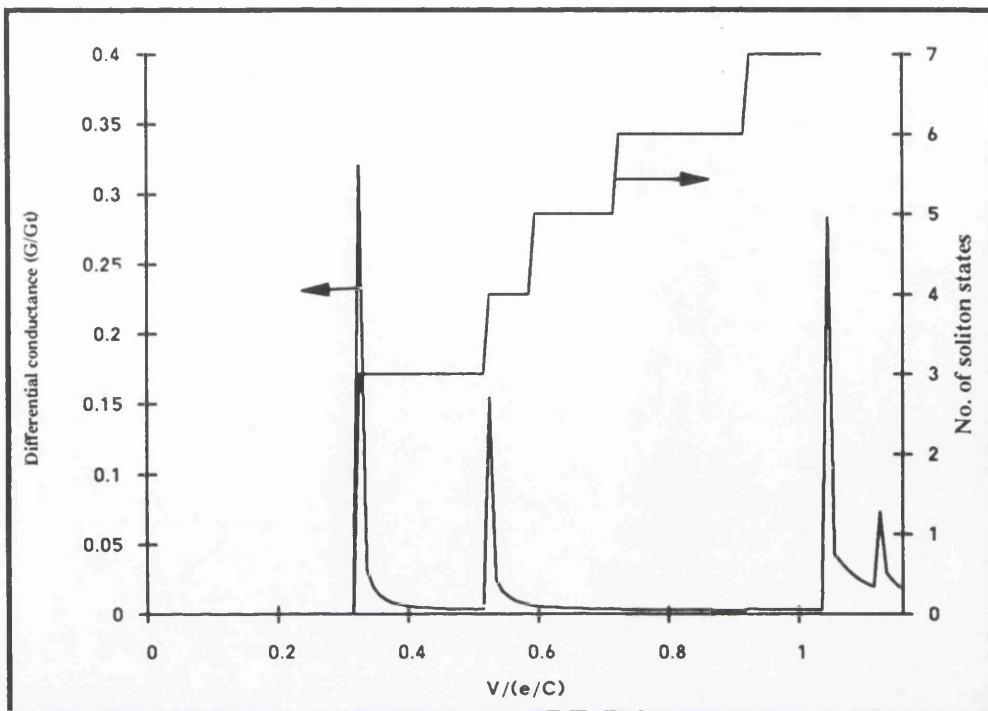
Figure(5.7): Line conductance of a double-junction system calculated using the Birth-Death model (solid lines) and Monte-Carlo techniques (circles). A: $V=0.2e/C$, B: $V=0.5e/C$ and C: $V=e/C$



Figure(5.8): I-V curves of a double-junction system and the number of soliton states (NSS) contributing to the conduction process in case of discrete energy levels at the central electrode: $E_F=7E_c$, $C/C_o=1$, $E_x=3E_c$ & $\Delta E=E_c$.



Figure(5.9): Effect of the discrete energy levels at the dot on the conductance of the double-junction system; $C/C_o=1$, $E=0.5E_c$.



Figure(5.10):Differential conductance of asymmetric 3-junction array:
 $R_{t3} \gg R_{t1,2}$. Shown also the number of active soliton states. The symmetric structure exhibits the same shape for number of soliton states but less pronounced peaks for the differential conductance.

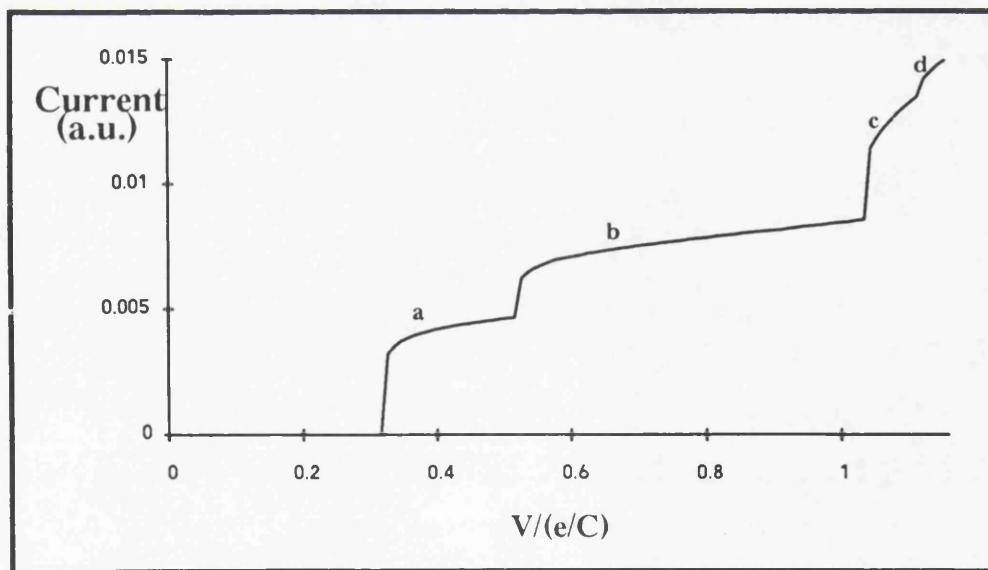


Figure (5.11): I-V characteristics of an asymmetrical three junction array.

Chapter (6)

Killer Processes

6.1 Introduction:

It was shown in chapter (2) that the Coulomb-blockade phenomenon and SET oscillations may be studied within a semiclassical model. The charging/discharging processes are represented by the classical capacitor charge/discharge curves; while the tunnel events are treated quantum-mechanically. The charge/discharge processes are represented by well-defined curves, if the initial and bias conditions of the circuit are known.

The semiclassical picture is extended in this chapter to cover the decay rate of the Coulomb-blockade state due to the thermal and quantum fluctuations. The macroscopic quantum tunnelling of the charge variable is also investigated using the same semiclassical approach. The acts of trapping/detrapping of single electronic charges near the junctions will also be treated in a classical way. The potential difference induced across the junction electrodes is calculated from simple electrostatic considerations.

6.2 General Model:

Several models have been used by different groups to study the characteristics of the single junction in the low-bias regime. Averin and Likharev (1986) and Likharev (1987) used a series RC circuit to represent the coupling leads and the tunnel junction and derived a Master Equation governing both the charge and tunnel processes. This technique was used in chapter (2) and a numerical solution was implemented and used to study the time evolution of the system. Girvin and co-workers (1990) used a transmission-line model where the line is characterised by a resistance, inductance and capacitance of $r \Omega/m$, $l H/m$ and $c F/m$ respectively. The transmission line is then treated as a collection of harmonic oscillators. Cleland et al (1990 & 1992) adopted a simplified version of

the full transmission-line model and used lumped components in place of the distributed parameters of the line. Hu and O'Connell (1992) used a similar model and assumed that the tunnel resistance does contribute to the total fluctuations in the circuit and treated the tunnel resistance as an ohmic resistance connected in parallel with the tunnel junction. Hu and O'Connell and Cleland et al used the quantum Langevin equation approach to evaluate the charge fluctuations in the circuit.

In the following sections, it is assumed that the circuit in the Coulomb-blockade region may be represented by a simple RLC model, where R is the line resistance, L is the total line inductance and C is the junction capacitance. The capacitance of the line is modelled as a lumped component at the input of the line, and is then absorbed into the junction capacitance and represented by the normalised capacitance, C.

Using circuit analysis it is straight-forward to show that the classical charging/discharging processes for this model circuit may be described by the following differential equation:

$$L \frac{d^2q}{dt^2} + R \frac{dq}{dt} + \frac{q}{C} - V = F(t) \quad (6.2.1)$$

where q is the instantaneous charge observed across the junction at time t, F(t) is the instantaneous noise voltage level, satisfying:

$$\langle F(t) \rangle = 0.$$

The evolution of the charge with time in the single-junction system under study is analogous to the motion of a particle of mass m in a potential $U(x)$ in a medium of friction η . The motion of this particle is described by the following differential equation:

$$m \frac{d^2x}{dt^2} + \eta \frac{dx}{dt} + \frac{\partial U}{\partial x} = 0 \quad (6.2.2)$$

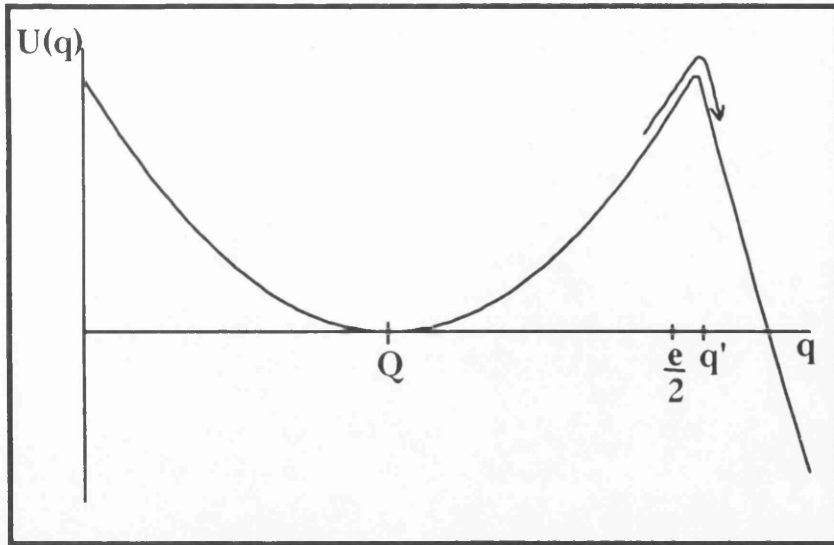


Figure (6.1): Potential profile if the tunnel event is thermally activated. The event takes place over the barrier.

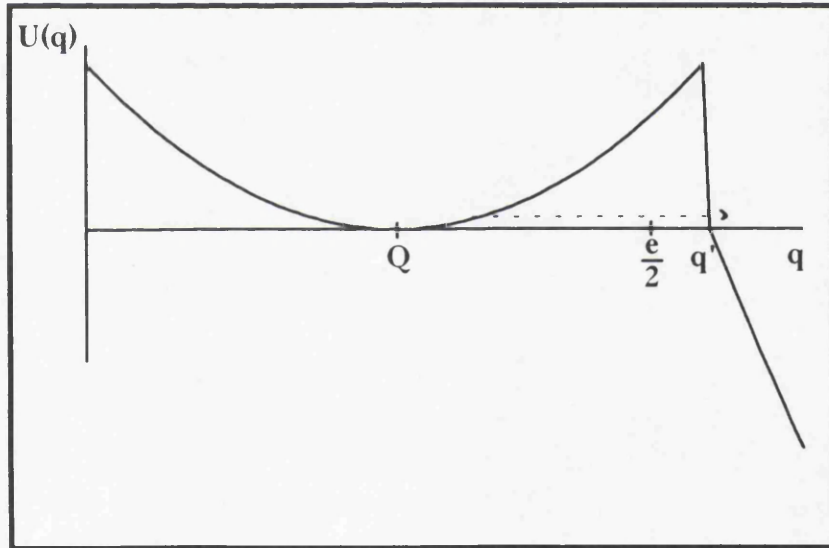


Figure (6.2): Potential profile in case of a Macroscopic Quantum Tunnelling event. The event takes place through the barrier.

It follows from direct comparison of (6.2.2) with (6.2.1) that the single-junction system may be described by a particle of mass L moving in a quadratic potential in a medium of friction R . The potential, $U(q)$, is given as:

$$U(q) = \frac{1}{2C}(q - Q)^2 , Q=CV \quad (6.2.3)$$

It is clear that the point $q=Q$ is the metastable point of the potential.

6.3 Thermal and Quantum Fluctuations:

The electron tunnelling rate from an electrode to another was derived in chapter (2). Formula (4.5.8) was shown to represent the tunnelling rate across any junction in a network of tunnel and non-tunnel junctions, provided that the electrodes have energy separation between the single-electron energy levels satisfying the relation: $\Delta \ll E_C$ and hence, a continuum of states can be adopted. The thermal effects are included in this formula through the Fermi-Dirac distribution function; thus accounting only for the energy levels that may contribute to the conduction process. The charge fluctuations are completely ignored and the charge is assumed localised at $q=Q$. This expression for the tunnel rate is also used within the Master-Equation formalism, considered in section (2.3), and the charge fluctuations are accounted for in the charge distribution function, $s(q,t)$.

A quantitative study of the effects introduced by the resistive and inductive elements can be performed by solving the quantum Langevin equation (6.2.1), e.g. Cleland et al (1990), which gives the fluctuations as:

$$\langle q^2 \rangle = \int_0^{\infty} \frac{C^2 S_V(\omega) d\omega}{(1 - \omega^2 LC)^2 + \omega^2 R^2 C^2} \quad (6.3.1)$$

where $S_V(\omega)$ is the noise power spectral density given by:

$$S_V(\omega) = \frac{\hbar R \omega}{\pi} \coth(\hbar \omega / 2k_B T) \quad (6.3.2)$$

The integral in (6.3.1) can be evaluated using contour methods in the complex domains. The value turns out to be a sum of an infinite series. It is possible to find an exact analytical expression for the integral in the high-temperature limit. Cleland et al (1990, 1992) evaluated the fluctuations at low temperatures assuming that the zero-temperature approximation is adequate at low temperatures. It will be shown that their approximation leads to large errors when this approximate value is used to evaluate the total tunnel rate and the low-bias resistance.

In the low-temperature regime $S_V(\omega)$ can be replaced by $\hbar R \omega / \pi$ for $\omega > \omega'$ where ω' is some positive value for which $\coth(\hbar\omega'/2k_B T) \approx 1$. The integration (6.3.1) may be split into two parts, viz.:

$$\langle q^2 \rangle = \int_0^{\omega'} + \int_{\omega'}^{\infty} = I_1 + I_2 \quad (6.3.3)$$

It is now possible to evaluate an exact expression for I_2 , and is found to be equal to:

$$I_2 = e^2 \frac{CRR_Q}{L\pi^2} \frac{1}{\omega_+^2 - \omega_-^2} \log \left[\frac{\omega_+^2 + \omega'^2}{\omega_-^2 + \omega'^2} \right] \quad (6.3.4)$$

where

$$\omega_{\pm}^2 = \left(\beta^2 - 2 \pm \beta \sqrt{\beta^2 - 4} \right) / 2$$

and $\beta = R \sqrt{C/L} > 2$.

The dependence of this term, I_2 , on temperature appears in cut-off frequency ω' . This term is sensitive to variations of temperature for high values of β . The zero-temperature approximation used by Cleland et al and Hu and O'Connell assumes $\omega' = 0$.

The first part of (6.3.3) retains the same integrand as in (6.3.1) and it may be evaluated using numerical methods. Splitting the integration into two parts

allows the investigation of the thermal effects on the low-bias properties. The charge fluctuations obtained using this method is always greater than the zero-temperature approximation ($\omega=0$) used by Cleland et al and Hu and O'Connell. The low-bias resistance, R_0 , is therefore less than the value obtained in the $T=0$ approximation. It is to be pointed out that the low-bias resistance is a strong function of the charge fluctuations, $\langle q^2 \rangle$, which is in turn a function of temperature and it will not be a fair approximation to use the zero-temperature value at all low temperatures.

Let the charge fluctuations at any temperature, $\sigma^2(T)$, be represented by an equivalent temperature, T_e , such that:

$$\sigma^2(T) = k_B T_e C \quad (6.3.5)$$

The equivalent temperature satisfies $T_e \geq T$; and the equality holds in the high-temperature limit where the charge fluctuation is given by the classical value $k_B T C$, which is used within the Master-Equation formalism , section (2.3).

At finite temperatures, a system that is biased inside the Coulomb-blockade region picks up energy from the thermodynamic fluctuations of the environment. If the electrostatic potential energy is overcome by the energy gained from the environment then there is a finite probability that an electron will tunnel through the dielectric barrier.

The behaviour of the charge variable during the motion can be divided into two sections, viz.:

- a. the region $|q| < e/2$ where tunnelling is completely blocked due to the Coulomb interactions ,
- b. the region $|q| > e/2$ where tunnelling of a single electron is possible.

The behaviour in the region $q > e/2$ is described by the stochastic nature of tunnelling; i.e. a junction that is driven from its metastable state, $q=Q$, to $q > e/2$ will allow a tunnel event to occur during a short time, Δt , with a probability equals to $\Gamma(q)\Delta t$, see figure (6.1). The total probability of decay of the blockade state due to the charge fluctuations can thus be obtained by summing the

contributions of all charge levels outside the Coulomb-blockade region. The total forward tunnel rate in case of a charge packet defined by the distribution $s(q,T)$ is then equal to:

$$\bar{\Gamma}(Q) = \int_{e/2}^{\infty} \Gamma(q,T).s(q,T).dq \quad (6.3.6)$$

The charge density can be modelled by a gaussian function, e.g. Schön (1985), characterised by a mean Q and a variance of $\sigma^2(T)=\langle(q-Q)^2\rangle=k_B T_e C$. Results obtained by numerical integration of (6.3.6) show that the tunnel rate, in the low-bias regime and at $T_e \ll T_c$, decreases exponentially with decreasing T_e . The noise removes the sharp discontinuity in the I-V characteristics, at the critical voltage, and hence a non-zero conductance will be observed inside the Coulomb-blockade region. In the high-temperature regime, the charge fluctuations change linearly with temperature ; and increasing the temperature above the critical value, T_c , tends to wash out, and eventually remove, the Coulomb gap and an ohmic I-V relationship is regained.

The effectiveness of the Coulomb-blockade state in the presence of fluctuations is reflected in the low-bias conductance or resistance. The ideal junction is one that presents an infinite resistance in the circuit if the charge on that junction is less than half the electronic charge. The fluctuations will cause random tunnel events across the junction and will, therefore, reduce the resistance.

The conductance in the Coulomb-blockade region can be evaluated from the total current due to the noise. This current is simply given by:

$$i = e\{\bar{\Gamma}(Q) - \bar{\Gamma}(-Q)\}$$

from which the conductance is evaluated as:

$$G(Q) = C \frac{\partial i}{\partial Q} = C \frac{(2\kappa)^{3/2}}{\sqrt{2\pi e^3}} \int_{e/2}^{\infty} \Gamma(q) \left\{ (q - Q) \exp\left(-\kappa\left(\frac{q-Q}{e}\right)^2\right) + (q + Q) \exp\left(-\kappa\left(\frac{q+Q}{e}\right)^2\right) \right\} dq \quad (6.3.7)$$

where $\kappa = E_c/k_B T_e$. Figure (6.6) shows the dependence of the junction conductance on the applied terminal voltage. The conductance asymptotically approaches the classical value at high voltages; and attains the maximum level faster in the low-temperature regime. At $T_c/T_e \approx 1$, the conductance is equal to $\sim 0.75 G_t$ inside the Coulomb-blockade region and increases slowly towards the $G=G_t$ limit; the I-V relationship approaches the ohmic behaviour at $T > T_c$.

In the regime $T_c/T \gg 1$, $\Gamma(q)$ may be replaced by its value at zero temperature and the thermal contribution can be retained in the distribution function. The integral (6.3.1) then evaluates to:

$$\bar{\Gamma} = \frac{G_t}{e^2 C} \sqrt{\frac{\kappa}{\pi}} \left(\frac{e}{2} - Q \right) \int_{e/2-Q}^{\infty} \exp\left(-\kappa\left(\frac{q}{e}\right)^2\right) dq + \frac{G_t}{2C\sqrt{\pi\kappa}} \cdot \exp\left(-\kappa\left(\frac{1}{2} - \frac{Q}{e}\right)^2\right) \quad (6.3.8)$$

Inside the Coulomb-blockade region, $|Q| \ll e/2$, the first term in (6.3.8) is vanishingly small and the second term approximately gives the rate of thermally excited events. This is written as:

$$\begin{aligned} \bar{\Gamma} &\approx \frac{G_t}{2C\sqrt{\pi\kappa}} \cdot \exp\left(-\kappa\left(\frac{1}{2} - \frac{Q}{e}\right)^2\right) \\ &= \frac{G_t}{2C\sqrt{\pi\kappa}} \exp\left(-\frac{U(e/2)}{k_B T_e}\right), \quad Q \ll e/2 \quad \& \quad \kappa \gg 1 \end{aligned} \quad (6.3.9)$$

The zero-bias conductance is approximately given by:

$$G_o = C \frac{\partial i}{\partial Q} \Big|_{Q=0} = G_t \sqrt{\frac{\kappa}{\pi}} \exp\left(-\frac{\kappa}{4}\right), \quad \kappa \gg 1 \quad (6.3.10)$$

which indicates a fast decrease in the zero-bias conductance with decreasing temperature, e.g. with $\kappa=50$ the conductance has the value $G_o \approx 1.5 \times 10^{-6} G_t$.

Relation (6.3.9) is similar to the well-known Kramer's rule for tunnelling at temperature T across a barrier of height V_0 : rate $\propto \exp\left(-V_0/k_B T\right)$.

The effect of the environment on the low-bias characteristics is clearly observed in figure (6.7). The noise power spectral density (6.3.2) indicates that the total fluctuations in the circuit increase with the increase of the external resistance (as this resistance is the source of the noise). It is also this resistance that effectively reduces the total average fluctuations that are monitored across the tunnel junction.

The method suggested here for calculating the fluctuations gives improved agreement with experimental data. The high-resistance single junctions studied by Cleland et al are reported to have the following parameters: $C=5\text{fF}$, $L=4.5\text{nH}$, $R=130\text{K}\Omega$ and the measurements were carried out at $T=20\text{mK}$. The method of splitting the integration gives a ZBR of $R_o/R_t=4.7$; in good agreement with the experimental result of $R_o/R_t=4$. The zero-temperature approximation gives $R_o/R_t=7$ and $\langle q^2 \rangle$ is 22% less than the value obtained using (6.3.3).

Hu and O'Connell (1992) treated the tunnel resistance of the junction as an ohmic resistance and used the zero-temperature approximation to find the ZBR of the above-mentioned junction as $R_o/R_t=3.75$.

The zero-bias resistance (ZBR) of the single junction increases with the increase in the impedance of the environment. This is the result of the reduced total averaged noise power delivered to the junction. For moderate values of β , e.g. $\beta=3$ and 10 corresponding to $R=30\text{K}\Omega$ and $100\text{K}\Omega$ respectively, the fluctuations vary slowly with temperature and the ZBR saturates at low temperatures indicating a weak dependence of $\langle q^2 \rangle$ on T . For $\beta \gg 2$, the fluctuations are linearly related to temperature, $T_e \approx T$, and the ZBR increases exponentially with the decreasing temperature, indicating that the noise in this regime is dominated by the thermal fluctuations.

With low external circuit impedance, the discrepancy between the two schemes is small, e.g. for $R=9K\Omega$, the difference in $\langle q^2 \rangle$ is only 0.4% and $R_o/R_t=1.17$ is obtained for this junction compared with the experimental value of 1.3. The data presented by Cleland and co-workers shows that the quantum Langevin approach allows good predictions for junctions with high tunnel resistance coupled to a high impedance environment.

6.4 Charge Macroscopic Quantum Tunnelling:

The fluctuations of the charge variable due to quantum and thermal noise in the environment were investigated. These fluctuations give rise to the increase of the junction energy and the system will oscillate along the potential profile around the metastable minimum. The quantum Langevin approach showed that the low-bias conductance decays exponentially with decreasing equivalent temperature. At $T_e \approx 0$ K, formula (6.3.9) gives a negligible escape rate from the metastable state $q=Q$, for $|Q| < e/2$, and the charge will be localised at $q=Q$. The principal mechanism by which the system can leave the metastable state in this regime is the quantum tunnelling of the charge variable through the electrostatic barrier. The electron has to tunnel not only through the barrier associated with the insulating region between the electrodes but also through the barrier arising due to the Coulomb interactions.

Quantum fluctuations of the charge will have the dominant effect in the low-temperature regime when $k_B T_e \ll \hbar \omega_0 / 2$ where escape rate due to thermal fluctuations can be ignored. Quantum tunnelling of the charge takes place through the barrier (not above the barrier) when $\hbar \omega_0 / 2 < U(e/2)$; which defines the range of validity of the following analysis.

Equation (6.2.1), governing the classical evolution of the charge, represents the motion of a particle of mass L attracted to a fixed centre, $q=Q$, by a force $F=q/C$ (Hook's law). This is a typical linear harmonic oscillator system; the Schrödinger equation for which is:

$$-\frac{\hbar^2}{2L} \frac{d^2\psi}{dq^2} + \frac{1}{2C}(q - Q)^2 \psi = E\psi \quad (6.4.1)$$

The solution of the above equation is a well-known result, e.g. Bransden and Joachain (1989); the wave-functions are expressed in terms of the Hermite polynomials, viz.:

$$\psi_n(q) = \left(\sqrt{\frac{\pi}{\alpha}} 2^n n! \right)^{-1/2} \exp\left(-\frac{\alpha}{2} \left(\frac{q-Q}{e} \right)^2 \right) H_n\left(\sqrt{\alpha} \left(\frac{q-Q}{e} \right) \right) \quad (6.4.2)$$

where $\alpha=2E/\hbar\omega_0$. The energy spectrum of the system is given by the set $E_n = \left(n + \frac{1}{2}\right)\hbar\omega_0$, $n=0,1,2,\dots$

Let the system be at the ground state $n=0$; the wave-function is then given by:

$$\psi_0(q) = \left(\sqrt{\frac{\alpha}{e^2 \pi}} \right)^{1/2} \exp\left(-\frac{\alpha}{2} \left(\frac{q-Q}{e} \right)^2 \right) \quad (6.4.3)$$

The probability density, $p(q)$, can be calculated from the wave-function in the usual way:

$$p(q) = |\psi_0(q)|^2 \quad (6.4.4)$$

which is a gaussian distribution function. The fluctuations of the charge level can be calculated from the distribution function, giving:

$$\langle (q-Q)^2 \rangle = \hbar\omega_0 C / 2 \quad (6.4.5)$$

The above analysis is valid only in the absence of dissipation, $R=0$. Finite external resistance dampens the charging/discharging processes and reduces the quantum fluctuations. When the charging process is completed the charge variable will be localised at $\langle q \rangle = Q$.

In the case of no dissipation, $R=0$, the quantum fluctuations cause the system to oscillate in a charge region $Q \pm \varepsilon$ in the classically allowed region, where ε is given from the relation: $C\hbar\omega_0 = \varepsilon^2$. The fluctuations may drive the charge variable to $q > Q + \varepsilon$ and the system will spend some time below the barrier. An

electron may tunnel from one side of the junction to the other (with probability = $\Gamma \times \Delta t$) if the system spends a time Δt at the state $q > e/2$, thus causing the system to escape from its metastable state. The exit point in this case may be defined by the set $\{q' \rightarrow q'-e\}$. The quantum fluctuations are responsible for the transition, below the barrier, from Q to q' and the possible tunnel event eventually takes the system to the state $q'-e$. The recharging process takes the system back to the metastable state, $q=Q$, in a finite time determined from the classical charging curve. The total escape rate from the metastable state is therefore given as the sum of the contributions of all states satisfying $q > e/2$, viz.:

$$\Gamma_m(Q) = \int_{e/2}^{\infty} \Gamma(q) \cdot p(q) \cdot dq \quad (6.4.6)$$

where $\Gamma(q)$ is the zero-temperature tunnelling rate. It is straight forward to use the same method implemented in section (5.3) to show that the tunnel junction at zero temperature will have a non zero conductance, G_m , given by:

$$G_m(Q) = 2C \frac{\alpha^{3/2} G_t}{\sqrt{\pi e^3}} \int_{e/2}^{\infty} (q - e/2) \left\{ (q - Q) \exp\left(-\alpha \left(\frac{q-Q}{e}\right)^2\right) + (q + Q) \exp\left(-\alpha \left(\frac{q+Q}{e}\right)^2\right) \right\} dq \quad (6.4.7)$$

where $\alpha = 2E_0/\hbar\omega_0$. The dependence of G_m on the ground-state energy, $\hbar\omega_0/2$, is similar to the variation of the conductance with the thermal energy. The conductance decreases exponentially with the ratio α ; in other words, the conductance decreases exponentially with increasing \sqrt{L} . This is expected because the inductance, L , plays the role of the mass attached to the string. If the inductance of the connecting leads satisfies the relation $\alpha \gg 1$, the quantum fluctuations will be equivalent to the thermal fluctuations at an equivalent temperature T_e defined by the relation:

$$k_B T_e = \hbar \omega_0 / 2 \quad (6.4.8)$$

The single-junction circuits studied by Cleland et al (1990) are reported to have capacitances $\approx 4\text{fF}$ and inductances in the connecting paths of the order of 4.5nH . Ignoring the dissipative elements in the circuit, the quantum fluctuations are equivalent to a temperature of $T_e=0.9\text{K}$ corresponding to the value $\alpha=0.26$, which indicates that the quantum fluctuations are higher than the charging energy and the charge-MQT can not be observed in such circuits. The quantum fluctuations are dominant at the low-temperature regime; and are responsible for the fixed low-bias conductance.

It has been argued that the tunnelling electron will probe the electromagnetic environment that lies in an area of some radius around the junction. Thus, a tunnelling electron will be affected by the environmental modes in this area and will excite some modes as well. Devoret et al (1990) studied the transport characteristics in an R-L environment taking these modes into account and found the tunnel rate in the case of zero dissipation as:

$$\Gamma_D = \frac{G_t}{e^2 C} \exp\left(-\frac{\alpha}{2}\right) \sum_0^{n_{\max}} (eQ - n\hbar\omega_0 C) \quad (6.4.9)$$

where n_{\max} corresponds to the highest excited mode. The above equation suggests that the differential conductance displays a series of steps located at voltage levels $V_n = n\hbar\omega_0/e$. At low voltages the I-V curves will be dominated by the mode $n=0$ corresponding to the elastic channel and the differential conductance is estimated from this model to be $G_D = G_t \exp(-\alpha/2)$.

6.5 Effect of External Resistance:

The problem of tunnelling in a dissipative medium was studied by Caldeira and Leggett (1981 & 1983) and Waxman and Leggett (1985). It was shown that the effect of dissipation in a circuit is to suppress the tunnelling process in that circuit. The dissipative environment is treated as a collection of linear oscillators that interact with the system. The tunnelling rate out of the metastable state into the continuum of states is calculated using path integral methods. Ford et al

(1988) also studied the tunnelling process through a local maximum of a potential barrier in the presence of dissipation using the quantum Langevin equation approach. They assumed that the dissipative system can be replaced by a non-dissipative system if a modified potential is used in place of the original potential. This technique resulted in the same conclusion: the dissipative element tends to reduce the macroscopic quantum tunnelling rate.

The potential profile studied here is well defined in the range (-e/2, e/2). For charges satisfying: $|q| > e/2$, the potential is modified due to the stochastic nature of tunnelling. A tunnel event at q' takes the system from the point $q=q'$ on the potential (6.2.3) to the point $q=q'-e$ on the same potential. Subsequently, the system moves classically on the potential profile and the behaviour can be determined by the charging curves of a normal capacitor.

Let it be assumed that it is possible to replace the potential profile in which the charge variable moves by an equivalent continuous *cubic* potential satisfying at least the conditions:

$$U(q) \approx U'(q) , \quad q < q_1;$$

$$\text{and} \quad U(Q) = U(q_m)$$

where $U'(q)$ is the modified potential, q_1 is a value of the order of $e/2$ and q_m is the charge level at which tunnelling is most likely to occur. The value q_m is obtained from (6.4.6) as:

$$q_m = \left\{ \frac{e}{2} + Q + \sqrt{(e/2 - Q)^2 + 2\hbar\omega_0 C} \right\} / 2 \quad (6.5.1)$$

If $U(e/2) \gg \hbar\omega_0/2$ then

$$q_m \approx \frac{e}{2} + \frac{\hbar\omega_0 C}{e/2 - Q}.$$

Under the new potential, the exit point, $\{q' \rightarrow q'-e\}$, is replaced by a single exit point, viz. q' . Such an approximation was used by Averin and Odintsov (1989), on dealing with the charge macroscopic quantum tunnelling in Josephson junctions where the potential profile is basically quadratic. Caldeira and Leggett

(1983) showed that the dissipative element in a cubic potential will reduce the tunnelling rate by a factor $\approx \exp\left(-\frac{\zeta R|\Delta q|^2}{\hbar}\right)$, where ζ is a factor of the order unity and Δq is the distance under the barrier. For the model under study, Δq is given by:

$$\Delta q = \frac{e}{2} - Q + \frac{\hbar\omega_0 C}{e/2 - Q}, \quad Q \ll e/2 \quad (6.5.2)$$

The suppression factor in the low-bias regime is approximately given by $\exp\left(-\frac{e^2 R}{4\hbar}\right)$ which is comparable to the exponential term obtained by Devoret et al (1990), viz.:

$$\Gamma_D = \frac{G_t Q}{eC} \frac{1}{\Gamma(2+r)} \left(\frac{\pi r Q}{2e}\right)^r \exp\left(-\frac{e^2 R}{5.44\hbar}\right) \quad (6.5.3)$$

where $r=R/R_Q$ and $\Gamma(x)$ on the RHS is the gamma function. The relation (6.5.3) above suggests a weak power-law zero-bias anomaly, $dI/dV \propto V^r$.

Averin and Odintsov (1989), treated the tunnel term in the Hamiltonian (2.3.4) as a perturbation term and showed that the tunnel rate in the regime $R \ll R_Q$, for small voltages is expressed by:

$$\Gamma_{AD} = \frac{G_t Q}{eC} \frac{1}{\Gamma(2+r)} \left(\frac{\pi r Q}{e}\right)^r \quad (6.5.4)$$

which is similar to (6.5.3) in the limit of vanishing dissipation and identical zero-bias anomalies are obtained.

6.6 MQT in Multi-Junction Arrays:

The charge-MQT in a multi-junction system is an important process that should be carefully considered if the system is to be used in digital logic circuits. At voltages less than the threshold voltage, a tunnel event across any junction will result in an increase in the total Coulomb energy of the system and, therefore, the event is classically suppressed by the Coulomb interactions. However, the thermal

fluctuations can cause a tunnel event despite the Coulomb gap as explained for the single junction. Any junction may be treated as an isolated single junction probing an environment of total impedance $Z(\omega)$. The total tunnel rate across this junction can be evaluated in a way similar to that discussed in section (6.3) where it was found to decrease exponentially with the decrease in temperature. Therefore, the decay of the Coulomb-blockade state due to thermal noise can be neglected if $T \ll T_c$.

In an array of N tunnel junctions, at low temperatures, the quantum fluctuations of the charge across each tunnel junction can cause simultaneous tunnel events across each junction. This is equivalent to a single-electron tunnel act through the whole array. It was shown by Averin and Odintsov (1989) using the quantum golden rule that the inelastic charge-MQT rate through the array of N tunnel junctions may be expressed as:

$$\Gamma_{AO}(N) \propto \frac{\prod \left(G_{ti} / G_Q \right)}{(2N-1)!} V^{2N-1}$$

which suggests that the charge-MQT rate in an array of identical junctions decreases as the N -th power of G_t/G_Q . Longer arrays are more reliable than shorter arrays and the low-bias anomaly has the form $\partial I / \partial V \propto V^{2N-2}$. Charge-MQT has been observed by Geerligs et al (1990) in a double-junction configuration. Their data showed reasonable agreement with the inelastic charge-MQT formula given above which predicts an I-V relationship of the form $I \propto V^3$ inside the Coulomb-blockade region. Elastic charge-MQT is predicted to result in a current that is linearly related to V . This has been observed by Hanna et al (1992).

In chapter (3) the double-junction system -the turnstile- was studied as a candidate device for a memory element in logic systems. The charge-MQT presents a menace that will degrade the reliability of this device. It was mentioned above that increasing the tunnel resistance would result in enhanced suppression of

MQT events. On the other hand, this increased R_t would impose a longer waiting time, at the Store and Retrieve states, to ensure that the required event will occur during that period (with a high probability).

Series resistive components in the turnstile circuit were proposed to favour the occurrence of the wanted events and dramatically reduce the chances of the unwanted events. Fortunately, resistive elements in the turnstile circuit tend to suppress the MQT of the charge.

Golubev and Zaikin (1992) used the Caldeira-Leggett formulation to show that in the presence of a dissipative element the tunnel rate across an array of N tunnel junctions is given by:

$$\Gamma_{GZ}(N) \propto \frac{\prod \left(\frac{G_{ti}}{G_Q} \right)}{\Gamma(2N+r/2)} V^{2N-1} (rVR_Q)^{r/2}$$

6.7 Charge Trapping Effects:

It was shown that the conductance of a multi-junction system is greatly affected by slight changes in the gate potential. This is due to the modulation of the potential of the inner nodes with respect to the fixed-potential outer nodes. A system will also be affected by other systems if mounted on the same chip; the degree of coupling being dependent on the stray capacitances between adjacent nodes, Roy (1992).

Modulation of the potential at the nodes may be caused by single charges being trapped or released in the vicinity of the nodes. This process has been studied in semiconductor devices. The charge trapping/detrapping in the semiconductor-oxide interface of MOSFETs is responsible for the 1/f noise observed in the drain current of the device, e.g. Reimbold (1984) and Uren et al (1985). When a trap centre is charged it acts as a scatterer producing a change in the channel conductance. In short devices, with few trap centres, the phenomenon

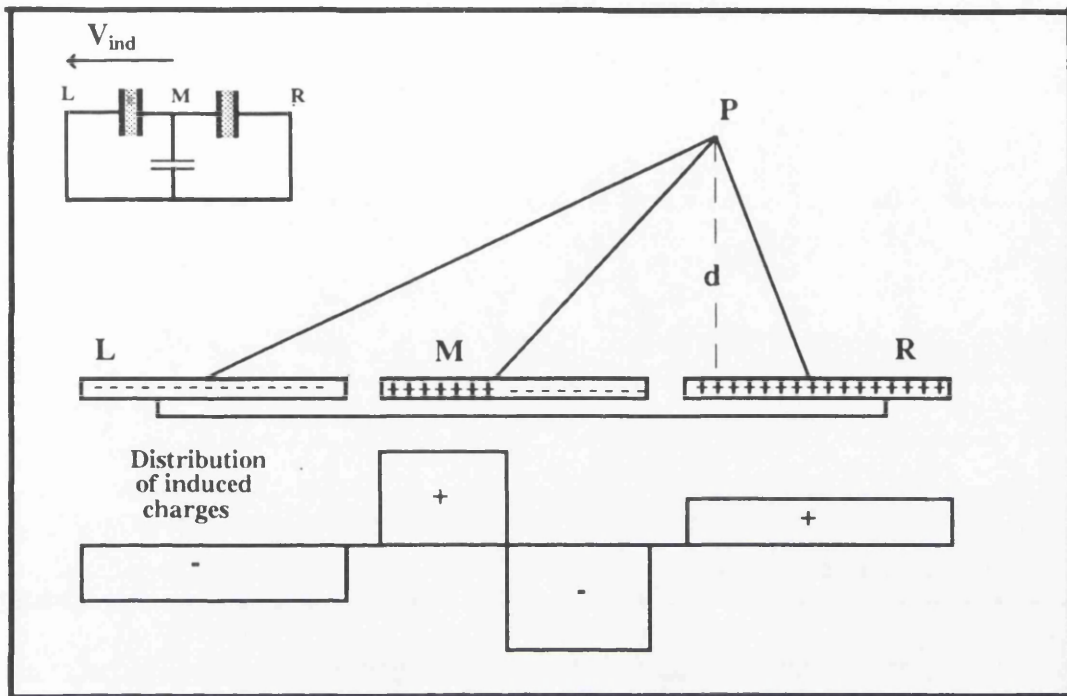


Figure (6.3): The distribution of the induced charges at the three segments of the one-dimensional electron gas due to a single electronic charge located at P. Shown also the induced potential difference between the electrodes.

is seen as a telegraphic noise superimposed on the current through the channel, Ralls et al (1984) and Skocpol (1986).

The effects of single trapped charges at the surface of, or inside, the material on which single-electronic devices are built are studied here with reference to the double-junction structures used by Meirav et al (1990), see section (3.2). Current flow takes place through the electron gas at the GaAs-AlGaAs interface. The negative bias on the top gates depletes the electron gas beneath these electrodes and creates a one-dimensional electron gas. The experiments carried out on these structures showed that the behaviour of the device changes each time the device is cycled to room temperature and back to low temperatures. The changes are visible in the conductance oscillation peaks and positions of the peaks. The variations may be explained in terms of charges being permanently trapped at the surface of the semiconductor.

The conducting channel is modelled as a conducting line divided by the tunnel barriers into three segments: left, central and right. The left and right portions are connected to the voltage source and will always be held at fixed potentials. The potential of the central segment is controlled by the GaAs substrate potential. Single trapped charges will modify the potential of the central 1-DEG and hence affect the characteristics of the device.

Let a single electron be trapped at point P at a distance d from the 1-DEG. The circuit may be investigated under zero-bias conditions: $V_\ell=V_r=V_g=0$, and the conducting channel is assumed to be independent of the voltage sources, i.e. the three-segment structure shown in figure (6.3) will be preserved under these conditions. The trapped charge at P will induce charges on the left and right segments which are assumed to be evenly distributed on each segment creating charge densities of ρ_ℓ and ρ_r on the left and right segments respectively. The central electrode develops zero net charge, but will be polarised as shown in the figure.

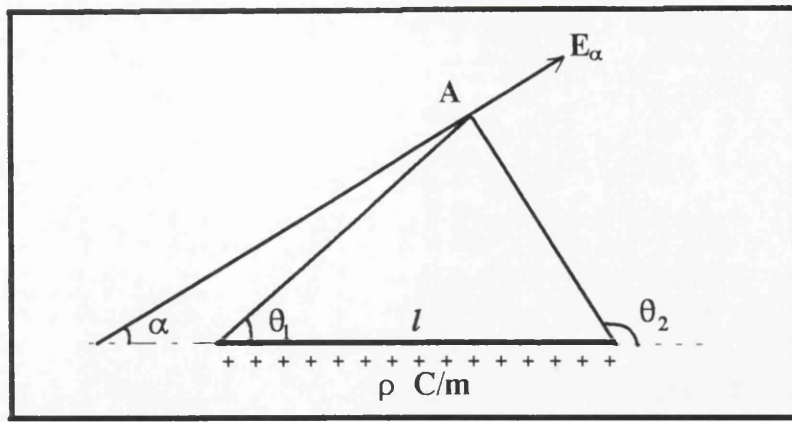


Figure (6.4): Electric field strength due to a uniformly distributed charge

Let \bar{E}_l , \bar{E}_r and \bar{E}_m be respectively the electric field strength at a point (e.g. A) due to the left, right and central sections of the 1-DEG. The total field strength at this point (A) in the direction RP is then calculated as:

$$E_{RP}^A = \frac{e}{4\pi\epsilon x^2} + (\bar{E}_l + \bar{E}_r + \bar{E}_m) \cdot \bar{u}_{RP} \quad (6.7.1)$$

where \bar{u}_{RP} is a unit vector in the direction RP and x is measured from P. Similar expressions are readily obtainable for the fields in the directions LP and MP.

Consider a uniform distribution of charge (ρ C/m) on a line of finite length, l . The field strength in a direction making an angle α with the line at a point A, figure (6.4), can be obtained from Coulomb's law as:

$$E_\alpha = \frac{\rho}{4\pi\epsilon d} (\sin(\theta_2 - \alpha) - \sin(\theta_1 - \alpha)) \quad (6.7.2)$$

where d is the distance between the point and the line, θ_1 and θ_2 are defined as in the figure. This relation can be used to evaluate the field strength (at any point in space at any direction) due to the induced charge distribution. The fields due to the left and right segments are obtained directly from relation (6.7.2). The central segment can be divided into two sections each with a different charge density and different θ 's.

Under the zero-bias conditions considered here, the left and right segments of the 1-DEG will lie on an equi-potential surface. The distribution of the charge

on the channel can be obtained by equating the potential differences between the trap centre and the left and right segments:

$$\int_{r_1}^{R_{RP}} E_{RP} \cdot dR_1 = \int_{r_1}^{R_{LP}} E_{LP} \cdot dR_2 \quad (6.7.3)$$

where r_1 is the radius of the 1-DEG. The induced potential difference between the outer and central segments is then calculated as:

$$V_{ind} = \int_{r_1}^{R_{RP}} E_{RP} \cdot dR_1 - \int_{r_1}^{R_{MP}} E_{MP} \cdot dR_o \quad (6.7.4)$$

Figure (6.9.A) shows the variation of the induced potential difference, V_{ind} , as a function of the location of the trapped electron on the surface of the (Meirav) double-junction system. The parameters of the device are $\ell_l = \ell_r = 1\mu\text{m}$, $\ell_m = 0.8\mu\text{m}$, $d = 50\text{nm}$. The capacitances are taken to be $C = C_o = 10\text{aF}$. The critical voltage with no trapped charges is 4mV. The induced voltage attains the extreme values when the trapped electron is located nearest to any of the three segments. The induced voltage modifies the p.d.'s across the left and right junctions; the critical voltage is then related to the induced voltage by:

$$V_{th} = \frac{1}{C + C_o} \left(C_T V_{ind} + \frac{e}{2} \right); |V_{ind}| < e/2C_T \quad (6.7.5)$$

For an induced p.d. greater than $e/2C_T$, an electron can tunnel into or out from the central segment, thus changing the charge distribution on the electrodes at the zero-bias condition. The critical voltage is then given as:

$$V_{th} = \frac{1}{C + C_o} \left(C_T V_{ind} - \frac{e}{2} \right); |V_{ind}| > e/2C_T \quad (6.7.6)$$

Figure (6.9) indicates that an electron trapped nearest to the central segment induces the maximum negative potential difference between the outer and central electrodes and the critical voltage is then minimum, (0.3 mV). Increasing the separation between the 1-DEG and the semiconductor surface reduces the induced

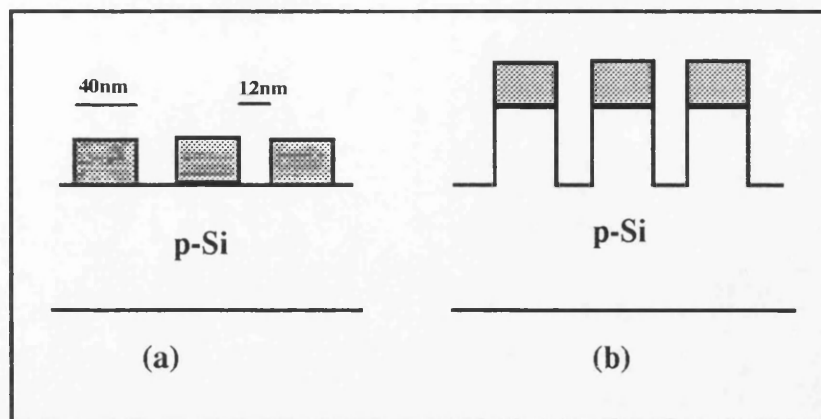
p.d. between the segments and hence reduces the variability of the critical voltage. Figure (6.9.B) shows the variation of the critical voltage for a device with $d=100\text{nm}$. The device is found to have a critical voltage varying in the range (2.5-5.3mV) and is clearly less sensitive to the single trapped charges when compared with the previous device ($d=50\text{nm}$ and V_{th} in the range 0.3-5.3mV). The data shown in figure (6.9.C) is taken for a similar device with $d=100\text{nm}$ but the capacitance is chosen as $C=C_0=1\text{aF}$. The device is more stable ($37\text{mV} < V_{th} < 44\text{mV}$).

It is clear from the above analysis that the performance of the double-junction system is sensitive to single charges being trapped near the electrodes. The behaviour is also a function of the exact location of the trapped charge and the geometry of the system. In the above arguments, only negative charges were considered. However, the extension to cover positive charges is straight-forward and similar results are expected. The induced p.d.'s are of the same magnitude as the p.d.'s due to negative charges. The effect on the critical voltages can be obtained using relations (6.7.5 & 6.7.6).

Trapping a charge while the system is in operation will shift V_{th} to a new level and this will either (a) switch the device on, (b) switch the device off or (c) cause a change in the current that is already passing through the device (in general: $I \propto (|V| - V_{th})$ if $|V| > V_{th}$). The acts of trapping and detrapping single electronic charges in localised trap centres produce telegraphic type of noise in the current passing through the device, similar to the noise in short channel MOSFETs; see e.g. Skocpol (1986). The behaviour depends on the initial state of the system and the location of the trapped charge. The trapping/detrapping processes are of prime importance if the device is intended to be used in logic circuits.

The effect of surface trap centres on single electronic systems has been studied by Asenov (1993) on a system of metallic particles deposited on p-type silicon, figure (6.5.A). It is assumed that the effects may be determined if the capacitances of the junctions, which are modified due to the presence of the

trapped charges, are known. The trap centres are assumed to lie in the middle of the band gap. The potential profile is determined from the self-consistent solution of Poisson's equation for the system.



Figure(6.5): a: Model used to determine the effects of surface charges on the metallic quantum dot structures. b: Modified structure to reduce the effects.

Asenov has shown that the capacitance between the metallic dots remains fairly unchanged in the presence of both donor and acceptor surface states (of concentration = $10^{10}/\text{cm}^2$). The capacitance to ground, C_o , is found to be constant in the presence of donor states while it is ($\sim 25\%$) higher with acceptor surface states. It was also suggested that the capacitance to ground may be stabilised by using etched structures similar to those shown in figure (6.5.B), see Roy et al (1993).

Finally, it must be pointed out that such results reflect only the average expected properties of these arrays. Solution of Poisson's equation in the presence of single or few trapped charges will be required to determine the exact effects of these charges.

6.8 Killer Processes and the Traffic Model:

The decay of the Coulomb-blockade state due to the several processes mentioned in this chapter can be easily embodied in the Traffic Model discussed in

the previous chapter. The effect of thermal and quantum fluctuations at any bias condition is to modify the tunnel rate from a given node to the other (normally, rate in presence of thermal and quantum fluctuations > rate with no fluctuations). The modified tunnel rates simply replace all rates defining the parameters of the Traffic Model. Similarly, the charge trapping/detrapping effects can be accommodated in the model, except that the tunnel rate may increase or decrease according to the type and location of the trapped charges.

A macroscopic quantum tunnel event in a multi-junction system (e.g. array) is accomplished by several tunnel events taking place simultaneously. Such an event will leave the state of the system unchanged. A system that is initially found at state ψ_i will leave this state and enter other states with different probabilities that can be calculated by solving the traffic equations. However, there is also a non-zero probability that the system will re-enter the same state at a rate that is equal to the charge-MQT rate, i.e.

$$\mu_i = \Gamma_{MQT}(i)$$

and the occupancy of states are then calculated in the usual way.

Summary:

The thermal and quantum fluctuations have been studied using the Langevin equation approach. The fluctuations are calculated using an accurate numerical technique and proved to yield better agreement with experimental data. It is shown that the low-bias resistance is enhanced when the junction is coupled to the source via a higher impedance environment. The charge-MQT is investigated and shown to decrease exponentially with dissipation in a single-junction circuit.

The effect of charges being momentarily or permanently trapped in the vicinity of tunnel junctions is found to have detrimental effects on the performance of the circuit. The effects can be reduced by keeping the junctions away from the surface and by using high quality materials, with the minimum possible trap centres.

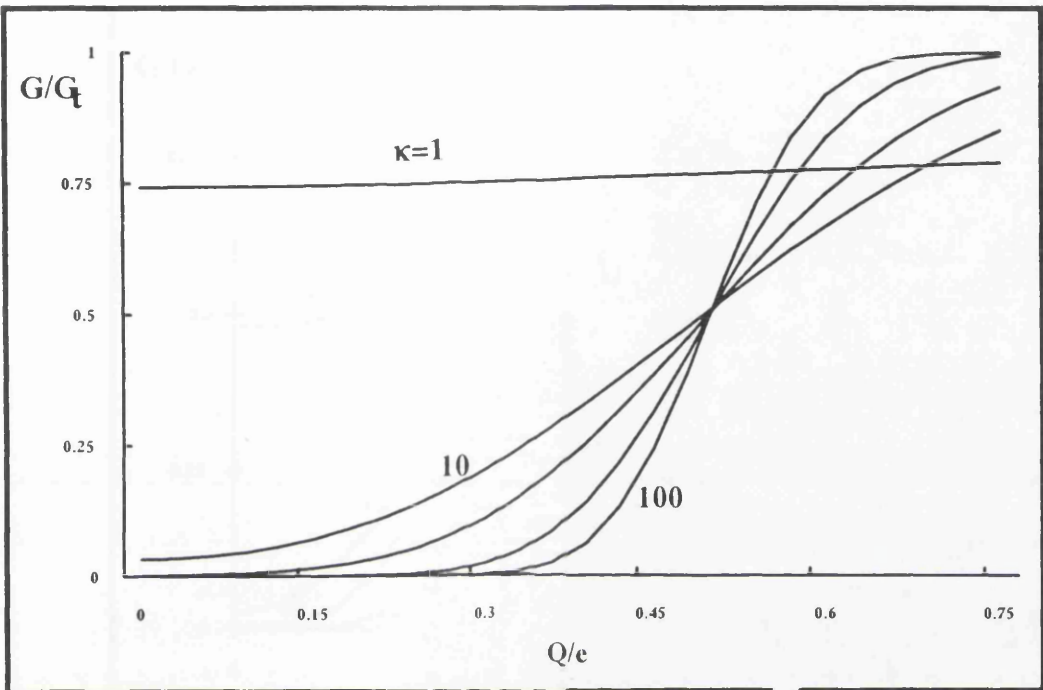
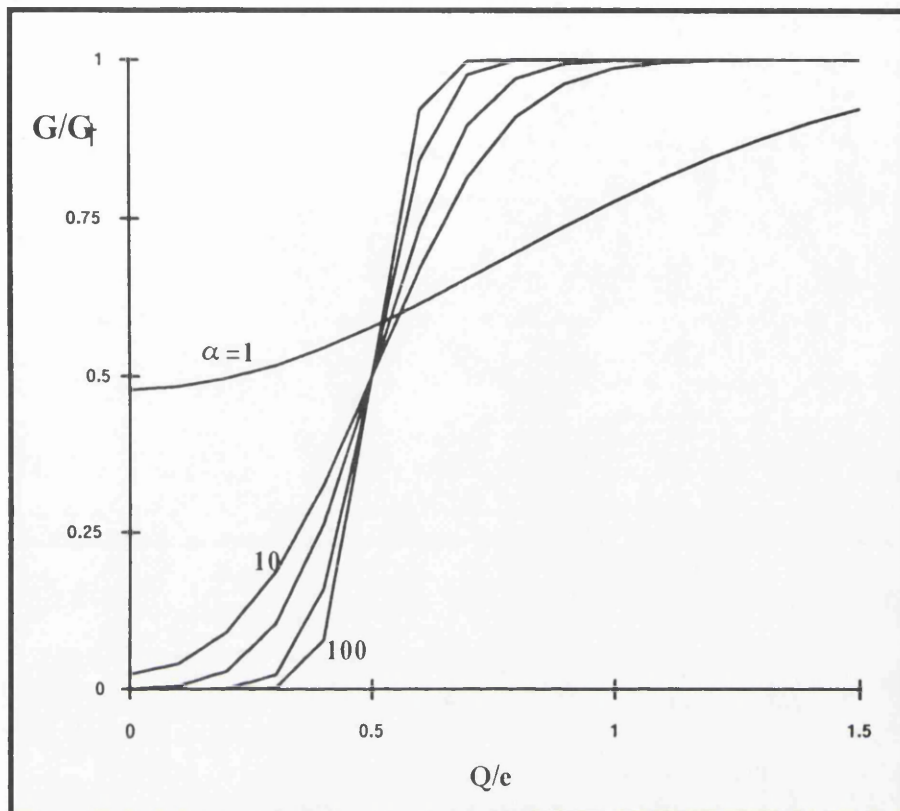


Figure (6.6): Effect of temperature on the conductance of a single tunnel junction.

$\kappa=1, 10, 20, 50$ and 100 .



Figure(6.6A): Conductance of the single junction due to the macroscopic quantum tunnelling of the charge variable: $\alpha=2E_C/\hbar\omega_0=1, 10, 20, 50$ & 100 .

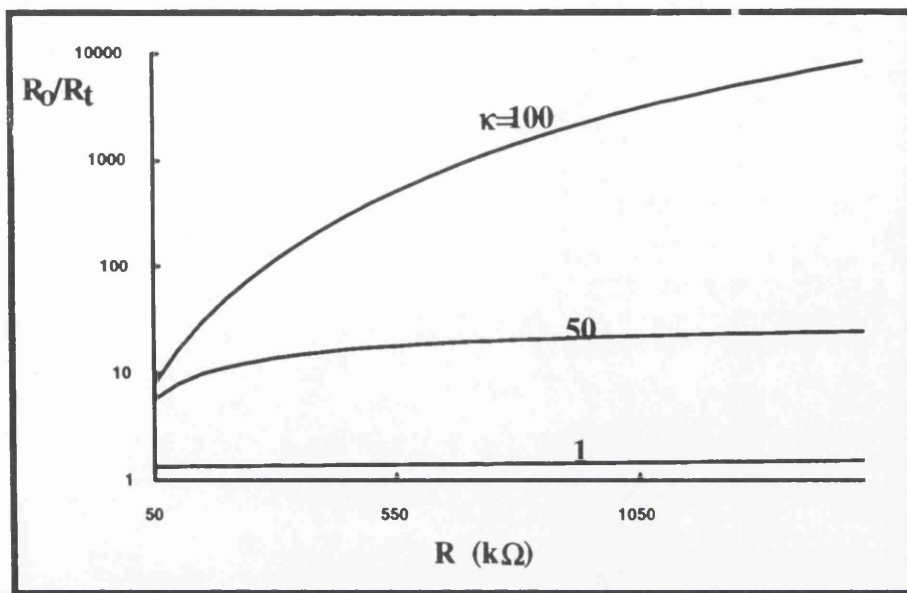


Figure (6.7): Effect of the environmental impedance on the zero-bias resistance of a single junction: $C=0.5\text{af}$, $L=5\text{nH}$, $E_c/k_B T=1, 50 \& 100$.

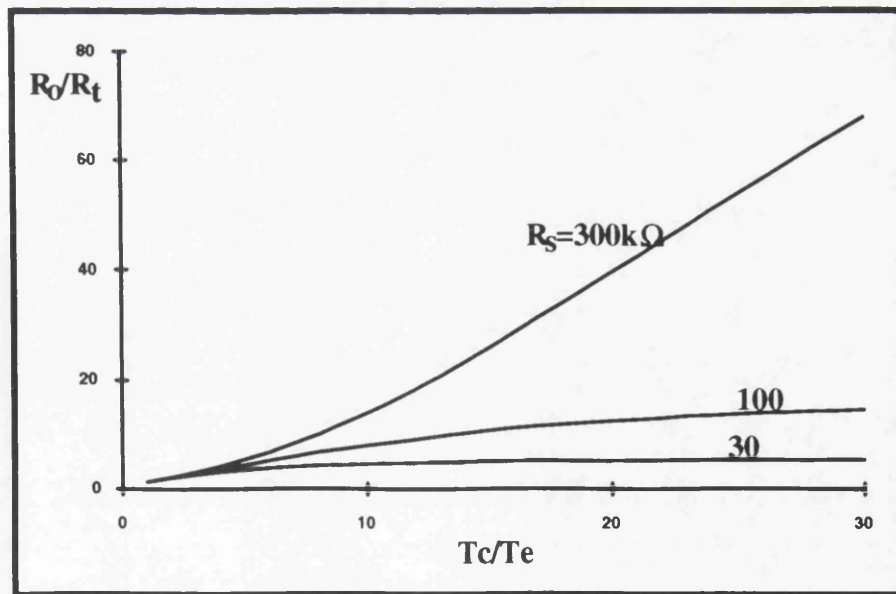
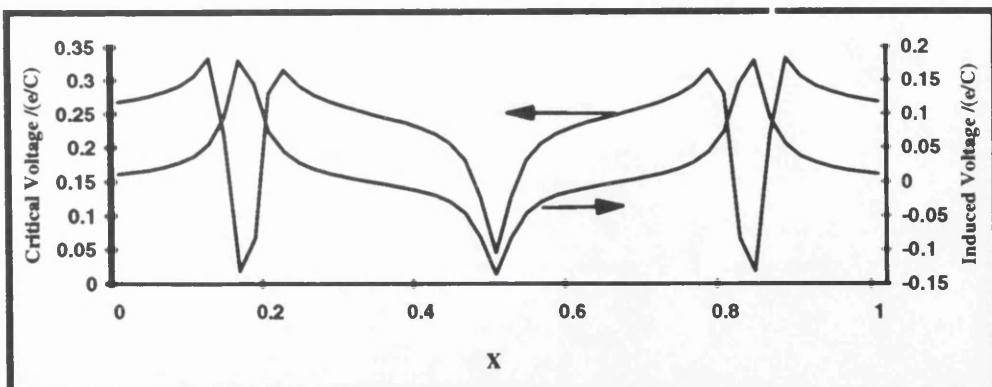
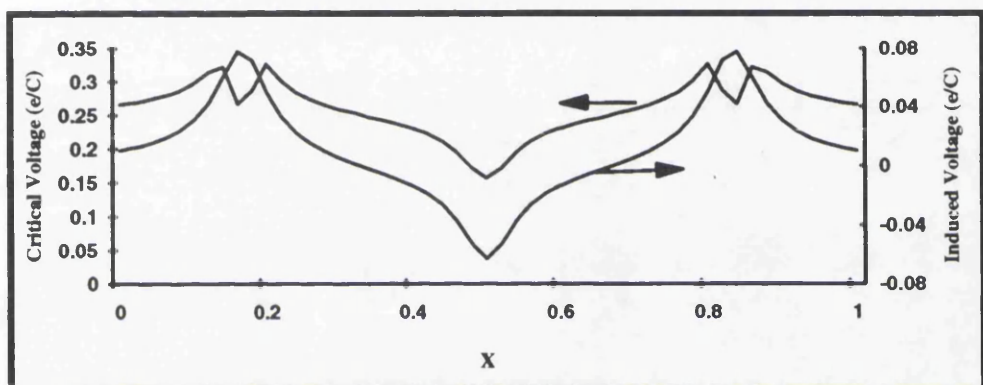


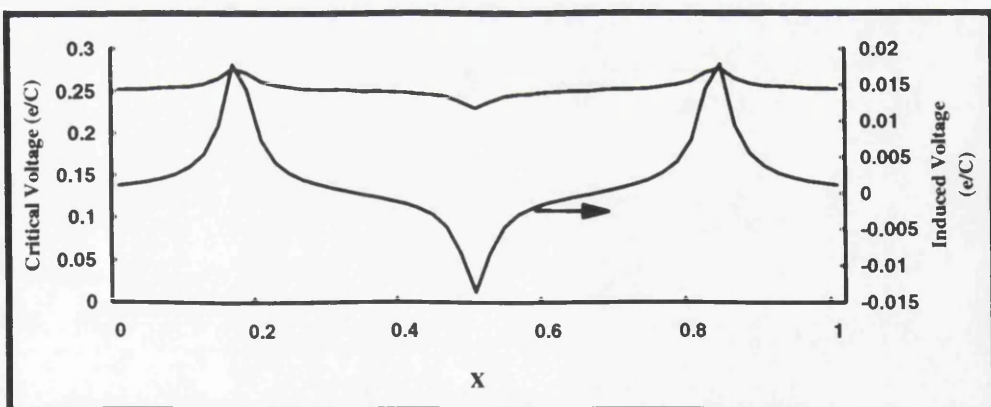
Figure (6.8): Variation of zero-bias resistance with temperature: $C=0.5\text{af}$, $L=5\text{nH}$, $R_s=30, 100$ and $300\text{k}\Omega$.



(A)



(B)



(C)

Figure (6.9): Induced p.d. and resulting critical voltage as a function of the location of the trapped electron: $\ell_l = \ell_r = 1\mu m$, $\ell_m = 0.8mm$, (A) $d = 50nm$, $C = C_o = 10aF$ (B) $d = 100nm$, $C = C_o = 10aF$ and (C): $d = 100nm$, $C = C_o = 1aF$. (x =distance/length).

Conclusion

In this thesis a new technique to model the steady-state behaviour of single-electronic systems has been introduced. The technique was successfully used to study the properties of the double-junction structure and linear arrays of tunnel junctions. It is to be emphasised that the technique formulated in chapter (5) is quite general and is applicable to any network of normal tunnel junctions. Tunnelling dynamics in networks of superconducting tunnel junctions may also be studied within this new formalism.

Although the Traffic Model has been extensively used to study the flow of messages and calls in communication systems, it was largely ignored in other fields. In fact, this method seems promising in areas where the systems under study contain few interacting or non-interacting objects and can be found in finite and well-defined set of states. It can be used, e.g., in modelling transport in systems where few electrons are involved in the process.

Another important feature of the new technique is that it allows the most probable evolution of the system to be determined. This is crucial in systems where the single-electronic device is intended to control other events in the system according to a given input. The technique helps study these events in the time domain and the possible delays in the circuit can thus be obtained.

Some single-electronic devices are shown to function efficiently and effectively as switching elements in analogue circuits. On the other hand, their performance in digital circuits is not very promising. This is due to the high sensitivity of these devices to slight changes of the potential at the electrodes. It is possible to dramatically reduce the thermal and quantum fluctuations in single-electronic circuits, viz. by keeping the operational temperature much lower than the critical temperature and by coupling to a high impedance environment. The charge-macroscopic quantum tunnelling process is another fatal process that

should be carefully considered. It is shown that this process can be reduced by the addition of resistive components to the circuit.

Charges being momentarily or permanently trapped in the vicinity of the electrodes are shown to introduce the most severe effect in the circuit. The other fluctuations; viz. thermal and quantum fluctuations, cause occasional tunnel events (in the Coulomb-blockade regime) while the basic behaviour is preserved. Trapped charges change the overall characteristics of the system. It is shown that the effect, in turnstile circuits, is manifested as a shift in the threshold voltage of the device. This, in effect, shifts the I-V characteristics of the device and the current is either increased or decreased depending on the type of the trapped charge and its location. The device may also change its state.

Elimination or reduction of the effects of trapped charges can be achieved by using high quality materials and by keeping the (tunnel and non-tunnel) nodes away from the surface. The method used to calculate the effects of the trapped charges at the surface of (or inside) the device is an approximate method that gives a qualitative idea about the induced potential difference between the electrodes and hence the modified critical voltage. An accurate technique would be the self-consistent solution of the Poisson's equation in the presence of the trapped charges.

References

- Abeles B, " *Granular Metal Films*", in 'Applied Solid State Science' e.d. R.Wolfe, Academic Press, 1976.
- Abeles B, Sheng P, Gouts M and Arie Y, Adv. Phys. 1975, 24, 407.
- Amman M and Mullen K, "The charge-effect transistor", J. App. Phys, 1989, 65, 339.
- Amman M, Ben-jacob B and Mullen K, "Charge Solitons in 1-D Array of Mesoscopic Tunnel junctions", Phys. Lett. (A), 1989, 142, 431.
- Asenov A, 1993, Private Communications.
- Averin D and Likharev K, "Coulomb Blockade of SET and Coherent Oscillations in small Tunnel Junctions", J. Low Temp. Phys., 1986, 62, 345.
- Averin D and Likharev K, "New Results of the Theory of SET and Bloch Oscillations in Small Tunnel Junctions.", IEEE Trans, Magn, 1987, 23, 1138.
- Averin D and Odintsov D, "Macroscopic Quantum Tunnelling of the electric charge in small tunnel junctions", Phys. Lett. A, 1989, 140, 251.
- Averin D and Korothov A, "Influence of discrete energy spectrum on correlated S.E.T. Via a mesoscopically small metal granule", JETP, 1990, 70, 937.
- Averin D and Nazarov Y, "Virtual Electron Diffusion during Quantum Tunnelling of the Electric Charge", Phys. Rev. Lett., 1990, 65, 2446.
- Averin D and Likharev K, in "Quantum Effects in Small Disordered Systems", eds B.L.Al'lshuler, P.Lee and R.Loeb, (Elsevier, Amsterdam), 1990.
- Averin D, Korothov A and Nazarov Y, "Transport of Electron-Hole Pairs in Arrays of small tunnel junctions", Phys. Rev. Lett, 1991, 66, 2818.
- Babikir S, Barker J & Asenov A, "Queuing theoretic simulation of metal-semiconductor single-electronic devices and systems", Proc. of International Workshop on Computational Electronics, Leeds, 1993, 260.
- Bakhvalov N, Kazacha N, Likharev K and Serdyukova S, "Single-electron solitons in one-dimentional tunnel structures", JETP, 1989, 68, 581.
- Barker J, "Grranular Electronics", Lecture notes, Glasgow University, 1991.
- Barker J, Private communications, 1993
- Barker J, Weaver J, Babikir S and Roy S, "On the theory, modelling and construction of electronic systems", Proc. of Second International Symposium on New Phenomena in Mesoscopic Structures, Hawaii, 1992.

- Barker J, Roy S and Babikir S, "Trajectory representations, fluctuations and stability of granular electronic devices", in *Science and Technology of Mesoscopic Structures*, ed. S.Namba, C.Hamaguchi and T.Ando Springer-Verlag, chapter (22), Tokyo, 1992.
- Barner J and Ruggiero S, "Observation of the Incremental Charging of Ag Particles by single Electrons." Phys. Rev. lett., 1987, 59, 807.
- Baskett F, Chandy K, Muntz R and Palacios F, "Open, Closed and Mixed Networks of Queues with Different Classes of Customers", J. of the ACM, 1975, 22, 248.
- Beaumont G, "Introductory Applied Probability", Ellis Horwood Ltd, 1983.
- Beenakker C, "Theory of Coulomb-blockade oscillations in the conductance of a quantum dot.", Phys. Rev. B., 1991, 44, 1646.
- Ben-jacob E, Mullen K and Amman A, "Charge-effect Solitons", Phys. Lett. (A), 1989, 135, 390.
- van Bentum P, van Kempen H, van Leemput L and Teunissen P, "SET observed with Point-Contact Tunnel Junctions", Phys. Rev. Lett., 1988, 60, 369.
- van Bentum P, Smokers R and van Kempen H, "Incremental Charging of Single Small Particles", Phys Rev. Lett., 1988, 60, 2543.
- Bransden B and Joachain C, "Introduction to Quantum Mechanics", Longman, 1989.
- Caldeira A and Leggett A, "Influence of Dissipation on Quantum tunnelling in Macroscopic System.", Phys. Rev. Lett., 1981, 46, 211.
- Caldeira A and Leggett A, "Quantum Tunnelling in a Dissipative System", Annals of Physics, 1983, 149, 374.
- Celasco M, Masoero A, Mazzetti P and Stepanescu A, "Electrical conductoin and current noise mechanism in discontinuous metal films", Phys. Rev. (B), 1987, 17, 2553.
- Chang L, Esaki L and Tsu R, "Resonant tunnelling in semiconductor double barriers", App. Phys. Lett., 1974, 24, 593.
- Cleland A, Schmidt J and Clarke J, "Charge Fluctuations in Small-Capacitance Junctions", Phys. Rev. Lett., 1990, 64, 1565.
- Cleland A, Scmidt J and Clarke J, "Influence of the environment on the Coulomb blockade in submicrometer normal-metal tunnel junctions", Phys. Rev. (B), 1992, 45, 2950.
- Cohn J, Ben-jacob E and Uher C, "Low-temperature electronic. transport and the Coulomb blockade in oxidised films of bismuth", Phys. Lett. (A), 1990, 148, 110.

- Delsing P, PhD Thesis, unpublished, 1990.
- Delsing P, Likharev K, Kuzmin L and Claeson T, "Single-Electron Oscillation in 1-D arrays of ultra small Tunnel junctions", Physica (B), 1990, 165-166, 929.
- Devoret M, Esteve D, Grabert H, Ingold G, Pothier H and Urbina C, "Effect of Electromagnetic Environment on Coulomb Blockade in Ultra-small Tunnel Junctions", Phys. Rev. Lett., 1990, 64, 1824.
- Dietz R, McRae E and Campbell R, "Saturation of the Image Potential Observed in Low Energy Electron Reflection at Cu(001) Surface", Phys. Rev. Lett., 1980, 45, 1280.
- Duke C, "Tunnelling in Solids", Solid State Physics, Supplement 10, 1969.
- Duke C, "Tunnelling and Negative Resistance Phenomena in Semiconductors", Chapter (1), ed. B.Pamplin, Pergamon Press, 1987.
- Eade J, "Performance Engineering", Lecture notes, Essex University, 1987.
- Eisenstein J, Pfeiffer L and West K, "Coulomb Barriers to Tunnelling between Parallel Two-dimensional Electron Systems", Phys. Rev. Lett., 1992, 69, 3804.
- Ford G, Lewis L, O'Connell R, "Dissipative Quantum tunnelling: Quantum Langevin Equation Approach", Phys. Lett. (A), 1988, 128, 29.
- Foxman E, McEuen P, Meirav U, Wingreen N, Meir Y, Belk P, Belk N, Kastner S and Wind S, "Effects of quantum levels on transport through Coulomb island", Phys. Rev. (B), 1993, 47, 10020.
- Fulton T and Dolan G, "Observation of Single-Electron Charging effects in Small Tunnel Junctions", Phys. Rev. Lett., 1987, 59, 109.
- Fulton T, Gammel P and Dunkleberger L, "Determination of Coulomb-Blockade Resistances and Observation of Tunnelling of Coulomb-Blockade Resistances and observation of the Tunnelling of Single Electrons in Small-Tunnel-Junction Circuits", Phys. Rev. Lett., 1991, 67, 3148.
- Furusaki A and Ueda M, "Semiclassical theory of small Josephson junctions: Solutions of the master equation", Phys Rev. (B), 1992, 45, 10576.
- Geerligs L and Mooij M, "Charge Quantisation and Dissipation in Arrays of Small Josephson Junctions", Physica(B), 1988, 152, 212.
- Geerligs L, Ph.D Thesis, unpublished, 1989.
- Geerligs L, Anderegg V, van Der Jeugd C, Romijn J and Mooij J, "Influence of Dissipation on the Coulomb Blockade in Small Tunnel Junctions", Europhys Lett., 1989, 10, 79.

- Geerligs L and Mooij J, "Charging effects and 'turnstile' clocking of single electrons in small tunnel junctions", NATO ASI on Granular Nanoelectronics, 1990.
- Geerligs L, Averin D and Mooij J, "Observation of Macroscopic Quantum Tunnelling through the Coulomb Energy Barrier", Phys. Rev. Lett., 1990, 65, 3037.
- Geerligs L, "Charge Quantisation Effects in Small Tunnel Junctions", Physics of Nano-structures, ed. J.Davies and A.Lang, Bristol-England, 1991, 171.
- Geigenmuller U and Schon G, "Single Electron Effects and Bloch Oscillations in Normal and Superconducting Tunnel Junctions", Physica(B), 1988, 152, 186.
- Giaever I and Zeller H, "Superconductivity of Small Tin Particles Measured by Tunnelling", Phys. Rev. Lett., 1968, 20, 1503.
- Girvin S, Glazman L, Jonson M, Penn D and Stiles M, "Quantum Fluctuations and the Single-Junction Coulomb Blockade", Phys. Rev. Lett, 1990, 64, 3183.
- Golubev D and Zaikin A, "Charge fluctuations in systems of mesoscopic tunnel junctions", Phys. Lett. (A), 1992, 169, 475.
- Golubev D and Zaikin A, "Quantum dynamics of ultrasmall tunnel junctions: Real-time analysis", Phys. Rev. (B), 1992, 46, 10903.
- Gorter C, Physica, 17, 1951, 777.
- Groshev A, "Coulomb-Blockade of resonant tunnelling", Phys. Rev. (B), 1990, 42, 5895.
- Hanna A, Touminen M and Tinkham T, "Observation of Elestic MQT of the charge variable", Phys. Rev. Lett., 1992, 68, 3228.
- Hartstein A and Weinberg Z, "Unified theory of photoemission and photon-assisted tunnelling", Phys. Rev. (B), 1979, 20, 1335.
- Hartstein A, Weinberg Z and DiMaria D, "Experimental test of the quantum mechanical image-force theory", Phys. Rev.(B), 1982, 25, 7174.
- Hill R, Proc. R. Soc. Ser. A, 1969, 309, 377.
- Hooge F, Kleinpenning T and Vandamme L, "Expeimental studies on 1/f noise", Rep. Prog. Phys., 1981, 44, 31.
- Hu G and O'Connell R, "Charge Fluctuations and zero-bias Resistance in Small Capacitance Tunnel Junctions", Phys. Rev. (B), 1992, 46, 14219.
- Jackson J, "Networks of Waiting Lines", Operations Research, 1959, 518.
- Joseph T, "Engineering Mathematics Handbook", McGraw-Hill Book Company.

- Kastner M, "The single-electron transistor", Rev. Mod. Phys., 1992, 64, 849.
- Kleinrock L, "Queuing Systems", New York London 1974-1976.
- Korotkov A, Averin D and Likharev K, "Single-Electron Charging of the Quantum Wells and Dots", Physica (B), 1990, 165-166, 927.
- Kouwenhoven L, Johnson A, van der Vaart N, Harms C and Foxon C, "Quantised Current in a Quantum-Dot Turnstile Using Oscillating Tunnel Barriers", Phys. Rev. Lett., 1991, 67, 1626.
- Kulik I and Shekhter R, "Kinetic phenomena and charge discreteness effects in granulated media", JETP, 1975, 41, 308.
- Kuzmin L and Likharev K, "Direct experimental observation of discrete correlated single electron-tunnelling", JETP Lett., 1987, 45, 495.
- Kuzmin L, Delsing P, Claeson T and Likharev K, "Single-Electron Charging Effects in Arrays of Ultra-Small Tunnel Junctions", Phys. Rev. Lett., 1989, 62, 2539.
- Kuzmin L, Nazarov Y, Haviland D, Delsing P and Claeson T, "Coulomb Blockade and Incoherent Tunnelling of Cooper Pairs in Ultrasmall Junctions Affected by Strong Quantum Fluctuations", Phys. Rev. Lett., 1991, 67, 1161.
- Lambe J and Jaklevic R, "Charge Quantisation Studies using a Tunnel Capacitor", Phys. Rev. Lett., 1969, 22, 1371.
- Landauer R, "Fluctuations in Bistable Tunnel Diode Circuits", J. Appl. Phys., 1962, 33, 2209.
- Lang S, "Complex Analysis", Addison-Wesley Pub-company, 1977.
- Levine A, "Theory of Probability", Addison-Wesley, 1971.
- Likharev K, "Single-Electron Transistors: Electrostatic Analogs of the DC SQUIDS", IEEE Trans. on Magnetics, 1987, 23, 1142.
- Likharev K, "Correlated discrete transfer of single electrons in ultrasmall tunnel junctions", IBM. J. Res. Develop., 1988, 32, 144.
- Likharev K, Bakhvalov N, Kazacha G and Serdyukova S, "Single-Electron Tunnel Junction Array, An Electrostatic Analog of the Josephson Transmission Line", IEEE Trans. Mgn, 1989, 25, 1436.
- Lipschutz S, "Linear Algebra", Mc-Graw-Hill, 1981.
- Mead C and Conway L, "Introduction to VLSI Systems", Addison-Wesley, 1980.
- Meirav U, Kastner M and Wind S, "Single-Electron Charging and Periodic Conductance Resonances in GaAs Nanostructures", Phys. Rev. Lett., 1990, 65, 771.

- Mel'nikov V, "Cotunnelling rate in a series array of tunnel junctions", Phys. Lett. (A), 1993, 176, 267.
- Meurer B, Heitmann D and Ploog K, "Single-Electron Charging of Quantum-Dot Atoms", Phys. Rev. Lett, 1992, 68, 1371.
- Milgram A and Lu C, "Field Effect and Electrical Conduction Mechanism in Discontinuous Thin Metal Films", J.Appl. Phys., 1966, 37, 4773.
- Mullen K, Ben-Jacob E and Ruggiero S, "Charging effects in coupled superconducting tunnel junctions and their implications for tunnelling measurements of high T_c superconductors", Phys. Rev. (B), 1988, 38, 5150.
- Mullen K, Ben-Jacob E and Schuss Z, "Combined Effect of Zener and Quasiparticle Transitions on the Dynamics of Mesoscopic Josephson Junctions", Phys. Rev. Lett., 1988, 60, 1097.
- Mullen K, Gefen Y and Ben-Jacob E, "The Dynamics of Mesoscopic Normal Tunnel Junctions", Physica (B), 1988, 152, 172.
- Mullen K and Ben-Jacob E, "I-V characteristics of coupled ultrasmall-capacitance normal tunnel junctions", Phys. Rev. (B), 1988, 37, 98.
- Nazarov Y, "Coulomb-Blockade of Tunnelling in isolated junctions", JETP Lett., 1989, 49, 126.
- Neuegebauer C and Webb M, "Electrical Conduction Mechanism in Ultrathin, Evaporated Metal Films", J.Appl. Phys., 1961, 33, 74.
- Newell G, "Applications of Queueing Theory", Chapman & Hall, London New York, 1982.
- Pasquier C, Meirav U, Williams F, Glattli D, Y.Jin Y and B.Etienne, "Quantum Limitation on Coulomb Blockade Observed in a 2D Electron System", Phys. Rev. Lett., 1993, 70, 69.
- Ralls K, Skocpol W, Jackel L, Howard R, Fetter L, Epworth R and Tennant D, "Discrete Resistance Switching in Submicrometer Silicon Inversion Layers: Individual Interface Traps and Low-Frequency (1/f) Noise", Phys. Rev. Lett., 1984, 52, 228.
- Raven M, "Charge transport and conductance oscillations in gold island films", Phys. Rev. (B), 1984, 29, 6218.
- Reed M, Randall J, Aggarwal R, Matyi R, Moore T and Wetsel A, "Observation of Discrete Electronic States in a Zero-Dimensional Semiconductor Nanostructure", Phys. Rev. Lett., 1988, 60, 535.

- Reimbold G, "Modified $1/f$ Trapping Noise Theory and Experiments on MOS Transistors Biased from Weak to Strong Inversion-Influence of Interface States", IEEE Trans. Electron Devices, 1984, 31, 1190.
- Rogers C and Buhrman R, "Composition of $1/f$ Noise in Metal-Insulator-Metal Tunnel Junctions", Phys. Rev. Lett., 1984, 53, 1272.
- Rogers C and Buhrman R, "Nature of Single-Localized-Electron-States Derived for Tunnelling Measurements", Phys. Rev. Lett., 1985, 55, 859.
- Roy D, "Tunnelling and negative Resistance phenomena in Semiconductors", e.d. B.R.Pamplin, Pergamon Press, 1977.
- Roy S, Barker J and Asenov A, "System simulation tools for single-electronic devices", Proc. of International Workshop on Computational Electronics, 1993, Leeds, 257.
- Roy S, Unpublished, 1992.
- Schön G, "Quantum shot noise in tunnel junctions", Phys. Rev. (B), 1985, 32, 4469.
- Schwartz M, "Computer Communication Network Design and Analysis", Prentice-Hall, 1977.
- Scott-Thomas J, Field S, Kastner M, Smith H and Antoniadis D, "Conductance Oscillations Periodic in the Density of a One-Dimensional Electron Gas", Phys. Rev. Lett., 1989, 62, 583.
- Shekhter R, "Zero Anomalies in the Resistance of a Tunnel Junction Containing Metallic Inclusions in the Oxide Layer", JETP, 1973, 36, 747.
- Sheng P, Abeles B and Arie Y, Phys. Rev. Lett., 1973, 31, 44.
- Shikin V, Leao S and Hipolito O, "Current-voltage characteristic of a double tunnel junction under Coulomb-blockade conditions", JETP, 1993, 76, 325.
- Simmons J, "Potential Barriers and Emission-limited Current Flow Between Closely Spaced Parallel Metal Electrodes", J.Appl. Phys., 1964, 35, 2472.
- Simmons J, "Generalised Thermal J-V Characteristics for the Electric Tunnel Effect", J.Appl. Phys., 1964, 35, 2655.
- Skocpol W, "Transport Physics of Multicontact Si MOS Nanostructures", Europhysics, Conference on Physics and Fabrication of Nanostructures, 1984, 255.
- Ueda M and Yamamoto Y, "Exact time-domain description of the crossover from random to Coulomb-regulated single-electron tunnelling in Ultrasmall normal tunnel junctions", Phys. Rev. (B), 1990, 41, 3082.

- Ueda M, "Probability-density-function description of mesoscopic normal tunnel junctions", Phys. Rev. (B), 1990, 42, 3087.
- Uozumi K, Nishiura M and Kinbara A, "On the field effect of the electrical conductance of discontinuous thin metal films", J. Appl. Phys., 1977, 48, 818.
- Uren M, Day D and Kirton M, "1/f and random telegraph noise in silicon metal-oxide-semiconductor FET's", Appl. Phys. Lett., 1985, 47, 1195.
- Waxman D and Leggett A, "Dissipative quantum tunnelling at finite temperatures", Phys. Rev. (B), 1985, 32, 4450.
- Weinberg Z and Hartstein A, "Photon Assisted Tunnelling from Aluminium to Silicon dioxide", Solid State Comm., 1976, 20, 179.
- Wilkins R, Ben-Jacob E and Jaklevic R, "Scanning-Tunnelling-Microscope Observations of C.B. and Oxide Polarisation in Small Metal Droplets", Phys. Rev. Lett., 1989, 63, 801.
- Williams J and Burdett R, "Current noise in thin gold films", J. Phys. (C), 1969, 2, 298.
- Williams J and Stone I, "Current noise on thin discontinuous films", Phys. Lett. (C), 1972, 5, 2105.
- Yoshihiro K, "Observation of 'Bloch Oscillations in Granular Tin Films", Physica (B), 1988, 152, 207.
- Zeller H and Giaever I, "Tunnelling, Zero-Bias Anomalies, and Small Superconductors", Phys. Rev. 1968, 181, 789.

Appendices

Appendix (A): Coefficients of the set of equations (2.4.20)

To simplify the calculations the following transformations are used:

$$Q=qe, \quad t=R_s C \tau; \quad \text{giving} \quad I(t) = \frac{e}{R_s C} i(\tau)$$

where q and τ are dimensionless quantities. The coefficients are then obtained as:

$$A_1 = -\frac{\Delta\tau}{2} \Gamma_2 \quad A_2 = -A_1$$

$$B_1 = -\frac{\Delta\tau}{2} \frac{D}{(\Delta q)^2} \quad B_2 = -B_1$$

$$C_1 = 1 - \frac{\Delta\tau}{2} \left(1 + \gamma - \frac{\beta}{\Delta q} - \frac{2D}{(\Delta q)^2} \right) \quad C_2 = 1 + \frac{\Delta\tau}{2} \left(1 + \gamma - \frac{G}{\Delta q} - \frac{2D}{(\Delta q)^2} \right)$$

$$D_1 = -\frac{\Delta\tau}{2} \left(\frac{G}{\Delta q} + \frac{D}{(\Delta q)^2} \right) \quad D_2 = -D_1$$

$$E_1 = -\frac{\Delta\tau}{2} \Gamma_1 \quad E_2 = -E_1$$

where

$$\gamma = \Gamma_3 + \Gamma_4, \quad G = q - \bar{q} - i(t), \quad D = \frac{k_B T C}{E_c} \quad \text{and} \quad \beta = \frac{R_s}{R_t}.$$

Appendix(B): Linear Programming relations for the operational areas of the *undamped turnstile*:

Clocking-in Phase:

At bias voltages V_g , V_r and V_l , using the transformation,

$$u = \frac{1}{C_T} \{ CV_r - (C + C_o)V_l + C_o V_g \}$$

$$v = \frac{1}{C_T} \{ (C + C_o)V_r - CV_l - C_o V_g \}$$

the voltages V_1 and V_2 can be written as:

$$V_1(n) = u - \frac{ne}{C_T}$$

$$V_2(n) = v + \frac{ne}{C_T}$$

The first phase of the clocking cycle requires only one event to take place; while all other events are to be blocked, see FSM model shown in figure (3.7). This event is chosen to be $T(L,M,0)$. Using the transition conditions defined in equation (3.3.2) together with the transformation defined above, the following relations are obtained,

- | | |
|-----------------------------------------------------|-----------------------------------------------------|
| 1. $T(L,M,0) \rightarrow u > \frac{e}{2C_T}$ | 2. $\bar{T}(M,R,0) \rightarrow v < \frac{e}{2C_T}$ |
| 3. $\bar{T}(R,M,0) \rightarrow v > -\frac{e}{2C_T}$ | 4. $\bar{T}(L,M,1) \rightarrow u < \frac{3e}{2C_T}$ |
| 5. $\bar{T}(M,L,1) \rightarrow u > \frac{e}{2C_T}$ | 6. $\bar{T}(M,R,1) \rightarrow v < -\frac{e}{2C_T}$ |
| 7. $\bar{T}(R,M,1) \rightarrow v > \frac{3e}{2C_T}$ | |

Clocking-out Phase:

In Phase-II, V_{g2} is to excite the excess electron already stored at M to tunnel through the RHS junction and the event is therefore $T(M,R,1)$. Again, all other events should be blocked. Using the same transformation mentioned above, the following set of relations should hold:

- | | |
|-----------------------------------------------------|------------------------------------------------------|
| 1. $T(M,R,1) \rightarrow v > -\frac{e}{2C_T}$ | 2. $\bar{T}(M,R,0) \rightarrow v < \frac{e}{2C_T}$ |
| 3. $\bar{T}(R,M,0) \rightarrow v > -\frac{e}{2C_T}$ | 4. $\bar{T}(R,M,1) \rightarrow v > -\frac{3e}{2C_T}$ |
| 5. $\bar{T}(M,L,1) \rightarrow u > \frac{e}{2C_T}$ | 6. $\bar{T}(L,M,1) \rightarrow u < \frac{3e}{2C_T}$ |
| 7. $\bar{T}(L,M,0) \rightarrow u < \frac{e}{2C_T}$ | 8. $\bar{T}(M,L,0) \rightarrow u > -\frac{e}{2C_T}$ |

Appendix (C): Damped double-junction system:

In this case the tunnelling electron senses the change of the charge on the junction through which the event is performed. Using the strict local limit (*critical charge*= $e/2$) the following set of relations is obtained:

Clocking-In Phase:

The required event is $T(L,M,0)$ and all other events should be eliminated.

$$\bar{T}(L,M,0) \rightarrow u > e/2C$$

$$\bar{T}(L,M,1) \rightarrow u < e/C_T + e/2C$$

$$\bar{T}(R,M,0) \rightarrow v > -e/2C$$

$$\bar{T}(R,M,1) \rightarrow v < e/2C - e/C_T$$

Clocking-out Phase:

The event expected to take place here is $T(M,R,1)$. The most important relations in this case are given below:

$$T(M,R,1) \rightarrow v > e/2C - e/C_T$$

$$\bar{T}(M,R,0) \rightarrow v < e/2C$$

$$\bar{T}(L,M,0) \rightarrow v < e/2C$$

$$\bar{T}(M,L,0) \rightarrow u > -\left(e/2C - e/C_T\right)$$

